Thesis

Pairing symmetry and gap structure in heavy fermion superconductors

Takuya Nomoto

Department of Physics, Kyoto University

January, 2017

Abstract

Since the discovery of high-T_c cuprates, the unconventional superconductivity has been attracted much attention for its novel property, pairing mechanism and potential applicability to the engineering. In particular, the class of heavy fermion superconductors often exhibits various interesting phenomena such as spin-triplet pairing and coexistence with a magnetic order. However, the presence of strong electronic correlations and complicated multi-degrees of freedom has prevented us from fully understanding such novel properties. In this situation, group theoretical classification of gap functions, which provides definite statements independent of the details of materials, has played an essential role for an analysis. Early works, however, were devoted to the gap classification for single orbital systems, as is summarized in the review by Sigrist and Ueda [1], and thus, the attention should be paid in its use since the actual gap structure does not exactly have such simple momentum dependence or nodal structure.

In this thesis, we first propose an exotic multi-gap structure in the heavy fermion superconductor UPt_3 as a remarkable example, from a gap analysis based on the first-principles calculations [2]. The obtained E_{2u} state has in-plane twofold vertical line nodes, axial point and horizontal line nodes on each Fermi surface, which is completely different from the previous phenomenological models. Such a nodal structure can be hardly understood based on the results in Ref. [1] and requires careful consideration on the gap functions in the basis of $j = 5/2$ space. In addition, Micklitz and Norman demonstrated in their pioneering work that new types of symmetry protected nodes can appear at the Brillouin zone boundary in UPt_3 [3], which is also observed in the microscopic calculations [2]. These facts imply that it is necessary to revisit the gap classification in symmorphic/non-symmorphic superconductors by explicitly considering the multi-degrees of freedom including the spin, orbital, and sublattice degrees of freedom. Motivated by such observations, we then provide general group theoretical classification of the gap functions in multiorbital superconductors [4] and in nonsymmorphic superconductors [5]. In the former study [4], we perform the gap classification by introducing generalized Cooper pairs, which possess spin-orbital coupled (multipole) degrees of freedom, instead of the conventional spin-singlet/triplet in the single orbital systems. From the classification, we realize that a gap function with $\Gamma_9 \otimes \Gamma_9$ in D_6 possesses nontrivial momentum dependence that is different from the usual spin 1/2 classification. Indeed, the

present classification can describe the emergent twofold vertical line nodes in E_{2u} pairing states of UPt_3. Furthermore, we show that unconventional gap structure can be realized in the BCS approximation for a purely local interaction, which implies the emergence of the electron-phonon mediated unconventional superconductivity. In the latter study [5], we extend the gap classification to the non-symmorphic magnetic space groups, which have been less understood in spite of the growing interest in the superconductors coexisting with a magnetic order. The obtained results are applied to the analysis of superconductivity in UCoGe and UPd_2Al_3. Based on the weak coupling BCS theory, we show that the UCoGe-type ferromagnetic superconductors must have horizontal line nodes on either the $k_z = 0$ or $k_z = \pm\pi/c$ plane. On the other hand, in UPd_2Al_3-type antiferromagnetic superconductors, A_g-type gap functions possess line nodes in the antiferromagnetic Brillouin zone boundary perpendicular to the c-axis, namely, the conventional fully gapped s-wave superconductivity is forbidden regardless of the pairing mechanism. Our present gap classification as well as the exotic multi-gap structure in UPt_3 shed new light on the understanding of various unconventional superconductors with spin-orbit coupling and multi-degrees of freedom.

Contents

List of publications

Published papers related to the thesis

1. Takuya Nomoto and Hiroaki Ikeda,
   Exotic multi-gap structure in UPt_3 unveiled by the first-principles analysis,
   Phys. Rev. Lett. **117**, 217002 (2016).

2. Takuya Nomoto, Kazumasa Hattori, and Hiroaki Ikeda,
   Classification of multipole superconductivity in multiorbital systems and its implications,
   Phys. Rev. B **94**, 174513 (2016).

3. Takuya Nomoto and Hiroaki Ikeda,
   Symmetry-Protected Line Nodes in Non-symmorphic Magnetic Space Groups: Applications to UCoGe and UPd_2Al_3,
   J. Phys. Soc. Jpn. **86**, 023703 (2017).

Published papers not included in the thesis

4. Takuya Nomoto and Hiroaki Ikeda,
   Effect of magnetic criticality and Fermi-surface topology on the magnetic penetration depth,
   Phys. Rev. Lett. **111**, 167001 (2013).

5. Takuya Nomoto and Hiroaki Ikeda,
   Fermi surface evolution and d-wave superconductivity in $CeCoIn_5$: Analysis based on LDA+DMFT method,
   Phys. Rev. B **90**, 125147 (2014).

6. Shunichiro Kittaka, Yusei Shimizu, Toshiro Sakakibara, Yoshinori Haga, Etsuji Yamamoto, Yoshichika Ōnuki, Yasumasa Tsutsumi, Takuya Nomoto, Hiroaki Ikeda, and

Kazushige Machida,
Evidence for Chiral d-Wave Superconductivity in URu_2Si_2 from the Field-Angle Variation of Its Specific Heat,
J. Phys. Soc. Jpn. **85**, 033704 (2016).

7. Yusei Shimizu, Shunichiro Kittaka, Toshiro Sakakibara, Yasumasa Tsutsumi, Takuya Nomoto, Hiroaki Ikeda, Kazushige Machida, Yoshiya Homma, and Dai Aoki,
Omnidirectional Measurements of Angle-Resolved Heat Capacity for Complete Detection of Superconducting Gap Structure in the Heavy-Fermion Antiferromagnet UPd_2Al_3,
Phys. Rev. Lett. **117**, 037001 (2016).

8. Taichi Terashima, Naoki Kikugawa, Hai Lin, Xiyu Zhu, Hai-Hu Wen, Takuya Nomoto, Katsuhiro Suzuki, Hiroaki Ikeda, and Shinya Uji,
Upper critical field and quantum oscillations in tetragonal superconducting FeS,
Phys. Rev. B **94**, 100503(R) (2016).

9. Yasumasa Tsutsumi, Takuya Nomoto, Hiroaki Ikeda, and Kazushige Machida,
Nodal gap detection through polar angle resolved density-of-states measurements,
Phys. Rev. B **94**, 224503 (2016).

Chapter 1

Introduction to the superconductivity with multi-degrees of freedom

In the celebrated microscopic theory by Bardeen, Cooper, and Schrieffer (BCS) in 1957 [6], the superconducting state is described as a condensation of Cooper pairs. The resulting Cooper pair wave function or gap function plays a role of the superconducting order parameter, which spontaneously breaks the U(1) gauge symmetry below the transition temperature T_c.

The BCS theory excellently explained interesting phenomena in the traditional superconductivity. However, the class of heavy fermion superconductors discovered around 1980 [7] and also the high-T_c cuprates [8] did not fit the BCS theory. The power-law temperature behavior in various thermodynamic quantities at low temperatures observed in these superconductors was drastically different from the conventional BCS superconductors. In the early stage, it was clear that an extension of the BCS theory is inevitable. It was soon discussed that spin-fluctuations can lead to anisotropic pairing states [9, 10], in connection with superfluid ^{3}He [11]. In such unconventional superconductivity, one or more symmetries in addition to the U(1) symmetry are broken below T_c.

For instance, phase sensitive experiments such as π-junction and angle-resolved measurements clarified that the high-T_c cuprates and also $CeCoIn_5$ possess the $d_{x^2-y^2}$-wave pairing state [12, 13, 14], which breaks the C_4 rotational symmetry in the tetragonal crystal structure. In such a case, low-energy excitations below T_c are dominated by nodal quasi-particle excitations around symmetry protected line nodes (gap zeros) on the Fermi surfaces. This situation is incompatible with the fully gapped s-wave state in the conventional BCS theory. The gap structure is closely related to the pairing symmetry and the pairing mechanism. Thus, the superconducting gap function, which is one of the most fundamental quantities, continues to be hotly debated in this research field.

In this context, group theoretical classification of the superconducting gap functions is important and useful to investigate a variety of superconductors. Indeed, the early works [15, 16, 17] of classification have been indispensable for the analysis of various uncon-

ventional superconductors including heavy fermion [18, 19, 20], cuprate [21], and ruthenate superconductors [22, 23, 24].

1.1 Overview of the early works

One of the main assumptions of early works is the presence of space inversion and time reversal symmetries. In such a case, there appears twofold degeneracy at every $\boldsymbol{k}$ point in energy spectra, which is a consequence of the Kramers theorem. Furthermore, in the presence of spin-orbit coupling, momentum (or orbital) and spin degrees of freedom are no longer independent each other, and then only simultaneous transformations of the real and spin spaces can be the symmetry operations, which leave the system invariant. Thus, if we regard the Kramers degrees of freedom as those come from *pure* spin 1/2, the transformation of the Bloch states $\psi(\boldsymbol{k})$, or the corresponding creation operators $c^\dagger(\boldsymbol{k})$ in the second quantization, is given by

$$p\, c^\dagger_{n\sigma}(\boldsymbol{k})\, p^{-1} = \sum_{\sigma'} c^\dagger_{n\sigma'}(p\boldsymbol{k}) D^{(1/2)}_{\sigma'\sigma}(p), \tag{1.1.1}$$

for any rotation $p \in \mathrm{SU}(2)$, which acts on both the real and spin spaces. Here, n denotes the band index and σ denotes the Kramers index. $D^{(1/2)}(p)$ is the two dimensional representation matrix of the irreducible representation $\ell = 1/2$ in SU(2) group, which corresponds to the electron spin. Note that with respect to the symmetry, the superconducting gap functions $\Delta(\boldsymbol{k})$ can be regarded as the Cooper pair wave functions. Therefore, for the zero momentum Cooper pairs, Eq. (1.1.1) implies that (the inter-band components of) the gap functions are transformed as [1],

$$p\ :\ \Delta_{\sigma_1\sigma_2}(\boldsymbol{k}) \to \sum_{\sigma'_1\sigma'_2} D^{(1/2)}_{\sigma_1\sigma'_1}(p) \Delta_{\sigma'_1\sigma'_2}(p^{-1}\boldsymbol{k}) (D^{(1/2)}_{\sigma'_2\sigma_2}(p))^T. \tag{1.1.2}$$

Equation (1.1.2) gives us the basis of gap classification. Here, A^T denotes the transpose matrix of the matrix A. Note that in the absence of spin-orbit coupling, the real and spin space transformations can be treated independently. The classification based on such a limit was developed in Refs. [25, 26], although we do not consider in this thesis.

On the other hand, Landau theory for the second order phase transition tells us that the order parameter of the symmetry broken phase has to belong to an irreducible representation of the broken symmetry through the transition. In the class of superconductors called *anisotropic* superconductors, the point group symmetry in addition to the U(1) symmetry is broken below T_c, and thus, the order parameters also belong to an irreducible representation of the point group symmetry. For example, when the order parameter belongs to ith basis of Γ, which is an irreducible representation in the point group symmetry P, the corresponding

gap function $\Delta^{(\Gamma,i)}(\boldsymbol{k})$ satisfies,

$$p\ :\ \Delta^{(\Gamma,i)}_{\sigma_1\sigma_2}(\boldsymbol{k}) \to \sum_j \Delta^{(\Gamma,j)}_{\sigma_1\sigma_2}(\boldsymbol{k}) D^{(\Gamma)}_{ji}(p), \tag{1.1.3}$$

for all $p \in P$ in addition to Eq. (1.1.2). Here, $D^{(\Gamma)}(p)$ is the representation matrix of p in Γ. Since the space inversion operator I is not an element of SU(2) group but may be that of P, we define that $D^{(\Gamma)}(I)$ for the Bloch states is identical with the identity matrix as usual. The equivalence between Eqs. (1.1.2) and (1.1.3) imposes the constraint to the momentum and the spin dependence, and in certain cases, can yield symmetry protected nodal structure.

In particular, we can immediately see that the even and odd parity representations cannot be mixed in the superconducting states in the presence of the space inversion symmetry, which is one of the key consequences of the classification based on the point group symmetry. Such superconductors are often called *centrosymmetric superconductors*. Because fermion antisymmetry imposes an additional constraint for the gap functions $\Delta(\boldsymbol{k}) = (\Delta(-\boldsymbol{k}))^T$, a spin-singlet pairing $\Delta^g(\boldsymbol{k})$ is of even parity and a spin-triplet $\Delta^u(\boldsymbol{k})$ is of odd parity in the centrosymmetric superconductors. These take the forms,

$$\Delta^g_{\sigma\sigma'}(\boldsymbol{k}) = \varphi(\boldsymbol{k})(i\sigma^y)_{\sigma\sigma'}, \tag{1.1.4}$$

$$\Delta^u_{\sigma\sigma'}(\boldsymbol{k}) = \boldsymbol{d}(\boldsymbol{k}) \cdot (i\boldsymbol{\sigma}\sigma^y)_{\sigma\sigma'}, \tag{1.1.5}$$

with an even $\varphi(\boldsymbol{k})$ and an odd function $\boldsymbol{d}(\boldsymbol{k})$ of momentum $\boldsymbol{k}$. Here, $\boldsymbol{\sigma} = (\sigma^x, \sigma^y, \sigma^z)$ denotes the usual Pauli matrix and the three dimensional vector $\boldsymbol{d}(\boldsymbol{k})$ defined in Eq. (1.1.5) is called $\boldsymbol{d}$-vector. As is well-known, $\boldsymbol{d}$-vector plays an important role for the nodal structure and the magnetic response in spin-triplet superconductors. By use of the definitions (1.1.2), (1.1.4), and (1.1.5), we find that $p \in P$ transforms each gap function as follows,

$$p\ :\ \varphi(\boldsymbol{k}) \to \varphi(p\boldsymbol{k}), \qquad \text{for even parity}, \tag{1.1.6}$$

$$p\ :\ \boldsymbol{d}(\boldsymbol{k}) \to (p\boldsymbol{d})(p\boldsymbol{k}), \quad \text{for odd parity}. \tag{1.1.7}$$

From Eq. (1.1.7), we find that $\boldsymbol{d}(\boldsymbol{k})$ transforms like a usual (pseudo) vector for the point group operations, which is the origin to be called $\boldsymbol{d}$-vector. Eqs. (1.1.6) and (1.1.7) are the basic equations to derive symmetry allowed gap functions composed of pairs of electrons with the pure spin 1/2. Note that the transformation property of Bloch states Eq. (1.1.1) is a fundamental assumption to derive that of gap functions (1.1.6) and (1.1.7). However, it is not so clear that such definition is always best to describe the superconductivity in *multiorbital* systems in the presence of strong spin-orbit coupling. Furthermore, in the systems with more than one atoms in a unit cell, each electron has atomic site (sublattice) degrees of freedom as well as the spin and orbital. It is also unclear whether the superconductivity in such systems can be well described by the above gap classification scheme. These are the main subjects in this thesis and will be discussed in more detail in later Chapters.

Table 1.1: Basis functions of irreducible representations (IRs) in D_{4h} group [1].

IR(even)	Basis functions	IR(odd)	Basis functions
A_{1g}	$\varphi(\boldsymbol{k}) = 1, k_x^2 + k_y^2, k_z^2$	A_{1u}	$\boldsymbol{d}(\boldsymbol{k}) = \hat{\boldsymbol{x}}k_x + \hat{\boldsymbol{y}}k_y, \hat{\boldsymbol{z}}k_z$
A_{2g}	$\varphi(\boldsymbol{k}) = k_x k_y (k_x^2 - k_y^2)$	A_{2u}	$\boldsymbol{d}(\boldsymbol{k}) = \hat{\boldsymbol{x}}k_y - \hat{\boldsymbol{y}}k_x$
B_{1g}	$\varphi(\boldsymbol{k}) = k_x^2 - k_y^2$	B_{1u}	$\boldsymbol{d}(\boldsymbol{k}) = \hat{\boldsymbol{x}}k_x - \hat{\boldsymbol{y}}k_y$
B_{2g}	$\varphi(\boldsymbol{k}) = k_x k_y$	B_{2u}	$\boldsymbol{d}(\boldsymbol{k}) = \hat{\boldsymbol{x}}k_y + \hat{\boldsymbol{y}}k_x$
E_g	$\varphi_1(\boldsymbol{k}) = k_x k_z$	E_u	$\boldsymbol{d}_1(\boldsymbol{k}) = \hat{\boldsymbol{x}}k_z, \hat{\boldsymbol{z}}k_x$
	$\varphi_2(\boldsymbol{k}) = k_y k_z$		$\boldsymbol{d}_2(\boldsymbol{k}) = \hat{\boldsymbol{y}}k_z, \hat{\boldsymbol{z}}k_y$

Based on the above (conventional) classification scheme, symmetry allowed gap functions in major point group symmetries were investigated in the early works[15, 16, 17]. For example, Table 1.1 shows the results in D_{4h} point group symmetry summarized in Ref. [1]. From the Table 1.1, we find that the $d_{x^2-y^2}$-wave gap function, proposed in cuprates and $CeCoIn_5$, belongs to B_{1g} irreducible representation in D_{4h} group, which guarantees the presence of line nodes on the symmetry lines along $k_x \pm k_y = 0$. Among spin-triplet superconductors, it has been believed that E_u representation in D_{4h} is realized in the zero magnetic field phase of Sr_2RuO_4 [24]. In this case, since two basis functions are degenerate, an arbitrarily linear combination of them are allowed just above T_c. Minimizing fourth order terms appearing in the Ginzburg-Landau (GL) functional [1], then we find that the time reversal symmetry breaking gap function $\boldsymbol{d}(\boldsymbol{k}) = \hat{\boldsymbol{z}}(k_x \pm ik_y)$, which has s a chirality given by the $\pm$ sign, is the most stable gap in the zero field phase. Another candidate of such chiral superconductivity is that in the hidden ordered phase of URu_2Si_2 [27], with the spin-singlet gap function $\varphi(\boldsymbol{k}) = (k_x \pm ik_y)k_z$ in E_g representation, which also can be seen in Table 1.1. In such ways, the classification table such as Table 1.1 is very helpful in a comprehensive understanding of anisotropic superconductivity, and as a result, has been indispensable for the analysis of various unconventional superconductors.

In the experiments, the nodal structure of the gap functions often is determined by following ways; In conventional s-wave superconductors, the existence of excitation gap in energy spectra leads to the exponential temperature dependence of various physical quantities including the specific heat, magnetic penetration depth, and relaxation rate of nuclear magnetic resonance (NMR). On the other hand, in the presence of nodes (gap zeros) on a part of Fermi surface, the excitation spectrum starts from zero energy due to the excitations across nodal points or lines, which leads to the power low behavior in the physical quantities. Thus, the low energy excitations of anisotropic superconductors often provides the crucial information about the nodal structure, and thus, also the pairing symmetry (namely, irreducible representation to which the order parameter belongs). For example, the temperature dependence

of the specific heat C depends on the topology of the gap structure in the following ways; $C \propto T$ in gapless, $C \propto T^2$ in line nodes, $C \propto T^3$ in point nodes cases at low temperatures. Observations of such power-law behavior are crucial for unconventional superconductivity. Moreover, phase sensitive techniques such as π-junction and angle-resolved measurements under magnetic field can provide the knowledge of nodal positions on the Fermi surface.

In the spin-triplet superconductors, the gap function has the spin component, denoted by the $\boldsymbol{d}$-vector, as well as the momentum. The direction of the $\boldsymbol{d}$-vector is a key property to determine the magnetic response of the triplet superconductors. For example, it is known that magnetic susceptibility parallel to $\boldsymbol{d}$-vector is suppressed in the superconducting phase as the same as the spin-single superconductivity, while that perpendicular to $\boldsymbol{d}$-vector remains unchanged. By use of that, in general, the direction of $\boldsymbol{d}$-vector can be determined by measuring the reduction of Knight shift in various field directions through the superconducting transition. The Pauli paramagnetic suppression of upper critical field H_{c2} is also helpful in the identification of $\boldsymbol{d}$-vector because this is only expected in $\boldsymbol{H} \parallel \boldsymbol{d}$. Note that $\boldsymbol{d}$-vector is defined with the *pseudo*-spin of electrons in the band basis as in Eq. (1.1.1). Thus, the response to the magnetic field does not have to be isotropic even with the isotropic triplet state as the BW state of ^{3}He. Such a behavior is generally expected in the multiorbital superconductors with the strong spin-orbit coupling. This is one of the reasons to complicate the identification of $\boldsymbol{d}$-vector in practice.

1.2 Recent developments

The early theories of classification have been a great success to unveil the fundamental properties of various unconventional superconductors [1]. However, in the last decade, novel superconductors beyond these major classifications have attracted much attentions. Here, we briefly summarize such superconductors.

1.2.1 Non-centrosymmetric superconductors

In the non-centrosymmetric superconductors, such as $CePt_3Si$ [28], UIr [29] and LaBiPt [30], lack of spatial inversion symmetry admits the presence of antisymmetric spin-orbit coupling, and then the spin part of the pairing state explicitly breaks SU(2) symmetry. Rashba spin-orbit coupling is a typical example of antisymmetric spin-orbit coupling, which has the form of $\boldsymbol{g}(\boldsymbol{k}) = \alpha(k_y, -k_x, 0)$ leading to the interaction $H = \boldsymbol{g}(\boldsymbol{k}) \cdot \boldsymbol{\sigma} = \alpha(k_y\sigma^x - k_x\sigma^y)$. In the presence of such antisymmetric spin-orbit coupling, each twofold degenerate band splits to non-degenerate two bands with the fixed spin components at each $\boldsymbol{k}$ point. Thus, in the case with much larger antisymmetric spin-orbit coupling than the superconducting gap amplitudes, the only one of three possible spin-triplet gap functions with $\boldsymbol{d}(\boldsymbol{k}) \propto \boldsymbol{g}(\boldsymbol{k})$ can be stable while the spin-singlet superconductivity is largely unaffected by the broken inversion

symmetry. In addition, broken inversion symmetry also permits that the so-called parity mixing occurs between spin-singlet and triplet states, which are separable under the space inversion symmetry [31]. Although the degree of the singlet-triplet mixing is determined by the pairing interactions as well as the spin-orbit coupling, such mixing can also lead to additional gap nodes that are not imposed by symmetry [32, 33] and may induces interesting topological properties [34]. Moreover, the effect of broken inversion symmetry also appears in the magnetic (Zeeman) field response. Namely, in the presence of $\boldsymbol{g}$-vector perpendicular to Zeeman field $\boldsymbol{H}$, there is no coupling to $\boldsymbol{H}$ in the Hamiltonian at the strong spin-orbit coupling limit [35]. This suggests that there will be no paramagnetic suppression of H_{c2} even for a spin-singlet superconductivity. The anisotropic Pauli suppression observed in the $CePt_3Si$ [35] is well described by this mechanism. Furthermore, many fascinating phenomena including topological [36] and novel magneto-electric effects [37, 38, 39] have been also attracted much attention in this class of superconductors.

1.2.2 Multiorbital superconductors

Regarding centrosymmetric superconductors, the importance of multiorbital character of gap functions has been gradually recognized, for example, through the study on iron based superconductors [40, 41, 42]. As mentioned above, in the early works, the Bloch states are assumed to have pure spin 1/2 degrees of freedom and the gap classification has been performed based on the band-based representation. Although this procedure is always possible, the electrons have other internal degrees of freedom such as orbital and sublattice in the realistic situations. Here, let us briefly consider the effect of orbital degree of freedom on the transformation property of gap functions.

The Hamiltonian describing electron systems can be expressed in terms of the Wannier states, as well as the Bloch states that diagonalize a quadratic term of the Hamiltonian. The Wannier states are constructed from the Bloch states to be localized at some site with the same symmetry as an atomic or a molecule orbital. In the presence of time reversal symmetry, such a local orbital has Kramers degrees of freedom. Here, we suppose a real atomic orbital with angular momentum ℓ. Then, the Wannier states $w^{(\ell)}(\boldsymbol{R})$, where $\boldsymbol{R}$ is a lattice vector (and also denotes the center of the Wannier states), are specified by bases of the orbital and spin, denoted by l and σ, respectively. Then, the transformation property of corresponding creation operator $c^{(\ell)\dagger}(\boldsymbol{R})$ is given by

$$p\, c^{(\ell)\dagger}_{l\sigma}(\boldsymbol{R})\, p^{-1} = \sum_{l'\sigma'} c^{(\ell)\dagger}_{l'\sigma'}(p\boldsymbol{R}) D^{(\ell)}_{l'l}(p) D^{(1/2)}_{\sigma'\sigma}(p), \tag{1.2.1}$$

for any $p \in \mathrm{SU}(2)$. Here, $D^{(\ell)}(p)$ is a representation matrix describing the transformation among the orbital bases with angular momentum ℓ, which results in various phenomena with respect to the orbital degrees of freedom.

Table 1.2: Pairing basis matrices carrying even parity irreducible representations (IRs) of the two-orbital model. [43]. The spin/orbital parity is shown as S(singlet) or T(triplet)/O(odd) or E(even) in the third column. The fourth column describes the behavior of the quasi-particle excitation gap in the momentum space.

IR	Basis	S/O	Gap	IR	Basis	S/O	Gap
A_{1g}	τ^0	S/E	Full	A_{1g}	$(\cos k_x + \cos k_y)\tau^0$	S/E	Nodal
A_{1g}	$(\cos k_x - \cos k_y)\tau^3$	S/E	Nodal	A_{2g}	$(\cos k_x - \cos k_y)\tau^1$	S/E	Nodal
A_{2g}	$i\tau^2$	T/O	Gapless	A_{2g}	$(\cos k_x + \cos k_y)i\tau^2$	T/O	Gapless
B_{1g}	τ^3	S/E	Nodal	B_{1g}	$(\cos k_x - \cos k_y)\tau^0$	S/E	Nodal
B_{1g}	$(\cos k_x + \cos k_y)\tau^3$	S/E	Nodal	B_{2g}	τ^1	S/E	Nodal
B_{2g}	$(\cos k_x + \cos k_y)\tau^1$	S/E	Nodal	B_{2g}	$(\cos k_x - \cos k_y)i\tau^2$	T/O	Gapless
E_g	$(\sin k_x + i \sin k_y)i\tau^2$	S/O	Gapless	E_g	$(\sin k_x + i \sin k_y)\tau^0$	T/E	Full
	$(\sin k_x - i \sin k_y)i\tau^2$				$(\sin k_x - i \sin k_y)\tau^0$		
E_g	$(\sin k_x + i \sin k_y)\tau^3$	T/E	Nodal	E_g	$(\sin k_x + i \sin k_y)\tau^1$	T/E	Nodal
	$(\sin k_x - i \sin k_y)\tau^3$				$(\sin k_x - i \sin k_y)\tau^1$		

If we reconstruct the Bloch states, by diagonalizing the Hamiltonian, from the Wannier states and discuss the symmetry allowed gap functions in the band-based representation, the previous classification scheme is then reproduced. However, we can consider the gap functions also in the local orbital-based representation, based on Eq. (1.2.1) or its momentum space form as

$$p\, c^{(\ell)\dagger}_{l\sigma}(\boldsymbol{k})\, p^{-1} = \sum_{l'\sigma'} c^{(\ell)\dagger}_{l'\sigma'}(p\boldsymbol{k}) D^{(\ell)}_{l'l}(p) D^{(1/2)}_{\sigma'\sigma}(p). \tag{1.2.2}$$

Here, $c^{(\ell)\dagger}(\boldsymbol{k})$ is defined by $c^{(\ell)\dagger}_{l\sigma}(\boldsymbol{k}) = \frac{1}{\sqrt{N}} \sum_{\boldsymbol{R}} e^{i\boldsymbol{k}\cdot\boldsymbol{R}} c^{(\ell)\dagger}_{l\sigma}(\boldsymbol{R})$, where N is the number of unit cell in the crystal. For example, the minimal model describing iron-based superconductor may be composed of two real atomic orbital d_{yz} and d_{zx} on a lattice with D_{4h} point group symmetry [44, 45, 46]. Thus, the gap functions in the local basis are represented by 4×4 matrix $\Delta_{l\sigma,l'\sigma'}(\boldsymbol{k})$ where l denotes the orbital d_{yz}/d_{zx} and σ the spin up/down. Then, the transformation of the gap functions can be obtained from Eq. (1.2.2) similar to Eq. (1.1.2) from Eq. (1.1.1). For instance, resulting basis functions for even-parity pairing states are shown in Table 1.2. Here, τ^μ represents the identity ($\mu = 0$) or the Pauli matrix ($\mu = 1, 2,$ or 3), which acts on the orbital space. We find that there appears spin-triplet (and orbital-triplet) gap functions in the even parity pairing, which is a characteristic of multiorbital systems. Indeed, the complete set of classification tables for the pairing states allowed in two or three orbital models has been provided in Refs. [47, 43, 48, 49, 50]. These works have

revealed many important aspects of the orbital properties in the gap functions and also in the pairing mechanism. However, in spite of such progress in iron based superconductors, there are few works of the extension to the other materials or the other point groups. In addition, many of the previous works are performed in the basis of real atomic orbital, and thus, the extension to the systems with strong spin-orbit coupling is also necessary. These are remaining issues of gap classification and one of the main subjects in this thesis.

1.2.3 Non-symmorphic superconductors

Next, let us focus on remaining electron degrees of freedom, namely, atomic sites (or sublattice) degrees of freedom. Indeed, the classification in several iron based superconductors requires an appropriate treatment for the sublattice character of gap functions [51, 52, 53]. One of the simplest examples with sublattice degrees of freedom may be the multilayered superconductors, which have been widely investigated in the context of high-T_c cuprates and recently attracted locally non-centrosymmetric superconductors [54, 55, 56, 57, 58]. Let us consider the gap functions in bilayer superconductors, which are examples of two sublattice systems. We denote by α or β one of the two layers and suppose that the inversion center is located at the center of the two layers. In this case, since the creation operator of the α-layer electron $c^\dagger_{\alpha\sigma}(\boldsymbol{k})$ transforms to that of the β-layer $c^\dagger_{\beta\sigma}(-\boldsymbol{k})$ by the space inversion operation, staggered spin-singlet (triplet) pairing states belong to the odd (even) parity representation. As a result, for example, finite magnetic susceptibility persists at low temperatures even in even parity pairing states [55]. These features are quite similar to the multiorbital systems when we identify a label of orbital degrees of freedom with that of sublattice. However, in *non-symmorphic* superconductors, it is known that such sublattice degrees of freedom often play more essential roles on the nodal structure than the orbital degrees of freedom [3].

In the presence of two or more equivalent atoms in each unit cell, the space group describing the systems often becomes *non-symmorphic*, some of whose elements include a point group operation p associated with a non-primitive translation $\boldsymbol{a}$. Screw or glide operations are examples of such non-symmorphic operations. For such an operation, which is denoted by $g = \{p|\boldsymbol{a}\}$ in the Seitz notation [59], $c^\dagger_{\alpha\sigma}(\boldsymbol{k})$ is transformed as followings,

$$\begin{aligned} g\, c^\dagger_{\alpha\sigma}(\boldsymbol{k})\, g^{-1} &= e^{-i\boldsymbol{k}\cdot\boldsymbol{a}} \sum_{\sigma'} c^\dagger_{\beta\sigma'}(p\boldsymbol{k}) D^{(1/2)}_{\sigma'\sigma}(p) \\ &= \sum_{\alpha'\sigma'} c^\dagger_{\alpha'\sigma'}(p\boldsymbol{k}) D^{\mathrm{site}}_{\alpha'\alpha}(g;\boldsymbol{k}) D^{(1/2)}_{\sigma'\sigma}(p), \end{aligned} \tag{1.2.3}$$

when g interchanges α with β-sites. Here, $D^{\mathrm{site}}_{\alpha'\alpha}(g;\boldsymbol{k}) = e^{-i\boldsymbol{k}\cdot\boldsymbol{a}}\delta_{\beta\alpha}$ is a representation matrix describing the interchange of the two sites. Note that Eq. (1.2.3) holds for $c^\dagger_{\alpha\sigma}(\boldsymbol{k})$, which is defined by the sublattice dependent Fourier transformation of that in the Wannier basis (see the discussion in Appendix A.2.3). Here, the transformation (1.2.3) appears to be very similar to Eq. (1.2.2) in multiorbital systems except for the $\boldsymbol{k}$ dependence in the representation matrix

$D^{\rm site}_{\alpha'\alpha}(g;\boldsymbol{k})$. However, it has been realized that this momentum dependence is crucial in the classification of gap functions in non-symmorphic superconductors, and indeed, can induce additional nodes on the Fermi surface. Lines nodes protected by such non-symmorphic space groups are investigated through the study on spin-triplet superconductivity of UPt_3 in the context of the breakdown of the Blount's theorem [3, 60, 61]. However, in spite of its general versatility, there are few works on the gap classification in non-symmorphic superconductors so far.

1.3 Heavy fermion superconductors

Among many strongly correlated electron systems, heavy fermion superconductors may be the most suitable systems for the investigation of unconventional superconductivity with multi-degrees of freedom [7, 20]. For instance, the first discovered heavy fermion superconductor $CeCu_2Si_2$ had been widely believed as the first example of the unconventional superconductors [62]. Many observations including T-linear behavior at low T in C/T [63], no coherence peak just below T_c and the T^3 behavior in the NMR relaxation rate $1/T_1$ [64, 65] support line nodal d-wave superconductivity. However, recent specific-heat measurements [66] show the exponential behavior below 60 mK and the H-linear dependence under the magnetic field H, which is more compatible with the multigapped s-wave pairing state. As a result, the importance of the multiband or the multiorbital nature of gap functions has been focused in this material [67, 68, 69].

Furthermore, other prototypical heavy fermion superconductors such as UBe_{13} [70] and UPt_3 [71] exhibit many fascinating phenomena including a spin-triplet pairing and a multiple phase diagram, which may be related to the complicated electronic structure due to the presence of multi-degrees of freedom. Indeed, the heavy fermion superconductor UPt_3 have attracted continuous attentions since its discovery [18, 19]. Although there have been steady progress in group theoretical considerations about the gap symmetry [18, 23, 19, 3], no consensus has been reached on the gap structure as well as the pairing mechanism. The subsequently discovered superconductivity in URu_2Si_2 [72, 73] appears to be more exotic because the superconducting transition occurs deep inside so called "hidden ordered" phase [27]. In this compound, the gap symmetry has been believed as the chiral d-wave of E_g representation in D_{4h} point group symmetry. However, in actual, the broken symmetry associated with the hidden ordered transition will affect the gap functions in the coexisting phase. Such coexisting between superconductivity and the other long range orders (typically, the magnetic orders) was discovered successively after that. Namely, the hexagonal UPd_2Al_3 [74] and UNi_2Al_3 [75] show the superconductivity coexisting with antiferromagnetism and the UGe_2 [76], URhGe [77], and UCoGe [78] show that with ferromagnetism. In such U-based compounds, nevertheless the underlying magnetic ordering is well-established, there are few study on the systematic gap classification in the coexisting phases [79, 80].

In most of heavy fermion superconductors, it is difficult to determine the pairing mechanism and also the gap structure in the microscopic calculations, which is due to the presence of strong electronic correlations as well as the spin-orbit coupling and the multi-degrees of freedom. However, in order to unveil the exotic properties in the heavy fermion superconductors more completely, such microscopic calculations are necessary. Recent progress of first-principles theoretical approach allows us to investigate the superconductivity considering the realistic electronic structure in heavy fermion systems [81, 67, 82], although the electronic correlations can be treated only in the perturbative level. In such situations, cooperation between the microscopic calculations and the group theoretical consideration is necessary to understand various fascinating phenomena inherent in the heavy fermion superconductors.

1.4 Organization of the thesis

In this thesis, we investigate the superconducting symmetry and the gap structure in various unconventional superconductors with spin-orbit coupling and multi-degrees of freedom. In Chapter 2, we first present an exotic multi-gap structure in the heavy fermion superconductor UPt_3, which is revealed based on the first-principles calculations [2]. The obtained E_{2u} pairing state has in-plane twofold vertical line nodes, point and horizontal nodes on each Fermi surface, which is completely different from the previous phenomenological models. This requires an explicit consideration of the multiorbital and the non-symmorphic character in UPt_3. Motivated by the study on UPt_3, we then provide general group theoretical classification of gap functions in the multiorbital superconductors with spin-orbit coupling [4] in Chapter 3 and in non-symmorphic space groups [5] in Chapter 4. In the former study [4], we perform the gap classification by introducing generalized Cooper pairs, which possess spin-orbital coupled (multipole) degrees of freedom, instead of the conventional spin-singlet/triplet in the single orbital systems. On the other hand, in Chapter 4, we extend the gap classification in non-symmorphic space groups to the magnetic crystals [5]. The results are applied to the analysis of superconductivity in UCoGe and UPd_2Al_3. Our present gap classification as well as the exotic multi-gap structure in UPt_3 shed new light on the understanding of various heavy fermion superconductors.

Chapter 2

Exotic multi-gap structure in UPt_3 unveiled by the first-principles analysis

The heavy fermion superconductor UPt_3 is one of the candidates for a spin-triplet superconductor. Because of the rareness of spin-triplet superconductivity and the presence of a multiple superconducting phase, this material has attracted great attention in the field of superconductivity. However, in spite of extensive efforts, its pairing gap structure remains unclear. For example, it has been widely believed that the most promising gap structure is the phenomenological E_{2u} models [18], while the state-of-the-art measurement of field-angle resolved thermal conductivity has indicated that the low-energy quasi-particle excitations are compatible with the E_{1u} representation [83, 84].

In this chapter, we provide the first report on the microscopic gap structure in the heavy fermion superconductor UPt_3 based on an advanced first-principles approach. We found that an unprecedented E_{2u} gap structure can consistently explain experimental observations. Our obtained E_{2u} gap structure has the following peculiar features; Nodal structure is completely different for each Fermi surface, and also the in-plane twofold vertical line nodes emerge on a small Fermi surface. These features cannot be explained in the conventional pseudo-spin representation, but are described with the representation of the Cooper pairs in the total angular momentum $j = 5/2$ space.

The organization is as follows. In Sec. 2.1, we introduce the experimental observations related to our work and also the phenomenological E_{1u} [83] and E_{2u} [18] models. Our results are summarized in Secs. 2.2-2.4. In Sec. 2.2, we derive a model Hamiltonian to describe the electronic structure of UPt_3 and focus on the orbital-resolved property of its Fermi surfaces. In Sec 2.3, we discuss the magnetic susceptibility obtained within our model calculations. Finally, in Sec 2.4, we present the phase diagram and the corresponding gap structure in our model. We also discuss the relation to the experiments and the phenomenological models.

2.1 Introduction to the superconductivity in UPt_3

Identifying a pairing state or a pairing mechanism is one of the most interesting and important issues in the field of unconventional superconductivity. In particular, a spin-triplet type of pairing state attracts much attention, since there are few examples except for the superfluid ^{3}He. In the strongly correlated electron systems, the heavy fermion superconductor UPt_3 is one of the rare candidates for a spin-triplet superconductor. The most impressive feature of this material is showing a multiple superconducting phase diagram under a magnetic field.

The left panel of Fig. 2.1 shows a schematic H-T phase diagram under the field parallel to and perpendicular to the c-axis determined by the sound velocity measurement [85]. At the zero field, there appears superconducting double transition into the A phase at the upper critical temperature $T_c^+ \sim 500$ mK, and then into the B phase at the lower $T_c^- \sim 440$ mK [86]. Moreover, the C phase appears at the high field and the low temperature [87]. The phase transition lines separating the three phases appear to meet at a tetracritical point both for $\boldsymbol{H} \parallel \boldsymbol{c}$ and $\boldsymbol{H} \perp \boldsymbol{c}$, although the case for a tetracritical point is strongest for $\boldsymbol{H} \perp \boldsymbol{c}$ [85]. In addition, the clear anisotropy between in and perpendicular to the basal plane is observed in the upper critical field H_{c2} [88]. The crossover in the anisotropy ratio of H_{c2} indicates the presence of paramagnetic suppression of H_{c2} for $\boldsymbol{H} \parallel \boldsymbol{c}$, but no suppression for $\boldsymbol{H} \perp \boldsymbol{c}$. Because of such prominent features, a lot of theoretical works have been devoted to understand its superconductivity [89, 90, 91, 92]. Today, two incompatible scenarios, called E_{2u} model proposed by the Sauls' group [18] and E_{1u} or spin model by the Machida's group [93], are widely believed as a possible pairing state in UPt_3. Here, we summarize key features of these two scenarios.

UPt_3 possesses hexagonal crystal structure with the space group $P6_3/mmc$ (see the right panel of Fig. 2.1). The presence of multiple phases implies that the order parameter has (nearly) degenerate two components which should be bases of an irreducible representation in D_{6h} point group symmetry. Moreover, considering the paramagnetic suppression, it is natural to assume that the order parameter belongs to an odd parity representation with $\boldsymbol{d}$-vector locked to the c-axis by strong spin-orbit coupling, because the Zeeman energy is then pair-breaking for $\boldsymbol{H} \parallel \boldsymbol{c}$, but not for $\boldsymbol{H} \perp \boldsymbol{c}$. Along this line, Sauls' group proposed the phenomenological E_{2u} model with following characteristics [94, 95, 18, 96, 97];

1. The order parameter belongs to E_{2u} irreducible representation in D_{6h}. Thus, the gap functions are represented by a linear combination of two basis functions as $\Delta(\boldsymbol{k}) = \eta_1\Delta_1(\boldsymbol{k}) + \eta_2\Delta_2(\boldsymbol{k})$, where $\boldsymbol{\eta} = (\eta_1, \eta_2)$ is a complex two-component vector corresponding to a GL order parameter [1]. Here, they suppose

$$\Delta_1(\boldsymbol{k}) = (k_x^2 - k_y^2)k_z\boldsymbol{z}, \quad \Delta_2(\boldsymbol{k}) = 2k_xk_yk_z\boldsymbol{z}, \tag{2.1.1}$$

as the basis functions. Since $\boldsymbol{d}$-vectors are locked to the c-axis, this can reproduce the observed crossover behavior in the anisotropy ratio of H_{c2} [94].

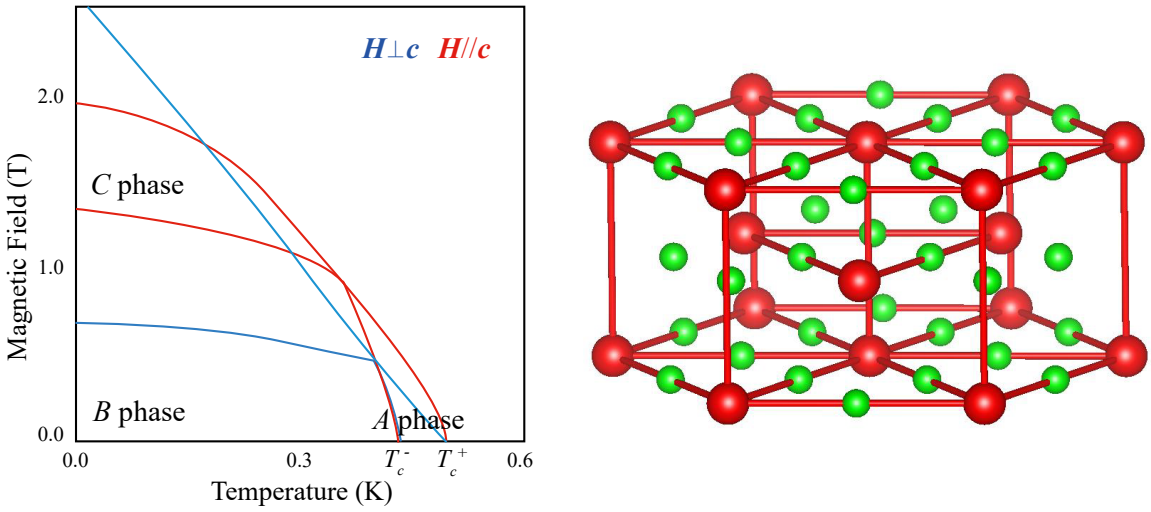

Figure 2.1: (Left) A schematic H-T phase diagram determined by the sound velocity measurement [85]. The phases separated by the red and blue lines correspond to those in $\boldsymbol{H} \parallel \boldsymbol{c}$ and $\boldsymbol{H} \perp \boldsymbol{c}$, respectively. (Right) Crystal structure of UPt_3. Red and green spheres indicate U and Pt atoms, respectively. The space group is non-symmorphic $P6_3/mmc$.

2. The two component order parameters, η_1 and η_2, are coupled with the tiny antiferromagnetic order observed in the neutron measurements [98, 99, 100]. As a result, the degeneracy of the transition temperatures is lifted and the double transition occurs. The three phases are specified by $\boldsymbol{\eta} = (\eta_1, 0)$ in A phase, (η_1, η_2) in B phase, and $(0, \eta_2)$ in C phase, respectively.

3. Since $\boldsymbol{d}$-vector is locked to the one direction, the time reversal symmetry breaking in B phase is promised within the GL theory [1, 96]. This is compatible with the observations in the μSR [101], the Josephson tunnel junctions [102], and the Kerr effect measurements [103].

4. One horizontal and two vertical line nodes are present in A and C phases while a point and a horizontal line nodes in B phase. Such hybrid structure between point and line nodes is well compatible with the nodal quasi-particle excitations observed in various quantities [104, 105, 106, 107].

Because of the above successes in the description of observations, the E_{2u} model has been believed to be the most promising scenario until recently. However, several contradicting observations, including the robust existence of the tetracritical point in the various field directions [85] and the absence of Knight shift in the NMR measurements [108], remain to be solved so far.

On the other hand, the recent measurement of field-angle resolved thermal conductivity has detected in-plane twofold oscillations in C phase [109]. This seems to be inconsistent with the E_{2u} model because fourfold oscillations are naively expected. Indeed, based on a group theoretical argument, it is believed that any gap function in the E_{2u} representations does not possess such an in-plane twofold symmetry, namely, a single vertical line node [1]. This is rather compatible with the E_{1u} model proposed by K. Machidia and the collaborators [110, 93, 83]. The key assumption of the E_{1u} model is that the spin-orbit coupling in the pairing channel is sufficiently weak compared to the energy scale of the magnetic field, and thus, the $\boldsymbol{d}$-vector can freely rotate to be in perpendicular to the field direction. The E_{1u} model also has the following properties.

1. The orbital (or momentum) part of the order parameter belongs to E_{1u} irreducible representation in $\mathrm{D_{6h}}$. Due to the approximate SU(2) symmetry in the spin space, gap functions are represented by a linear combination of six basis functions. The two orbital basis functions, $\lambda_1(\boldsymbol{k})$ and $\lambda_2(\boldsymbol{k})$, are supposed by

$$\lambda_1(\boldsymbol{k}) = k_a(5k_c^2 - 1), \quad \lambda_2(\boldsymbol{k}) = k_b(5k_c^2 - 1). \tag{2.1.2}$$

   By use of λ_1 and λ_2, for example in $\boldsymbol{H} \perp \boldsymbol{c}$, the order parameters of A, B, and C phases are identified with $\lambda_1\boldsymbol{b}$, $\lambda_1\boldsymbol{b} + \lambda_2\boldsymbol{c}$, and $\lambda_2\boldsymbol{c}$, respectively [109]. Note that the resulting gap functions do not belong to any irreducible representation in $\mathrm{D_{6h}}$ point group symmetry, and thus, often called a mixed representation theory.

2. While the assumption of the weak spin-orbit coupling is compatible with the Knight shift in the NMR[108], this is inconsistent with the paramagnetic suppression in $\boldsymbol{H} \parallel \boldsymbol{c}$. Similar difficulty appears also in the superconductivity of $\mathrm{Sr_2RuO_4}$ [24].

3. In A (C) phase, there exists one vertical line node at $k_a = 0$ ($k_b = 0$), which is consistent with the twofold oscillations observed in the thermal transport measurements [109]. In addition, point ant line nodes are present in the B phase, which is also consistent with the various observations [104, 105, 106, 107].

4. The orthogonality of $\boldsymbol{d}$-vectors in A and C phases promises the existence of the tetracritical point independently of the magnetic field directions. This is well compatible with the observations than that of the E_{2u} model, because the tetracritical point is guaranteed only at the spherical Fermi surface limit in the latter case.

In addition, the E_{1u} model is also supported by the following recent observations. A small residual thermal conductivity [84] suggests the presence of point nodes with linear dispersion, which is compatible with the E_{1u} models because the E_{2u} model has the point nodes with quadratic dispersion. The Josephson effect [111] with s-wave superconductor is also

compatible with E_{1u} planar states due to the existence of in-plane $\boldsymbol{d}$-vector components. As a result, recently, the E_{1u} model has been revisited.

Note that the revisit of the E_{1u} model has been strongly promoted by the field-angle resolved thermal transport measurement. However, the complementary specific heat measurements have not detected any signature of in-plane symmetry breaking in all phases [112]. Although this seems to be contradict with the thermal conductivity, it is expected to be explained by considering the multiband nature of UPt_3. Namely, if the twofold vertical line nodes are located on the Fermi surface with a light band mass, then the twofold oscillations will be more remarkable in the thermal conductivity than the specific heat measurement. In order to clarify how reasonable such plausible story is, the microscopic analysis of superconductivity including the electronic structure in UPt_3 is worth consideration [113, 114, 115]. In this regard, recent progress on the first-principles theoretical approach allows us to investigate the gap structure microscopically even in the complicated band structure like the heavy fermion compounds [116, 81, 67].

In this study, we provide the first report on a microscopic theory of superconductivity in UPt_3 based on the first principles approach. Based on the first principles approach, we find that the promising gap structure is an unprecedented E_{2u} pairing state, which is supported by the $j = 5/2$ representation of Cooper pairs, instead of conventional pseudo-spin representations. Its nodal structure is completely different on each Fermi surface; the point nodes with linear dispersion in the large hole Fermi surface, and the twofold vertical line nodes in small electron Fermi surfaces. These features are not expected in the well-known phenomenological E_{2u} model. The low-energy nodal excitations are similar to those in the E_{1u} model rather than the previous E_{2u} model. The peculiar properties can give a comprehensive explanation for the above-mentioned experimental observations, including the seemingly inconsistent result between the thermal conductivity and specific-heat measurement.

2.2 Model Hamiltonian and Fermi surface

In studying the superconductivity of UPt_3, the itinerant 5f model is considered to be a good starting point, since the Fermi surface in the first-principles calculations has been partially supported by the de Haas van Alphen measurements [117, 118]. Following the previous studies [116, 67], we here figure out the magnetic fluctuations in UPt_3, based on the first-principles theoretical approach.

First of all, we perform the *ab initio* band structure calculation in the paramagnetic state of UPt_3 using the WIEN2K package [119], in which the relativistic full-potential (linearized) augmented planewave (FLAPW) + local orbitals method is implemented. The crystallographical parameters are the space group $P6_3/mmc$ which holds the in-plane six-fold rotational symmetry and the experimental lattice constants $a = 5.764$ Å, $c = 4.899$ Å[19]. Note that the so-called symmetry breaking term [120, 121] is not included in the present

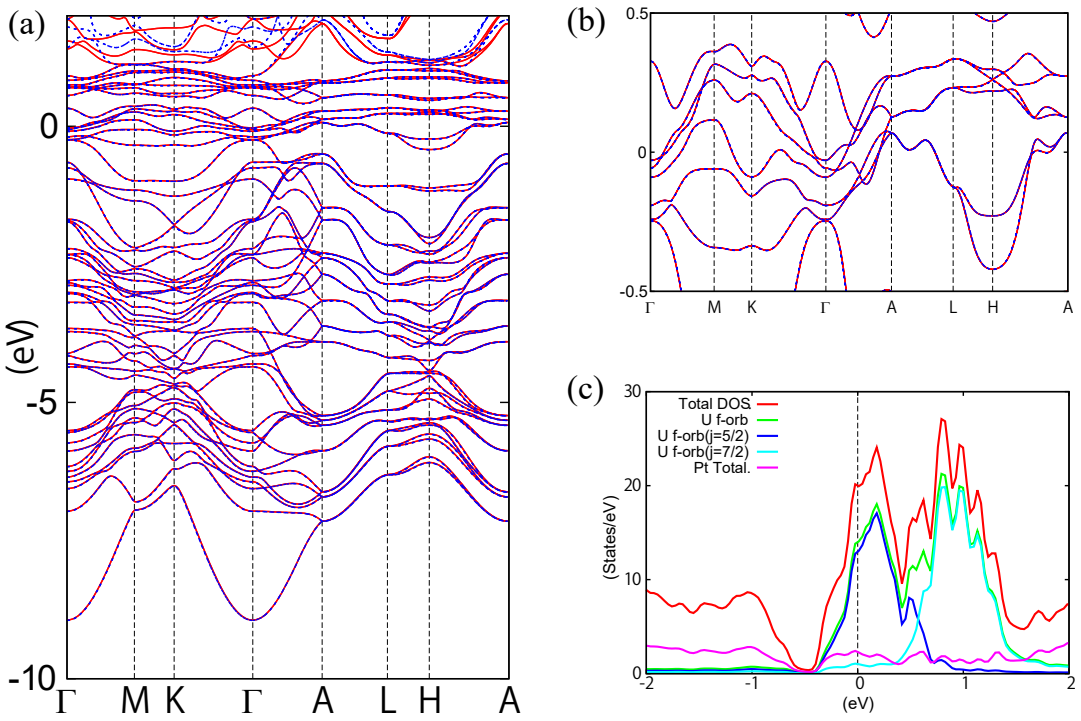

Figure 2.2: (a) Band structure along high-symmetry line and (b) enlarged one near the Fermi level. Red line is the result of *ab initio* calculation by WIEN2K. Blue dashed line is the Wannier fit. The dispersion below 1 eV is reproduced completely (c) The partial density of states near Fermi level.

calculations for simplicity. For the self-consistent calculations, we used PBE-GGA exchange-correlation potential [122], $12 \times 12 \times 12$ k-point grid in the Brillouin zone, and a cut-off parameter $RK_{max} = 13$. The spin-orbit interactions is included with the fully relativistic calculations. Using the self-consistent solutions, we then construct an effective tight-binding model in the Wannier bases using the `wien2wannier` interface [123] and the `wannier90` code [124, 125, 126]. The resulting model Hamiltonian is composed of 120 Wannier bases, containing U(5f), U(6d), Pt(5d), Pt(6s) orbitals and spin degrees of freedom. These bases are transformed into the bases of the total angular momentum j.

In Fig. 2.2, we illustrate the result of the band-structure calculations. Fig. 2.2(a) depicts the GGA band structure (red line) and its Wannier fit [127] (blue line). Fig. 2.2(b) is the enlarged figure near the Fermi level. We can see that the fitting works well. Fig. 2.2(c) shows the partial density of states (DOS). Blue, cyan, and magenta lines correspond to $j = 5/2$ and $7/2$ partial DOS of U(5f), and the total DOS of Pt atoms. We find that the states crossing the Fermi level are dominated by the U(5f) orbitals, especially, the $j = 5/2$ component. The

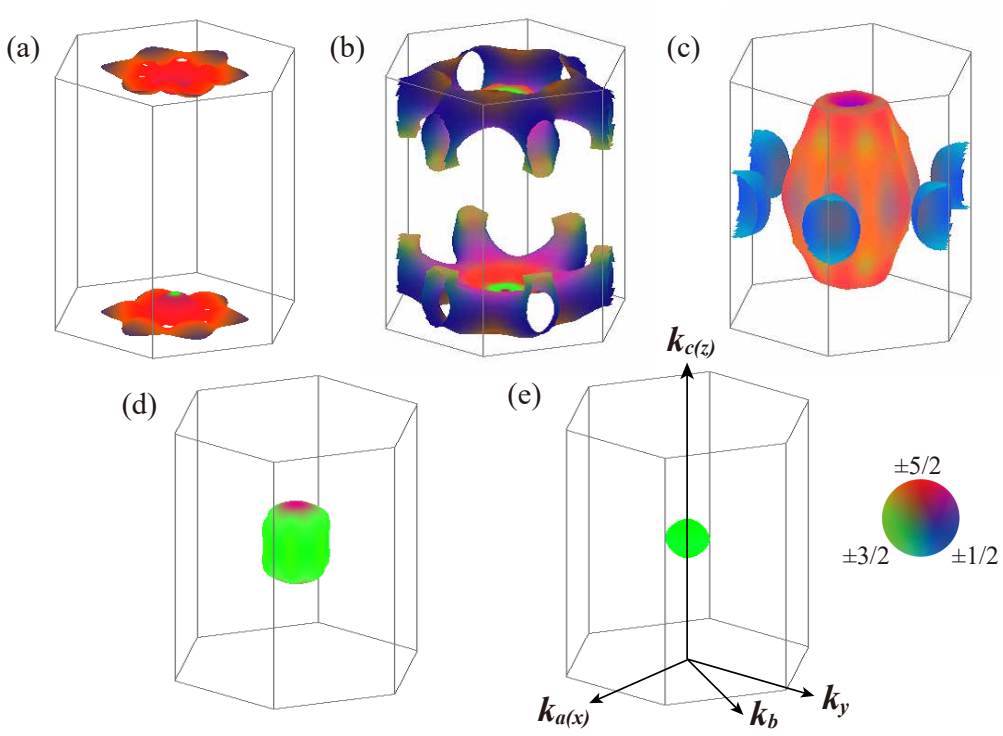

Figure 2.3: Orbital-resolved Fermi surfaces in our tight-binding model H_0, obtained by the first-principles calculations. The colors correspond to the weight of j_z component in the total angular momentum $j = 5/2$ space. In the text, (a)-(e) are referred to as band1-5, respectively.

$j = 7/2$ states are located around 1 eV higher due to the moderate spin-orbit coupling in U atoms. Therefore, we can expect that the low-energy excitations in this system are dominated by the $j = 5/2$ components. Thus, hereafter, we focus on the $j = 5/2$ electrons, and regards the other electrons as the conduction electrons. The resulting tight-binding Hamiltonian is formally expressed as

$$\begin{aligned} H_0 = &\sum_{\boldsymbol{k}} \sum_{12}^{f} \varepsilon^f_{12}(\boldsymbol{k}) f^\dagger_1(\boldsymbol{k}) f_2(\boldsymbol{k}) + \sum_{\boldsymbol{k}} \sum_{12}^{c} \varepsilon^c_{12}(\boldsymbol{k}) c^\dagger_1(\boldsymbol{k}) c_2(\boldsymbol{k}) \\ &+ \sum_{\boldsymbol{k}} \sum_{1}^{f} \sum_{2}^{c} \left(v_{12}(\boldsymbol{k}) f^\dagger_1(\boldsymbol{k}) c_2(\boldsymbol{k}) + v^*_{12} c^\dagger_2(\boldsymbol{k}) f_1(\boldsymbol{k}) \right), \end{aligned} \tag{2.2.1}$$

where $f^\dagger(\boldsymbol{k})(f(\boldsymbol{k}))$ and $c^\dagger(\boldsymbol{k})(c(\boldsymbol{k}))$ correspond to the creation (annihilation) operators of U(5f) electrons with $j = 5/2$ and the other electrons, which are denoted by f and c respectively in the following. Here, $\hat{\varepsilon}^f(\boldsymbol{k})$ is the dispersion relation of f electrons measured from the chemical potential μ and $\hat{\varepsilon}^c(\boldsymbol{k})$ is of c electrons. $\hat{v}(\boldsymbol{k})$ is a hybridization matrix between these states. The subscripts (1 and 2) symbolically represent both orbitals (in J-basis) and

atomic sites (sublattice) degrees of freedom. Taking into consideration the correlation effects, we need to add a Hubbard type interaction $H_{\rm int}$ to f electrons, which is given in the next Section, and then obtain a 120-orbital periodic Anderson Hamiltonian describing the electronic state of UPt_3.

The Fermi surface in our model Hamiltonian is illustrated in Fig. 2.3. Colors on the Fermi surface, red, green, and blue, correspond to each weight of $j_z = \pm 5/2$, $\pm 3/2$ and $\pm 1/2$ components, respectively. The obtained Fermi surface topology is well consistent with the previous studies [19, 128, 129]. The Fermi surfaces of Figs. 2.3(b) and (c) have a large contribution to the density of states at the Fermi level. Here, we realize that each Fermi surface possesses relatively separated orbital components, especially, the small Fermi surfaces in Figs. 2.3(d) and (e) roughly involve only $j_z = \pm 3/2$ component. This characteristic feature is the key to the emergence of the unprecedented E_{2u} gap structure as discuss later.

2.3 Magnetic susceptibility

Next we study the magnetic fluctuations in the model Hamiltonian, including the on-site Hubbard type repulsions, U, U', J, and J' between U(5f) electrons, where U is the intra-orbital Coulomb repulsion, U' the inter-orbital one, J the Hund's coupling, and J' the pair hopping interaction. The interactions between $j = 5/2$ electrons can be obtained by transformed the following LS-basis form into the representation of the $j = 5/2$ space,

$$H_{\rm int} = \frac{1}{4} \sum_{\boldsymbol{R}\alpha} \sum_{\zeta_1\zeta_2\zeta_3\zeta_4}^{f} \Gamma^{(0)}_{\zeta_1\zeta_4,\zeta_3\zeta_2} f^{\dagger}_{\alpha\zeta_1}(\boldsymbol{R}) f^{\dagger}_{\alpha\zeta_2}(\boldsymbol{R}) f_{\alpha\zeta_3}(\boldsymbol{R}) f_{\alpha\zeta_4}(\boldsymbol{R}), \tag{2.3.1}$$

where ζ_i denote both the orbital (angular) and spin quantum numbers. $\boldsymbol{R}$ denotes a lattice vector and $\alpha =$ U1 or U2 is a label of two U atoms in a unit cell. $\hat{\Gamma}^{(0)}$ is the Hubbard-type interaction, given by $\Gamma^{(0)}_{\zeta_1\zeta_4,\zeta_3\zeta_2} = -\frac{1}{2} S^{(0)}_{l_1 l_4, l_3 l_2} \boldsymbol{\sigma}_{\sigma_1\sigma_4} \cdot \boldsymbol{\sigma}_{\sigma_2\sigma_3} + \frac{1}{2} C^{(0)}_{l_1 l_4, l_3 l_2} \delta_{\sigma_1\sigma_4} \delta_{\sigma_2\sigma_3}$, where l_i and σ_i ($i = 1 \sim 4$) denote the orbital and spin quantum number respectively. The explicit forms of $\hat{S}^{(0)}$ and $\hat{C}^{(0)}$ are given by,

$$\hat{S}^{(0)} = \begin{cases} U \\ U' \\ J \\ J' \end{cases}, \qquad \hat{C}^{(0)} = \begin{cases} U & (l_1 = l_2 = l_3 = l_4) \\ 2J - U' & (l_1 = l_3 \neq l_2 = l_4) \\ 2U' - J & (l_1 = l_4 \neq l_2 = l_3) \\ J' & (l_1 = l_2 \neq l_3 = l_4) \end{cases} \tag{2.3.2}$$

In the actual calculations, we transform this representation of Eq.(2.3.1) into that of J-basis, and then neglect the interactions with $j = 7/2$ space, since we focus on the low-energy excitations of the $j = 5/2$ electrons as mentioned above. As demonstrated in Ref. [116], momentum dependence of susceptibilities, which is important in unconventional superconductivity, is well described within this approximation.

By use of resulting on-site interactions acting among $j = 5/2$ electrons, magnetic susceptibilities within the random phase approximation (RPA) can be obtained by the following way [116, 81]. First, the non-interacting Green's functions $\hat{G}(\boldsymbol{k}, i\omega_n)$, which are expressed as a 12×12 matrix in the $j = 5/2$ space of two U atoms in the unit cell, are given by

$$G_{12}(\boldsymbol{k}, i\omega_n) = -\int_0^\beta d\tau e^{i\omega_n \tau} \langle T_\tau (f_1(\boldsymbol{k}, \tau) f_2^\dagger(\boldsymbol{k}, 0)) \rangle , \tag{2.3.3}$$

$$= \sum_m \frac{u_{1m}(\boldsymbol{k}) u_{m2}^\dagger(\boldsymbol{k})}{i\omega_n - E_{mm}(\boldsymbol{k})}, \tag{2.3.4}$$

where $\hat{u}(\boldsymbol{k})$ and $\hat{E}(\boldsymbol{k})$ are the unitary matrix diagonalizing H_0 and the energy eigenvalues matrix, respectively. Here, $\langle \cdot \rangle$ denote a thermal average and T_τ is a time ordering operator with respect to a imaginary time τ. $\omega_n = \pi T(2n + 1)$ is a fermionic Matsubara frequency. The index m runs over all 120 degrees of freedom. Then, the irreducible susceptibilities $\hat{\chi}^{(0)}_{14,32}(\boldsymbol{q}, i\omega_q)$ are defined by

$$\chi^{(0)}_{14,32}(\boldsymbol{q}, i\omega_q) = -\frac{T}{N} \sum_{\boldsymbol{k},n} G_{13}(\boldsymbol{k} + \boldsymbol{q}, i\omega_n + i\omega_q) G_{24}(\boldsymbol{k}, i\omega_n). \tag{2.3.5}$$

By use of $\hat{\chi}^{(0)}(\boldsymbol{q}, i\omega_q)$, the RPA susceptibility $\hat{\chi}^{\mathrm{RPA}}(\boldsymbol{q}, i\omega_q)$ in the matrix form can be obtained as follows,

$$\hat{\chi}^{\mathrm{RPA}}(\boldsymbol{q}, i\omega_q) = (\hat{1} - \hat{\tilde{\Gamma}}^{(0)} \hat{\chi}^{(0)}(\boldsymbol{q}, i\omega_q))^{-1} \hat{\chi}^{(0)}(\boldsymbol{q}, i\omega_q). \tag{2.3.6}$$

Note that $\hat{\tilde{\Gamma}}^{(0)}$ is a 144×144 matrix describing a Hubbard type interaction restricted to the $j = 5/2$ electrons of two U atoms. In general, the magnetic (dipole) correlation functions, $\chi_{ab}(\boldsymbol{q})$, with $\hat{\chi}(q) = \hat{\chi}^{(0)}(q)$ or $\hat{\chi}^{\mathrm{RPA}}(q)$ are given by

$$\chi_{ab}(\boldsymbol{q}) = \sum_{\alpha\alpha'} e^{-i\boldsymbol{q}\cdot(\boldsymbol{x}_\alpha - \boldsymbol{x}_{\alpha'})} \int_0^\beta d\tau \langle T_\tau (J_a^\alpha(\boldsymbol{q}, \tau) J_b^{\alpha'\dagger}(\boldsymbol{q}, 0)) \rangle \tag{2.3.7}$$

$$\approx \sum_{1234} e^{-i\boldsymbol{q}\cdot(\boldsymbol{x}_{\alpha_1} - \boldsymbol{x}_{\alpha_3})} (\tilde{J}_a)_{12} \chi_{21,34}(\boldsymbol{q}, 0) (\tilde{J}_b)_{34}. \tag{2.3.8}$$

Here, we have used the definition of the dipole operator $J_a^\alpha(\boldsymbol{q}, \tau)$,

$$J_a^\alpha(\boldsymbol{q}, \tau) = \sum_{\boldsymbol{k}} \sum_{j_z j_z'} (J_a)_{j_z j_z'} f_{\alpha j_z}^\dagger(\boldsymbol{k}, \tau) f_{\alpha j_z'}(\boldsymbol{k} + \boldsymbol{q}, \tau), \tag{2.3.9}$$

where the matrix elements of $\hat{J}_a$ for $j = 5/2$ subspace can be obtained by the operator equivalent method as usual. $\hat{\tilde{J}}_a$ is the corresponding 12×12 matrix. $\boldsymbol{x}_\alpha$ is a position of atom α relative to the lattice vectors and $a, b = x, y$, or z. In the case of UPt_3, $\boldsymbol{x}_{\mathrm{U1}} = (\frac{1}{3}, \frac{2}{3}, \frac{1}{4})$ and $\boldsymbol{x}_{\mathrm{U2}} = (\frac{2}{3}, \frac{1}{3}, \frac{3}{4})$ in a unit of primitive lattice vector. Note that the phase factor in

Eq. (2.3.8) comes from the current definition of the Fourier transformation, given by (see also Appendix A.2.3),

$$f^{\dagger}_{\alpha j_z}(\boldsymbol{k}) = \frac{1}{\sqrt{N}} \sum_{\boldsymbol{R}} e^{i\boldsymbol{k}\cdot\boldsymbol{R}} f^{\dagger}_{\alpha j_z}(\boldsymbol{R}). \tag{2.3.10}$$

Such a sublattice independent definition is suitable for the calculation using the fast Fourier transformations. The magnetic fluctuation parallel (perpendicular) to the c-axis $\chi_{\parallel}(\boldsymbol{q})$ ($\chi_{\perp}(\boldsymbol{q})$) is defined by $\chi_{\parallel}(\boldsymbol{q}) = \chi_{zz}(\boldsymbol{q})$ ($\chi_{\perp}(\boldsymbol{q}) = (\chi_{xx}(\boldsymbol{q}) + \chi_{yy}(\boldsymbol{q}))/2$), given that a total magnetic moment $\hat{M}_a = \hat{L}_a + 2\hat{S}_a \simeq g\hat{J}_a$ with the Lande g-factor $g = 6/7$. From Eq.(2.3.8), the periodicity of $\chi_{ab}(\boldsymbol{q})$ in UPt_3 is $(3, 3, 2)$ in the unit of reciprocal lattice vector.

Fig. 2.4 depicts the wave-vector dependence of the magnetic fluctuations calculated with the bear susceptibility $\hat{\chi}^{(0)}(\boldsymbol{q}, i\omega_q)$. We find that the most dominant fluctuations are located at $\boldsymbol{Q} = (0, 0, 1)$ and $(1, 0, 0)$. The $\boldsymbol{Q}$ vector corresponds to the antiparallel alignment of the magnetic moment of two U atoms in the unit cell. This is well consistent with the observed dispersive magnetic excitations by inelastic neutron scattering measurements [130, 131]. On the other hand, the presence of the sub-dominant peaks at $\boldsymbol{Q} = (0, 0, 1/2)$ and $(1, 0, 1/2)$ may correspond to the fragile magnetic phase transition at $T_N \simeq 5$ K [[99, 98, 100]]. Indeed, this sub-dominant fluctuation is much enhanced within RPA. However, it needs further investigations along with a problem of magnetic anisotropy. Similarly to the previous study [81], the magnetic anisotropy of the uniform susceptibility is not so large, and slightly Ising-type, $\chi_{\parallel}(0) \geq \chi_{\perp}(0)$. Although this is the opposite to the experimental observation, we need to consider the large contribution from the localized f-electron part due to the strong electron correlations in the heavy fermion systems. This is a challenging issue in the future.

2.4 Superconductivity

Now, let us proceed to a study of the superconducting gap structure. Note that, for sufficiently large interaction parameters, magnetic fluctuations at $\boldsymbol{Q} = (0, 0, 1/2)$ and $(1, 0, 1/2)$ are enhanced, and those at $\boldsymbol{Q} = (0, 0, 1)$ and $(1, 0, 0)$ are concealed. On the other hand, the superconducting gap structure is not drastically changed for interaction parameters, irrespective of whether the pairing interaction $\hat{V}(\boldsymbol{q}, i\omega_q)$ is given by the second-order perturbation or RPA. Based on these results, we restricted ourselves to the weak-coupling approach for simplicity. The second-order perturbation for the renormalized interactions is valid as asymptotically exact weak-coupling limit. Here, we focus on probable spin-triplet states emerging in this limit.

By use of the effective pairing interaction $\hat{V}(\boldsymbol{q}, i\omega_q)$, possible candidates can be obtained by calculating the linearized gap equation at around T_c.

$$\lambda\Delta_{12}(k) = \sum_{k'} \sum_{343'4'} V_{13,42}(k - k') G_{33'}(k') G_{44'}(-k') \Delta_{3'4'}(k'), \tag{2.4.1}$$

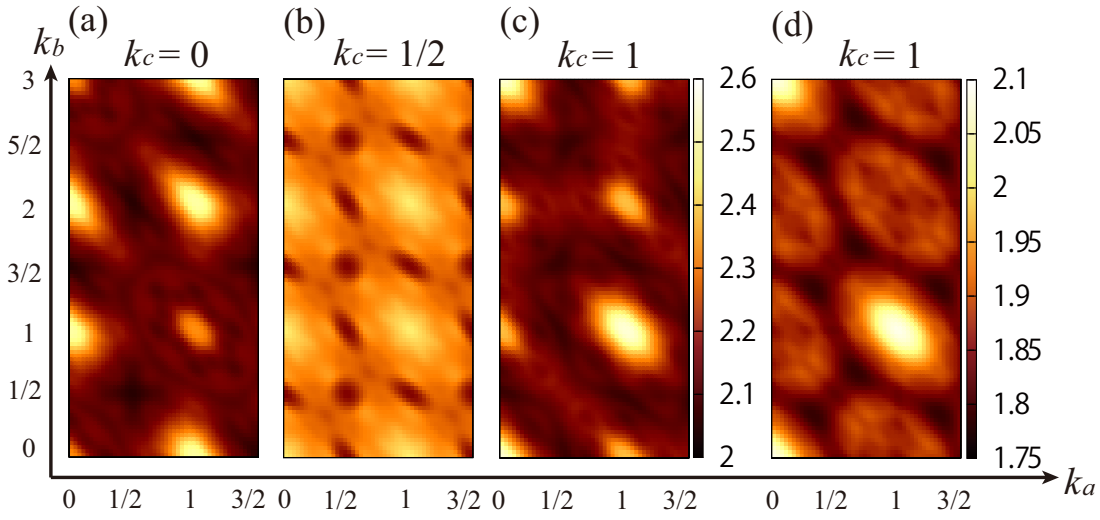

Figure 2.4: Magnetic structure of the bare susceptibilities. (a)-(c) show the magnetic susceptibilities parallel to c-axis, $\chi_{\parallel}(k_a, k_b, k_c)$, in $k_c = 0,\ 1/2$, and 1 plane. (d) shows the magnetic susceptibility perpendicular to c-axis, $\chi_{\perp}(k_a, k_b, k_c)$, in $k_c = 1$ plane. Difference between (c) and (d) corresponds to the magnetic anisotropy. Note that in actual, the angle between k_a and k_b axes is $\pi/3$.

where $\hat{\Delta}(k)$ is the J-basis gap functions. Here, k, k' denote both the momentum $\boldsymbol{k}$ and the Matsubara frequency $i\omega_n$. The maximum eigenvalue λ equals to 1 at T_c. Solving the self-consistent gap equations, we obtain two type of predominant spin-triplet pairing states with two dimensional representation E_{1u} and E_{2u}, as shown in Fig. 2.5. This means that the present microscopic theory supports the phenomenological candidates. In our calculations, the E_{2u} state is more dominant than the E_{1u} state over a wide parameter range. From these results, we conclude that the most promising candidate for the pairing state of UPt_3 is the E_{2u} odd-parity state.

Next, let us elucidate the detailed microscopic structure of these pairing states. In Fig. 2.6, we show the superconducting gap amplitude on each Fermi surface of band1, 3 and 4. Deep blue corresponds to the gap nodes and/or minima. Slight fluctuation of colors is attributed to the exemplification of the Blount's theorem [60] and some numerical errors. Strictly speaking, the Blount's theorem says that the symmetry protected line nodes cannot exist in odd-parity representation except for a rare case as discussed later. Therefore, when we do not single out a specific basis function as in the present calculations, the line nodes appear just as a "pseudo" line nodes, where the gap amplitude is not exact zero. Hereafter, we call the "pseudo" line nodes by the line nodes.

It is instructive to start with the E_{1u} state. In such two-dimensional representation, there

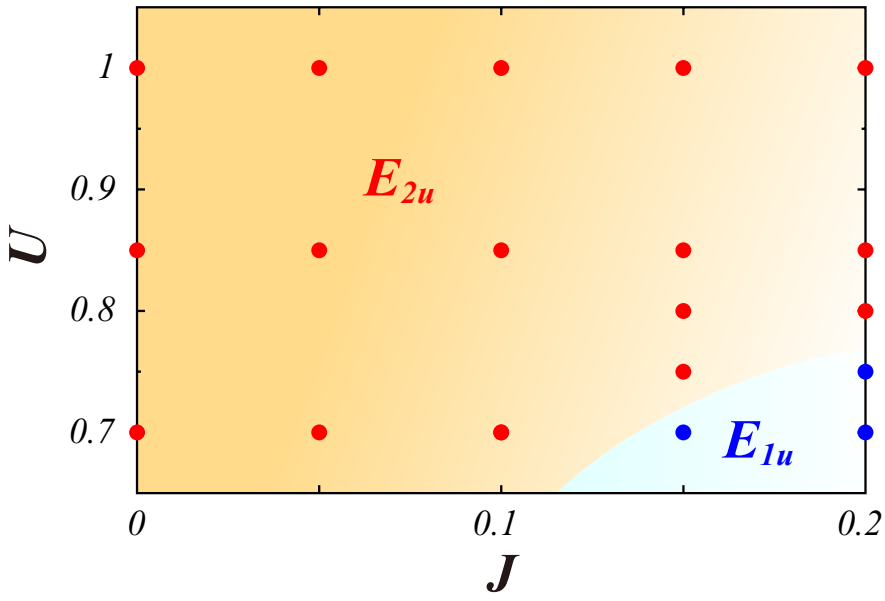

Figure 2.5: Superconducting phase diagram for the intra-orbital on-site repulsion U and Hund's coupling J. The unit of energy is eV. Here we set the inter-orbital interaction $U' = U$ and the pair hopping $J' = J$. E_{2u} state is predominant over the wide range. Even if assuming SU(2) condition, $U = U' + 2J$, the tendency is almost unchanged.

are two kinds of basis functions. Illustrated in Figs. 2.6(a)-(c) is one possible gap structure in the E_{1u} state. Another one is not shown here. Roughly speaking, the nodal structure on the Fermi surface at around the Γ point in Fig. 2.6(b) is the f-wave pairing state having one vertical line nodes and two horizontal line nodes at $k_z \neq 0$ plane. This nodal structure is identical to the E_{1u} model, which has been proposed based on the observations in the field-angle resolved thermal conductivity. Since the relevant Fermi surface has a large DOS, the in-plane twofold oscillation should be detected also in any experimental observations. However, this is incompatible with the observation in the field-angle resolved specific heat measurement [112].

Furthermore, let us consider the gap structure in the E_{2u} state in Figs. 2.6(d)-(f). Surprisingly, we find that the nodal feature is completely different on each Fermi surface; a horizontal nodes in Fig. 2.6(d), point nodes at the top of Fermi surface in Fig. 2.6(e), and in-plane twofold vertical line nodes in Fig. 2.6(f). Note that the point nodes at $k_x = k_y = 0$ are observed in all bands, but remarkable in band3. These nodal structures are completely different from those of the previous phenomenological E_{2u} models despite the same irreducible representation.

Generally, the superconducting order parameter is classified by the irreducible representations of the symmetry in the space group, since the linearized gap equation is separable

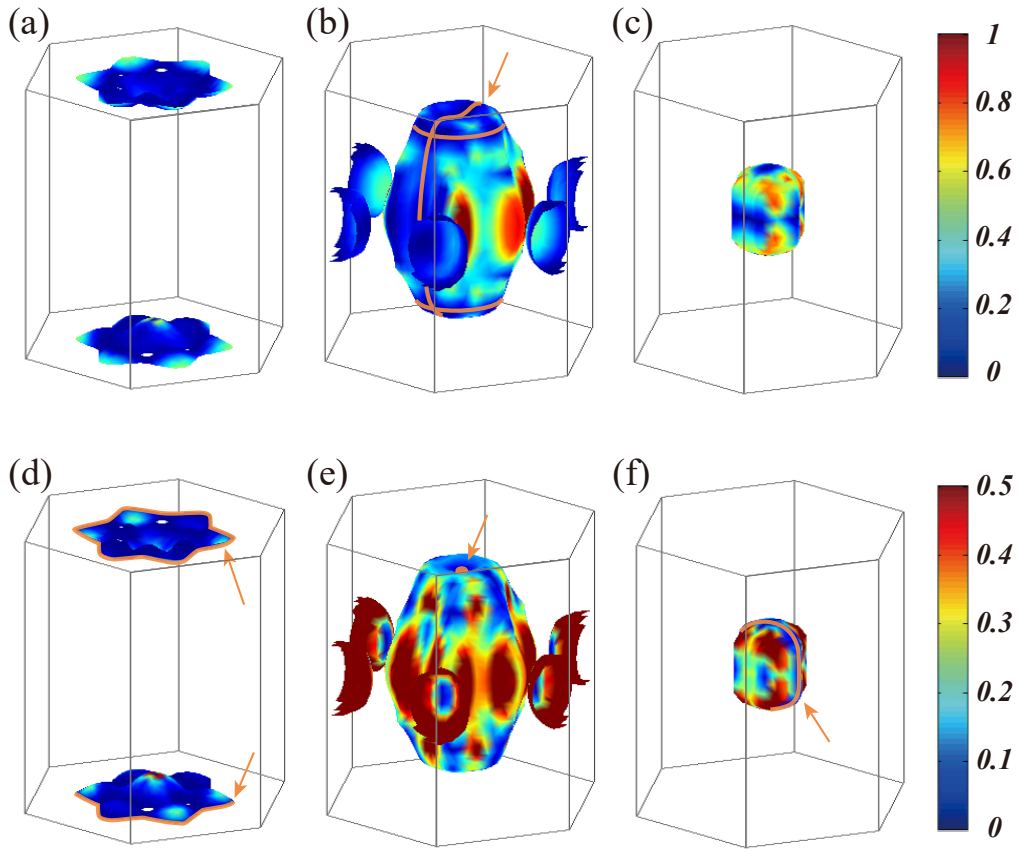

Figure 2.6: Superconducting gap amplitude, $\sum_{n'=\pm n} |\bar{\Delta}_{nn'}(\boldsymbol{k})|^2$, on the Fermi surfaces of band1, band3 and band4, where $\bar{\Delta}_{nn'}(\boldsymbol{k}) = \sum_{12} u^*_{1n}(\boldsymbol{k})\Delta_{12}u^*_{2n'}(-\boldsymbol{k})$ with the unitary matrix $u_{1n}(\boldsymbol{k})$ diagonalizing H_0. $n' = \pm n$ means a sum of the Kramers degeneracy for band$n$. (a)-(c) correspond to the E_{1u} state, and (d)-(f) the E_{2u} state. Line/point nodes colored by orange are pointed by arrows. We recognize that the nodal structure is completely different for each Fermi surface.

for each representation, by virtue of the identity property of the pairing interactions (see the discussion in Sec. 3.2). For the strong spin-orbit coupling, symmetry operations act on all the spin, orbital and wave-vector degrees of freedom in our case. If we as usual consider a spin one-half Fermion system without any other internal degrees of freedom, then following Refs. [19] and [1], we can see that the only a possible type of p-wave gap function in E_{2u} representation is $(\hat{d}_x k_x - \hat{d}_y k_y,\ -\hat{d}_x k_y - \hat{d}_y k_x)$ in the $\boldsymbol{d}$-vector notation. This minimal gap function has only a point node at the top of Fermi surface. Even if considering its higher-harmonics, there does not appear any twofold vertical line nodes. Therefore, it has been widely believed that in D_{6h} point group, twofold vertical line nodes are allowed only in E_{1u} representation, and generally forbidden in E_{2u} representation according to the group theoret-

ical argument [1]. In this regard, our E_{2u} gap structure seems to be very curious. However, in our case, we need to consider the Cooper pairs in the effective $j = 5/2$ space, instead of conventional pseudo-spin 1/2. Such extension can be performed with the help of projection operator method as in the case of spin 1/2. Thereby, we find that for the minimal p-wave pairing, one of two bases in E_{2u} representation can be described as follows,

$\Delta_1(\boldsymbol{k}) =$

$$\begin{array}{c} \begin{array}{cccccc} j_z = 5/2 & 3/2 & 1/2 & -1/2 & -3/2 & -5/2 \end{array} \\ \begin{pmatrix} c_1(k_x - ik_y) & c_2k_z & c_3k_x + c_4ik_y & c_5k_z & c_6(k_x + ik_y) & 0 \\ c_2k_z & c_7k_x + c_8ik_y & c_9k_z & c_{10}(k_x + ik_y) & 0 & c_6(-k_x + ik_y) \\ c_3k_x + c_4ik_y & c_9k_z & c_{11}(k_x + ik_y) & 0 & c_{10}(-k_x + ik_y) & c_5k_z \\ c_5k_z & c_{10}(k_x + ik_y) & 0 & c_{11}(-k_x + ik_y) & c_9k_z & -c_3k_x + c_4ik_y \\ c_6(k_x + ik_y) & 0 & c_{10}(-k_x + ik_y) & c_9k_z & -c_7k_x + c_8ik_y & c_2k_z \\ 0 & c_6(-k_x + ik_y) & c_5k_z & -c_3k_x + c_4ik_y & c_2k_z & c_1(-k_x - ik_y) \end{pmatrix} \end{array},$$

where c_i ($i = 1 \sim 11$) are material-dependent parameters. From the expressions of the second and fifth diagonal elements, we can verify that twofold vertical line nodes appear in the $j_z = \pm 3/2$ subspace. Similarly, we find that the gap functions in the $j_z = \pm 5/2$ or $\pm 1/2$ subspace yield only point nodes with the linear dispersion along c-axis, and the twofold vertical line nodes are forbidden. Anomalous twofold vertical line nodes in the E_{2u} representation emerge only in the $j_z = \pm 3/2$ space. For more complete discussions, see Sec. 3.1. In UPt_3, the Fermi surfaces in Figs. 2.2(d) and (f) involve plenty of $j_z = \pm 3/2$ component. Thus, it is natural that twofold vertical line nodes emerge in these Fermi surfaces even in E_{2u} gap symmetry. Moreover, it should be noted that these Fermi surfaces have a light band mass. In this case, it can be expected that the in-plane twofold oscillation in the field-angle resolved measurements is more prominent in the thermal conductivity than in the specific heat measurements. This can provide an explanation for the seemingly inconsistent observations between these measurements. In addition, since the Fermi surface around Γ in Fig. 2.2(c) is almost composed of $j_z = \pm 5/2$, we recognize that the point nodes observed in Fig. 2.6(e) have linear dispersion, which can be consistent with the small residual thermal conductivity [84].

In order to understand more about this unprecedented E_{2u} gap structure, let us dissect the superconducting gap structure in Fig. 2.6(f). Although the p-wave line nodes on the $k_x = 0$ plane are remarkable as mentioned above, we can realize additional gap minima on the $k_y = 0$ and $k_z = 0$ planes. This implies a mixing of f-wave component with the form of $k_xk_yk_z\hat{d}_z$, which is indeed allowed in the group theoretical arguments. Therefore, roughly speaking, the gap structure in Fig. 2.6(f) can be described as a linear combination between the p-wave $k_x\hat{d}_x$ and f-wave $k_xk_yk_z\hat{d}_z$ in the $\boldsymbol{d}$-vector representation in the $j_z = \pm 3/2$ space. Interestingly, in this case, under the applied field parallel to the c-axis, the Pauli-limiting behavior will be expected in the upper critical field. Although such suppression has been observed experimentally, we need further investigations, considering the magnetic anisotropy.

Here, we comment on the phase diagram expected within our calculations. Although it is very interesting to study the H-T phase diagram based on the gap structure we found, this is quite difficult in the present situation. Instead, we discuss the phase diagram with the help of the phenomenological E_{2u} theory [18]. In this case, we can identify the gap structure shown in Fig. 2.6 as that in A or C phase. Therefore, we can expect that the vertical line nodes appear in both A and C phases, although it may be difficult to observe the corresponding twofold oscillation in A phase. It should be noted that, in the present situation, gap functions below T_c cannot be obtained with high accuracy, since our model Hamiltonian includes numerical errors in the downfolding process. For this reason, we can discuss B phase only in the qualitative level. Following the E_{2u} theory in Ref. [18], we consider B phase as a time reversal symmetry breaking state, which are described by (η_1, η_2) with real η_1 and pure imaginary η_2 in the two-dimensional representation. In general, it will be a non-unitary state, and thus, it is unclear whether such a time reversal symmetry breaking state is really stabilized at low temperatures. In our case, for example in the $j_z = \pm 3/2$ Fermi surfaces, a (η_1, η_2) state with a pure p-wave (or f-wave) gap function is a unitary state without line nodes because there is only one $\boldsymbol{d}$-vector component. In this case, β_2 term in the GL functional (the definition is given in Ref. [1]) takes a positive value, and thus, the time reversal symmetry breaking state is favorable [18]. Therefore, also in our $p + f$-wave state, we may expect that the time reversal symmetry breaking state is stabilized, although it is a non-unitary state in this case. On the other hand, in $j_z = \pm 1/2$ or $\pm 5/2$ Fermi surfaces, pure p-wave states do not favor the time reversal symmetry breaking state, in contrast to the f-wave states. In the expected $p + f$-wave case, the time reversal symmetry breaking state with a number of Weyl point nodes may be realized, as recently proposed by Yanase [132]. However, in order to discuss its stability in our model Hamiltonian, we have to solve the gap equation with high accuracy, or calculate β_2 term in GL functional based on the microscopic electronic state and the gap structure. This is a challenging issue.

Finally, let us comment on the horizontal line nodes at $k_z = \pm\pi$ in Fig. 2.6(d). As mentioned above, in an ordinary case, there are only point nodes in E_{2u} representation. However, in the non-symmorphic system like UPt_3, there exists additional C_2 screw symmetry, which protects the horizontal line nodes. Such symmetry protected line nodes are known as exceptions to the Blount's theorem [3]. Note that as pointed out by Yanase [132], these horizontal line nodes appear only in the presence of spin-orbit coupling on the $k_z = \pm\pi$ plane. This is quite small in UPt_3, which can be seen as the small energy splitting between band1 and 2 on the $k_z = \pm\pi$ plane. Thus, the resulting gap structure has very sharp k_z dependence near the $k_z = \pm\pi$ plane as seen in Fig. 2.6(d). In addition, in the actual situation, the line nodes may be lifted, or slightly shifted from the plane, due to the presence of a weak symmetry-breaking term [100, 121]. This is also a challenge for the future.

2.5 Conclusion

Based on the advanced first-principles theoretical approach, we clarify the microscopic gap structure in the heavy fermion superconductor UPt_3. We find that the obtained antiferromagnetic fluctuations with $\boldsymbol{Q} = (0, 0, 1)$ and $(1, 0, 0)$, which are consistent with the neutron scattering measurements, lead to the spin-triplet pairing states with E_{1u} and E_{2u} representations in the D_{6h} space group. The obtained E_{1u} gap structure is consistent with the phenomenological f-wave pairing state. On the other hand, the latter E_{2u} state, having nodal structure different for each band, is distinct from the well-known E_{2u} models. In particular, the in-plane twofold vertical line nodes emerge on the small Fermi surface, which can consistently explain the field-angle resolved measurements in both the thermal conductivity and the specific heat. Such peculiar feature cannot be explained in the conventional pseudo-spin representation, but is described by the group theoretical representation of the Cooper pairs in the $j = 5/2$ space. Furthermore, the study of magnetic anisotropy and the mixture of p-wave and f-wave with different $\boldsymbol{d}$-vectors can provide a clue to understand the remaining problems of the Pauli limiting of the upper critical field [88, 94, 112] and the anomalous behavior of the Knight shift [108] and so on. These are interesting issues in future, together with the understanding of the multiple superconducting phases. Thus, our findings shed new light on the long-standing problems in the superconductivity of UPt_3.

Chapter 3

Classification of multipole superconductivity in multiorbital systems

As is demonstrated by the analysis on the superconductivity of UPt_3, the multiorbital nature of gap functions as well as the spin-orbit coupling can yield unusual nodal structure. In actual, most of superconductors possess the orbital degrees of freedom although this has been focused only in specific materials such as iron-based superconductors so far. Thus, motivated by a growing interest in multiorbital superconductors with spin-orbit interactions, we here perform the group theoretical classification of various superconducting gap functions. We focus on the pairing states with zero total momentum, and demonstrate the classification of unconventional superconductivity emerging in symmorphic O, D_4, and D_6 space groups. Complete sets of basis functions are summarized in several tables. Because of the spin-orbit coupling, multiorbital degrees of freedom appear as multipole characters. Similarly to $\boldsymbol{d}$-vector in spin-triplet states, they can be specified by multipole operators in the corresponding point groups. Thus, we here call the generalized pairing state "multipole" superconductivity. From its classification, we obtain the following key consequences.

1. A superconducting gap function with $\Gamma_9 \otimes \Gamma_9$ in D_6 possesses nontrivial momentum dependence different from that in the usual spin 1/2 classification. This is related to twofold symmetric line-nodes found in the microscopic study of UPt_3 [2].

2. Unconventional gap structure can be realized in the BCS approximation with purely local (on-site) interactions irrespective of attractive or repulsive. It implies the emergence of an electron-phonon driven unconventional superconductivity. Although the conventional electron-phonon interactions favor s-wave (A_{1g}) pairing states, the Hund's coupling and the electron-phonon interactions in magnetically ordered states can enhance such anisotropic pairing states.

3. In anisotropic s-wave (A_{1g}) states composed of the pairing of orbitals with different symmetries, there appear not symmetry protected but inevitable line nodes/gap minima. For examples, a B_{2g} pairing state of degenerate p_x and p_y orbitals in tetragonal crystals is an s-wave with line nodes along k_x/k_y axis in band based representation. A possibility of such anisotropic s-wave pairing via inter-orbital pairing can provide an interpretation for the emergence of accidental nodes/gap minima as observed in several superconductors. It is in sharp contrast to an anisotropic s-wave driven by two kinds of competing interactions, such as electron-phonon interactions and spin fluctuations, which was discussed for the appearance of point nodes in (Y,Lu)Ni_2B_2C [133].

This chapter is organized as follows. In Sec. 3.1, we will discuss the classification of superconducting order parameters in multiorbital systems in terms of the local orbital bases that transform as irreducible representations of the point group in the system. Complete tables of the Cooper pair basis functions for representative point group symmetries O, D_4, and D_6 will be demonstrated. The classification scheme used here is justified in Sec. 3.2. In Sec. 3.3, we will show the relations between the band based representation and the orbital one, and clarify how the band based Cooper pairs are related to the orbital based ones. In Sec. 3.4, we will discuss two models for the cubic O_h and tetragonal D_{4h} point groups as the applications of the present group theoretical theory. In the former case, we will discuss what kinds of anisotropic pairing states can emerge near quadrupole ordered phases. In the latter, we will point out the possibility of anisotropic pairs mediated by local fluctuations. Finally, in Sec. 3.5, we will summarize the present study.

3.1 Classification of superconducting order parameters

In this section, we explain how to classify superconducting order parameters in multiorbital systems. Our main interest is to extend the classification of unconventional superconductivity [15, 16, 17, 1] into generic multiorbital systems. Generally, the conventional BCS superconducting state is characterized by the presence of Cooper pairs with zero total momentum and the breaking of U(1) gauge symmetry. Unconventional superconductivity additionally breaks other symmetries, for example, point group symmetry of a given system.

Here, we consider the classification of the BCS superconductivity with zero total momentum in symmorphic-lattice systems with spacial inversion and time reversal symmetries. In this case, one-particle states possess the Kramers degeneracy, which can be labeled by a *pseudo*-spin 1/2 at each $\boldsymbol{k}$ point. Note that superconducting order parameters, i.e., the Cooper pair wave functions can be classified by irreducible representations of a point group symmetry P, regardless whether the systems belong to symmorphic or non-symmorphic space groups. That a consequence of the Landau theory of second order phase transition and can be directly confirmed by explicit mean field calculations. However, the classification given

below is not applicable to non-symmorphic systems because the sublattice degrees of freedom cannot be deduced into the local ones. In this section, we simply illustrate the classification under the above assumptions, and the detailed discussions will be provided in Sec. 3.2.

In the previous studies [15, 16, 17, 1], it was implicitly supposed that the transformation property of the *pseudo*-spin 1/2 equals to that of *pure*-spin 1/2. Although such convention in band based representation is always applicable in systems we consider, the knowledge of orbital character of band electrons contains interesting and rich physics, as the multipole degrees of freedom do. Thus, it will be useful to describe the pairing states not in the band but in the local orbital bases. In this study, we will explicitly write down the transformation property of the Kramers degeneracy in the orbital based representation. Since the classification of superconducting order parameters is very similar to that of localized multipole moment [134], we call the classified multiorbital superconductivity "multipole" superconductivity. In what follows, we will show several definitions and transformation rules, and then, summarize the consequences in several tables. Throughout this section, we will discuss pair amplitudes rather than the gap functions since the gap functions are readily calculated from the pair amplitudes and the symmetry properties are identical as seen in Sec. 3.2.

3.1.1 Pair amplitude

First of all, let us introduce an electron creation operator $c^\dagger_{\ell\alpha}(\boldsymbol{r})$ with the orbital ℓ and the spin α at the site $\boldsymbol{r}$. From a viewpoint of the classification, it is convenient to consider that ℓ indicates a basis function labeled by an irreducible representation of a given point group P, and α denotes the Kramers degrees of freedom rather than *pure*-spin 1/2. For the case containing two or more atoms in a unit cell, see Sec. 3.2.2. One-particle part of Hamiltonian is diagonalized by a unitary matrix $u_{\ell\alpha,n\sigma}(\boldsymbol{k})$ with the band n, the *pseudo*-spin σ and the wavenumber $\boldsymbol{k}$. A band based creation operator $\tilde{c}^\dagger_{n\sigma}(\boldsymbol{k})$ is given by

$$\tilde{c}^\dagger_{n\sigma}(\boldsymbol{k}) = \frac{1}{\sqrt{N}}\sum_{\boldsymbol{R}} e^{i\boldsymbol{k}\cdot\boldsymbol{R}} \sum_{\ell\alpha} c^\dagger_{\ell\alpha}(\boldsymbol{R}) u_{\ell\alpha,n\sigma}(\boldsymbol{k}), \tag{3.1.1a}$$

$$\equiv \sum_{\ell\alpha} c^\dagger_{\ell\alpha}(\boldsymbol{k}) u_{\ell\alpha,n\sigma}(\boldsymbol{k}), \tag{3.1.1b}$$

where N is the number of unit cells. The corresponding annihilation operator is obtained by the Hermite conjugate of Eq. (3.1.1).

In the orbital bases, a pair amplitude is defined as

$$F_{\ell\alpha,\ell'\alpha'}(\boldsymbol{k}) \equiv \langle c_{\ell\alpha}(\boldsymbol{k}) c_{\ell'\alpha'}(-\boldsymbol{k})\rangle, \tag{3.1.2}$$

where $\langle\cdot\rangle$ denotes the thermal average, and the fermion antisymmetry requires

$$F_{\ell\alpha,\ell'\alpha'}(\boldsymbol{k}) = -F_{\ell'\alpha',\ell\alpha}(-\boldsymbol{k}). \tag{3.1.3}$$

Hereafter, we will discuss the classification of $F_{\ell\alpha,\ell'\alpha'}(\boldsymbol{k})$.

3.1.2 List of irreducible representations for the Kramers sector

We perform the classification of the pair amplitude $F_{\ell\alpha,\ell'\alpha'}(\boldsymbol{k})$ in typical point groups O, D_4, and D_6. The classification consists of that in the orbital sectors $\ell\ell'$, the Kramers sector $\alpha\alpha'$, and the wavenumber $\boldsymbol{k}$. Once the orbital sectors are *fixed*, we can decompose F as,

$$F_{\ell\alpha,\ell'\alpha'}(\boldsymbol{k}) = \Big[\Big(\Phi_{\ell\ell'}(\boldsymbol{k})\sigma^0 + \boldsymbol{d}_{\ell\ell'}(\boldsymbol{k})\cdot\boldsymbol{\sigma}\Big)i\sigma^y\Big]_{\alpha\alpha'}, \tag{3.1.4}$$

where σ^0 is a 2×2 identity matrix, and $\boldsymbol{\sigma} = (\sigma^x, \sigma^y, \sigma^z)$ are the Pauli matrices in the Kramers sector. The explicit form of the Kramers pairs ($\alpha = \pm$) in each point group P is listed in Appendix A.2.2. From the transformation property under the point group operations, we classify the Kramers part,

$$\bar{\sigma}^\mu \equiv \sigma^\mu i\sigma^y, \ (\mu = 0, x, y, \text{and } z) \tag{3.1.5}$$

into the corresponding irreducible representations. The results are summarized in Tables 3.1-3.3. It should be noted that the generalized $\boldsymbol{d}$-vector, $\boldsymbol{d}_{\ell\ell'}(\boldsymbol{k})$, is no longer a net spin moment of Cooper pairs, although we conventionally use the unit vectors $\boldsymbol{x}$, $\boldsymbol{y}$, and $\boldsymbol{z}$.

Finally, the classification of $F_{\ell\alpha,\ell'\alpha'}(\boldsymbol{k})$ is completed by classifying $\boldsymbol{k}$ dependence of the basis functions, $\Phi_{\ell\ell'}(\boldsymbol{k})$ and $\boldsymbol{d}_{\ell\ell'}(\boldsymbol{k})$. Representative examples of these basis functions are listed in a column $\phi^\Gamma(\boldsymbol{k})$ in Tables 3.1-3.3. In space inversion invariant systems, all irreducible representations are classified into even/odd parity, which is conventionally labeled with g/u. By adding the label g/u to Γ in an appropriate manner, one can make tables for O_h, D_{4h}, and D_{6h} groups straightforwardly. For complete set of basis functions, $\phi^\Gamma(\boldsymbol{k})$, see Ref. [135].

Now, we discuss the consequence of the lists in Tables 3.1-3.3. We realize that even in a single-orbital system, orbital character can play crucial roles. Within the whole 32 point groups, there exists *one and only one* nontrivial combination whose transformation properties are completely different from the other cases. That is $\Gamma_9\otimes\Gamma_9$ in D_6 and the equivalent groups, which do not include E_1 representation in sharp contrast to the other products $\Gamma_7\otimes\Gamma_7$ or $\Gamma_8\otimes\Gamma_8$. In this case, the gap functions can show an anomalous $\boldsymbol{k}$ dependence, which explains the emergence of an exotic gap structure in the microscopic study for UPt_3 [2]. To the best of our knowledge, this point has not been recognized so far, which is one of nontrivial results in this study.

As highlighted in $\Gamma_9\otimes\Gamma_9$ in D_6 point group, it is noteworthy that, in Tables 3.1-3.3, the Kramers sector takes different irreducible representations, depending on the constituting orbitals. For example, direct products for *pure*-spin 1/2 s-orbital electrons in D_{4h} point group, which correspond to $\Gamma_{6g}\otimes\Gamma_{6g}$ in Table 3.2, include A_{1g} and A_{2g} representations. In contrast, $\Gamma_{6g}\otimes\Gamma_{7g}$ includes B_{1g} and B_{2g}, while it does not include A_{1g} and A_{2g} representations. Moreover, a spin-singlet state described by $\mathbf{0}$ in $\Gamma_{6g}\otimes\Gamma_{7g}$ belongs to B_{1g}, while that in $\Gamma_{6g}\otimes\Gamma_{6g}$ belongs to the identity representation. This is an essential aspect of the electron pairing in multiorbital systems. Note that we have used the word " spin-singlet/triplet " according to

Table 3.1: Basis functions of irreducible representations in O group. $\bar{\sigma}^\mu = i\sigma^\mu\sigma^y$ is represented by $\boldsymbol{\mu} = \mathbf{0}, \boldsymbol{x}, \boldsymbol{y}, \boldsymbol{z}$, symbolically. Index $a(b)$ of $\boldsymbol{\mu}_{a(b)}$ represents that the pair consists of one of the non-Kramers doublet $a(b)$ in Γ_8 (Appendix A.2.2) and the other orbital Γ_6 or Γ_7. $\boldsymbol{\mu}_{a\pm} = -\frac{1}{2}(\boldsymbol{\mu}_a \pm \sqrt{3}\boldsymbol{\mu}_b)$ and $\boldsymbol{\mu}_{b\pm} = \frac{1}{2}(-\boldsymbol{\mu}_b \pm \sqrt{3}\boldsymbol{\mu}_a)$. τ^μ's are the Pauli matrices in the orbital space spanned by the non-Kramers degrees of freedom (a/b). $\boldsymbol{\zeta} = \cos\theta(\tau^0, \tau^0, \tau^0) + \sin\theta(\tau^z_-, \tau^z_+, \tau^z)$ and $\boldsymbol{\eta} = \cos\theta(\tau^y, \tau^y, \tau^y) + i\sin\theta(\tau^x_-, \tau^x_+, \tau^x)$, where $\tau^z_\pm = -\frac{1}{2}(\tau^z \pm \sqrt{3}\tau^x)$ and $\tau^x_\pm = \frac{1}{2}(-\tau^x \pm \sqrt{3}\tau^z)$. θ is an arbitraly real parameter.

IR	$\phi^\Gamma(\boldsymbol{k})$	$\Gamma_6 \otimes \Gamma_6$ / $\Gamma_7 \otimes \Gamma_7$	$\Gamma_6 \otimes \Gamma_7$
A_1	$k_x^2 + k_y^2 + k_z^2$	$\mathbf{0}$	
A_2	$k_x k_y k_z$		$\mathbf{0}$
E	$(3k_z^2 - k^2, k_x^2 - k_y^2)$		
T_1	(k_x, k_y, k_z)	$(\boldsymbol{x}, \boldsymbol{y}, \boldsymbol{z})$	
T_2	$(k_y k_z, k_z k_x, k_x k_y)$		$(\boldsymbol{x}, \boldsymbol{y}, \boldsymbol{z})$
IR	$\Gamma_6 \otimes \Gamma_8$	$\Gamma_7 \otimes \Gamma_8$	$\Gamma_8 \otimes \Gamma_8$
A_1			$\tau^0\mathbf{0}$
A_2			$\tau^y\mathbf{0}$
E	$(\mathbf{0}_b, \mathbf{0}_a)$	$(\mathbf{0}_a, -\mathbf{0}_b)$	$(\tau^z, \tau^x)\mathbf{0}$
T_1	$(\boldsymbol{x}_{b+}, \boldsymbol{y}_{b-}, \boldsymbol{z}_b)$	$(\boldsymbol{x}_{a+}, \boldsymbol{y}_{a-}, \boldsymbol{z}_a)$	$(\zeta^1\boldsymbol{x}, \zeta^2\boldsymbol{y}, \zeta^3\boldsymbol{z})$
T_2	$(\boldsymbol{x}_{a+}, \boldsymbol{y}_{a-}, \boldsymbol{z}_a)$	$(\boldsymbol{x}_{b+}, \boldsymbol{y}_{b-}, \boldsymbol{z}_b)$	$(\eta^1\boldsymbol{x}, \eta^2\boldsymbol{y}, \eta^3\boldsymbol{z})$

the usual convention, although this means antisymmetrized/symmetrized representations for the pairs of Kramers degrees of freedom.

As seen in Table 3.1, the pairs including non-Kramers doublet Γ_8 are complicated because the Γ_8 bases labeled by a and b (see Appendix A.2.2) are inseparable under the point group operations. This degeneracy also can lead to the exotic pairing state, as recently proposed for the superconductivity in half-Heusler semimetal YPtBi [136, 137]. About the inter-orbital pairs including Γ_8 states, the classification can be performed by introducing the Pauli matrices $\tau^\mu_{a(b)}$ acting on $\Gamma_{8a(b)}$ and $\Gamma_{6,7}$, which represent a part of 3×3 orbital matrix space (see Eq. (3.1.7)).

Table 3.2: Basis functions of IRs in D_4 group.

IR	$\phi^{\Gamma}(\boldsymbol{k})$	$\Gamma_6 \otimes \Gamma_6$ / $\Gamma_7 \otimes \Gamma_7$	$\Gamma_6 \otimes \Gamma_7$
A_1	k_z^2	$\boldsymbol{0}$	
A_2	k_z	$\boldsymbol{z}$	
B_1	$k_x^2 - k_y^2$		$\boldsymbol{0}$
B_2	$k_x k_y$		$\boldsymbol{z}$
E	(k_x, k_y)	$(\boldsymbol{x}, \boldsymbol{y})$	$(\boldsymbol{x}, -\boldsymbol{y})$

Table 3.3: Basis functions of IRs in D_6 group. $i = 7(8)$ corresponds to upper(lower) expressions.

IR	$\phi^{\Gamma}(\boldsymbol{k})$	$\Gamma_i \otimes \Gamma_i$	$\Gamma_9 \otimes \Gamma_9$	$\Gamma_7 \otimes \Gamma_8$	$\Gamma_i \otimes \Gamma_9$
A_1	k_z^2	$\boldsymbol{0}$	$\boldsymbol{0}$		
A_2	k_z	$\boldsymbol{z}$	$\boldsymbol{z}$		
B_1	$k_y^3 - 3k_y k_x^2$		$\boldsymbol{y}$	$\boldsymbol{y}$	
B_2	$k_x^3 - 3k_x k_y^2$		$\boldsymbol{x}$	$\boldsymbol{x}$	
E_1	(k_x, k_y)	$(\boldsymbol{x}, \pm\boldsymbol{y})$			$(\boldsymbol{x}, \mp\boldsymbol{y})$
E_2	$(2k_x k_y, k_x^2 - k_y^2)$			$(i\boldsymbol{z}, \boldsymbol{0})$	$(i\boldsymbol{z}, \mp\boldsymbol{0})$

3.1.3 List of full irreducible representations

Now, let us complete a list of irreducible representations of gap functions, which is constructed via the subduction of

$$\Big(\boldsymbol{k} \text{ dependence } \phi^{\Gamma}(\boldsymbol{k})\Big) \otimes (\text{Kramers part}) \downarrow P, \tag{3.1.6}$$

(see Sec. 3.2.2). The results are summarized in Tables 3.4-3.6. These basis functions obtained by the subduction should still be antisymmetrized to meet the fermion antisymmetry. For this purpose, it is instructive to explicitly write down the pair amplitudes of Eq. (3.1.4) as,

$$F_{\ell\alpha,\ell'\alpha'}(\boldsymbol{k}) = \sum_{\mu\nu} d^{\mu\nu}(\boldsymbol{k}) \tau^{\nu}_{\ell\ell'} \bar{\sigma}^{\mu}_{\alpha\alpha'}, \tag{3.1.7}$$

where the matrix $\tau^{\nu}_{\ell\ell'}$ characterizes the orbital sector of the pair amplitudes. In the followings, we call $\tau^{\nu}_{\ell\ell'}\bar{\sigma}^{\mu}_{\alpha\alpha'}$ in Eq. (3.1.7) a multipole part of the pair amplitudes and denote $\boldsymbol{\tau}\bar{\boldsymbol{\sigma}}$

symbolically. In terms of $d^{\mu\nu}(\boldsymbol{k}), \Phi_{\ell\ell'}(\boldsymbol{k})$ and $d^{\mu}_{\ell\ell'}(\boldsymbol{k})$ in Eq. (3.1.4) are given by,

$$\Phi_{\ell\ell'}(\boldsymbol{k}) = \sum_{\nu} d^{0\nu}(\boldsymbol{k})\tau^{\nu}_{\ell\ell'}, \tag{3.1.8a}$$

$$d^{\mu}_{\ell\ell'}(\boldsymbol{k}) = \sum_{\nu} d^{\mu\nu}(\boldsymbol{k})\tau^{\nu}_{\ell\ell'}. \tag{3.1.8b}$$

The dimension of matrix $\tau^{\nu}_{\ell\ell'}$ depends on a given set of the two orbital (ℓ and ℓ'). For example, $\tau^{\nu}_{\ell\ell'}$ is the Gell-Mann matrix in three-orbital systems with $\Gamma_6 \otimes \Gamma_8$ and $\Gamma_7 \otimes \Gamma_8$ in O group, which is implicitly reflected in $\boldsymbol{\mu}_{a,b}$ in Table 3.1. In other cases, the $\tau^{\nu}_{\ell\ell'}$ is simply the Pauli matrix, which represents the different orbital degrees of freedom or the non-Kramers indices for Γ_8 in O group. Remember that we are considering a pair with a given set of orbital ℓ and ℓ', and the realized pair in reality is generally in a linear combination of such pairs.

Hereafter, let us consider two-orbital systems for simplicity. The generalization to generic multiorbital systems is straightforward. For the $\boldsymbol{\tau}\bar{\boldsymbol{\sigma}}$ pairing states, we can define orbital (o) singlet/triplet after spin (s) singlet/triplet. In what follows o-triplet s-singlet or o-singlet s-triplet is referred to be multipole (m) singlet, while o-singlet s-singlet or o-triplet s-triplet to be m-triplet. Note that the singlet(triplet) just means odd(even) under the exchange of the corresponding indices.

Let us discuss the properties of $d^{\mu\nu}(\boldsymbol{k})$. First, the fermion antisymmetry imposes a constraint,

$$d^{\mu\nu}(\boldsymbol{k})\tau^{\nu}\bar{\sigma}^{\mu} = -d^{\mu\nu}(-\boldsymbol{k})(\tau^{\nu})^{T}(\bar{\sigma}^{\mu})^{T}, \tag{3.1.9}$$

where A^T denotes the transpose of the matrix A. From this relation, one can see that $d^{\mu\nu}(\boldsymbol{k})$ should be even (odd) under the transform $\boldsymbol{k} \to -\boldsymbol{k}$ for m-singlet (triplet) pairings. Next, the time reversal symmetry imposes another constraint,

$$d^{\mu\nu}(\boldsymbol{k})\tau^{\nu}\bar{\sigma}^{\mu} = -d^{\mu\nu *}(-\boldsymbol{k})(\tau^{\nu})^{T}(\bar{\sigma}^{\mu})^{T}. \tag{3.1.10}$$

From Eqs. (3.1.9) and (3.1.10), we find that $d^{\mu\nu}(\boldsymbol{k})$ is real whenever the time reversal symmetry is preserved. Note also that the multipole part of pair amplitudes $\boldsymbol{\tau}\bar{\boldsymbol{\sigma}}$ is time reversal even (odd) for m-singlet (triplet), according to the fact $(\tau^{\nu})^{T}(\bar{\sigma}^{\mu})^{T} = -\tau^{\nu}\bar{\sigma}^{\mu}$ for m-singlet and $\tau^{\nu}\bar{\sigma}^{\mu}$ for m-triplet. Furthermore, the space inversion symmetry requires that pair amplitudes belong to the even or odd parity representation, which is denoted by the index g or u:

$$d^{\mu\nu}(\boldsymbol{k}) = (-)^{P} d^{\mu\nu}(-\boldsymbol{k}) \qquad \text{for } \Gamma_g \text{ irreducible representations,} \tag{3.1.11a}$$

$$d^{\mu\nu}(\boldsymbol{k}) = (-)^{P+1} d^{\mu\nu}(-\boldsymbol{k}) \qquad \text{for } \Gamma_u \text{ irreducible representations,} \tag{3.1.11b}$$

where $P = 0$ for $\nu = 0, z$ and is equal to the total parity of two orbitals ℓ and ℓ' for $\nu = x, y$. Therefore, the m-singlet/triplet pairing corresponds to the even/odd parity representation when the two orbitals have the same parity.

As a demonstration, let us mention a two-orbital system with Γ_{6g} and Γ_{7g} orbitals in D_{4h} point group. Both orbitals are twofold degenerate Kramers doublets. This two-orbital model has been studied as a minimal model of iron-based superconductors [47, 43]. The decomposition of direct products is given by $\Gamma_{6g} \otimes \Gamma_{6g} = \Gamma_{7g} \otimes \Gamma_{7g} = A_{1g} \oplus A_{2g} \oplus E_g$ and $\Gamma_{6g} \otimes \Gamma_{7g} = B_{1g} \oplus B_{2g} \oplus E_g$ (Table 3.2). Here, let us consider two examples of pairing states:

$$\boldsymbol{0} \ \text{ in } \ \Gamma_{6g} \otimes \Gamma_{6g} \quad (A_{1g}), \tag{3.1.12a}$$

$$\boldsymbol{z} \ \text{ in } \ \Gamma_{6g} \otimes \Gamma_{7g} \quad (B_{2g}). \tag{3.1.12b}$$

These basis functions can be easily read from the third and the fourth column in Table 3.2. Next, we attach a function $\phi^{\Gamma}(\boldsymbol{k})$ in Table 3.2 to the bases (3.1.12a) and (3.1.12b). For simplicity, we consider the following $\boldsymbol{k}$ dependence:

$$\phi^{B_{1g}}(\boldsymbol{k})\,\boldsymbol{0} \ \text{ in } \ \Gamma_{6g} \otimes \Gamma_{6g} \quad (B_{1g} = B_{1g} \otimes A_{1g}), \tag{3.1.13a}$$

$$\phi^{A_{2g}}(\boldsymbol{k})\,\boldsymbol{z} \ \text{ in } \ \Gamma_{6g} \otimes \Gamma_{7g} \quad (B_{1g} = A_{2g} \otimes B_{2g}). \tag{3.1.13b}$$

These two are both B_{1g} irreducible representations and we can find them in Table 3.5. However, they are not the final expression yet. Finally, we need to antisymmetrize Eqs. (3.1.13a) and (3.1.13b). Equation (3.1.13a) is already an antisymmetric expression, since $\phi^{B_{1g}}(\boldsymbol{k})$ is an even function and $\boldsymbol{0}$ is antisymmetric (odd). As for Eq. (3.1.13b), it is necessary to antisymmetrize the orbital sector, Γ_{6g} and Γ_{7g}. Since $\phi^{A_{2g}}(\boldsymbol{k})$ is even and $\boldsymbol{z}$ is symmetric (even), we should take an o-singlet τ^y. Thus, we obtain the final form of the gap function with B_{1g} m-singlet, $\phi^{A_{2g}}(\boldsymbol{k})\,\tau^y\boldsymbol{z}$. This is the outline to construct pair amplitudes with a specific irreducible representation in multiorbital systems.

Before the end of this section, let us make some remarks on inter-orbital pairings in Tables 3.4 and 3.6. One is that representations of some basis functions are *mixed*-parity and ambiguous. For example, $\phi^{A_1}(\boldsymbol{k}) \times (\boldsymbol{z}, i\boldsymbol{0})$ belongs to E_2 representations of $\Gamma_7 \otimes \Gamma_9$ in Table 3.6. Depending on $\phi^{A_1} = \phi^{A_{1g}}$ or $\phi^{A_{1u}}$, the basis functions are classified into two types of basis functions,

$$\phi^{A_{1g}}(\boldsymbol{k}) \times (\tau^y\boldsymbol{z}, \tau^x\boldsymbol{0}) \quad (m\text{-singlet}), \tag{3.1.14a}$$

$$\phi^{A_{1u}}(\boldsymbol{k}) \times (\tau^x\boldsymbol{z}, -\tau^y\boldsymbol{0}) \quad (m\text{-triplet}), \tag{3.1.14b}$$

after considering the fermion antisymmetry.

Another is a special case in $\Gamma_{6(7)} \otimes \Gamma_8$ of O group in Table 3.4 as noted in Sec. 3.1.2. Since the pair can be $\Gamma_{6(7)} \otimes \Gamma_{8a}$ or $\Gamma_{6(7)} \otimes \Gamma_{8b}$, we need two kinds of τ matrices: one for $\Gamma_{6(7)} \otimes \Gamma_{8a}$ and the other for $\Gamma_{6(7)} \otimes \Gamma_{8b}$.

Table 3.4: Basis functions of irreducible representations in O group. The following abbreviations are used; $\phi_i^{\Gamma} = \phi_i^{\Gamma}(\boldsymbol{k})$, $\phi_{1\pm}^E = \frac{1}{2}(-\phi_1^E \pm \sqrt{3}\phi_2^E)$, $\phi_{2\pm}^E = -\frac{1}{2}(\phi_2^E \pm \sqrt{3}\phi_1^E)$, and $\phi_i^{T_1}(\boldsymbol{k}) = k_i$, $\phi^{T_2}(\boldsymbol{k}) = \tilde{k}_i$ with $i = 1, 2, 3$. Basis fucntions in $\Gamma_6 \otimes \Gamma_8$ space are obtained by replacing $\boldsymbol{\mu}_a \to \boldsymbol{\mu}_b, \boldsymbol{\mu}_b \to -\boldsymbol{\mu}_a$ with $\boldsymbol{\mu} = \mathbf{0}, \boldsymbol{x}, \boldsymbol{y}, \boldsymbol{z}$ in the table of $\Gamma_7 \otimes \Gamma_8$ space. The other notations are the same as in Table 3.1.

IR		$\Gamma_6 \otimes \Gamma_6$ / $\Gamma_7 \otimes \Gamma_7$
A_1	$\phi^{A_1}\mathbf{0}$	$k_1\boldsymbol{x}+k_2\boldsymbol{y}+k_3\boldsymbol{z}$
A_2	$\phi^{A_2}\mathbf{0}$	$\tilde{k}_1\boldsymbol{x}+\tilde{k}_2\boldsymbol{y}+\tilde{k}_3\boldsymbol{z}$
E	$(\phi_1^E, \phi_2^E)\mathbf{0}$	$\left(\frac{k_1}{\sqrt{3}}\boldsymbol{x}+\frac{k_2}{\sqrt{3}}\boldsymbol{y}-\frac{2k_3}{\sqrt{3}}\boldsymbol{z}, k_2\boldsymbol{y}-k_1\boldsymbol{x}\right),\ \left(\tilde{k}_1\boldsymbol{x}-\tilde{k}_2\boldsymbol{y}, \frac{\tilde{k}_1}{\sqrt{3}}\boldsymbol{x}+\frac{\tilde{k}_2}{\sqrt{3}}\boldsymbol{y}-\frac{2\tilde{k}_3}{\sqrt{3}}\boldsymbol{z}\right)$
T_1	$(k_1, k_2, k_3)\mathbf{0}$	$(\phi^{A_1}\boldsymbol{x}, \phi^{A_1}\boldsymbol{y}, \phi^{A_1}\boldsymbol{z}),\ (k_2\boldsymbol{z}-k_3\boldsymbol{y}, k_3\boldsymbol{x}-k_1\boldsymbol{z}, k_1\boldsymbol{y}-k_2\boldsymbol{x}),$
		$(\phi_{1+}^E\boldsymbol{x}, \phi_{1-}^E\boldsymbol{y}, \phi_1^E\boldsymbol{z}),\ (\tilde{k}_2\boldsymbol{z}+\tilde{k}_3\boldsymbol{y}, \tilde{k}_3\boldsymbol{x}+\tilde{k}_1\boldsymbol{z}, \tilde{k}_1\boldsymbol{y}+\tilde{k}_2\boldsymbol{x})$
T_2	$(\tilde{k}_1, \tilde{k}_2, \tilde{k}_3)\mathbf{0}$	$(\phi^{A_2}\boldsymbol{x}, \phi^{A_2}\boldsymbol{y}, \phi^{A_2}\boldsymbol{z}),\ (k_2\boldsymbol{z}+k_3\boldsymbol{y}, k_3\boldsymbol{x}+k_1\boldsymbol{z}, k_1\boldsymbol{y}+k_2\boldsymbol{x}),$
		$(\phi_{2+}^E\boldsymbol{x}, \phi_{2-}^E\boldsymbol{y}, \phi_2^E\boldsymbol{z}),\ (\tilde{k}_2\boldsymbol{z}-\tilde{k}_3\boldsymbol{y}, \tilde{k}_3\boldsymbol{x}-\tilde{k}_1\boldsymbol{z}, \tilde{k}_1\boldsymbol{y}-\tilde{k}_2\boldsymbol{x})$

IR		$\Gamma_6 \otimes \Gamma_7$
A_1	$\phi^{A_2}\mathbf{0}$	$\tilde{k}_1\boldsymbol{x}+\tilde{k}_2\boldsymbol{y}+\tilde{k}_3\boldsymbol{z}$
A_2	$\phi^{A_1}\mathbf{0}$	$k_1\boldsymbol{x}+k_2\boldsymbol{y}+k_3\boldsymbol{z}$
E	$(\phi_2^E, -\phi_1^E)\mathbf{0}$	$\left(k_1\boldsymbol{x}-k_2\boldsymbol{y}, \frac{k_1}{\sqrt{3}}\boldsymbol{x}+\frac{k_2}{\sqrt{3}}\boldsymbol{y}-\frac{2k_3}{\sqrt{3}}\boldsymbol{z}\right),\ \left(\frac{\tilde{k}_1}{\sqrt{3}}\boldsymbol{x}+\frac{\tilde{k}_2}{\sqrt{3}}\boldsymbol{y}-\frac{2\tilde{k}_3}{\sqrt{3}}\boldsymbol{z}, \tilde{k}_2\boldsymbol{y}-\tilde{k}_1\boldsymbol{x}\right)$
T_1	$(\tilde{k}_1, \tilde{k}_2, \tilde{k}_3)\mathbf{0}$	$(\phi^{A_2}\boldsymbol{x}, \phi^{A_2}\boldsymbol{y}, \phi^{A_2}\boldsymbol{z}),\ (k_2\boldsymbol{z}+k_3\boldsymbol{y}, k_3\boldsymbol{x}+k_1\boldsymbol{z}, k_1\boldsymbol{y}+k_2\boldsymbol{x}),$
		$(\phi_{2+}^E\boldsymbol{x}, \phi_{2-}^E\boldsymbol{y}, \phi_2^E\boldsymbol{z}),\ (\tilde{k}_2\boldsymbol{z}-\tilde{k}_3\boldsymbol{y}, \tilde{k}_3\boldsymbol{x}-\tilde{k}_1\boldsymbol{z}, \tilde{k}_1\boldsymbol{y}-\tilde{k}_2\boldsymbol{x})$
T_2	$(k_1, k_2, k_3)\mathbf{0}$	$(\phi^{A_1}\boldsymbol{x}, \phi^{A_1}\boldsymbol{y}, \phi^{A_1}\boldsymbol{z}),\ (k_2\boldsymbol{z}-k_3\boldsymbol{y}, k_3\boldsymbol{x}-k_1\boldsymbol{z}, k_1\boldsymbol{y}-k_2\boldsymbol{x}),$
		$(\phi_{1+}^E\boldsymbol{x}, \phi_{1-}^E\boldsymbol{y}, \phi_1^E\boldsymbol{z}),\ (\tilde{k}_2\boldsymbol{z}+\tilde{k}_3\boldsymbol{y}, \tilde{k}_3\boldsymbol{x}+\tilde{k}_1\boldsymbol{z}, \tilde{k}_1\boldsymbol{y}+\tilde{k}_2\boldsymbol{x})$

IR		$\Gamma_7 \otimes \Gamma_8$ / $\Gamma_6 \otimes \Gamma_8$ $\quad(\boldsymbol{\mu}_a \to \boldsymbol{\mu}_b, \boldsymbol{\mu}_b \to -\boldsymbol{\mu}_a)$
A_1	$\phi_1^E\mathbf{0}_a-\phi_2^E\mathbf{0}_b$	$\left\{k_1\boldsymbol{x}_{a+}+k_2\boldsymbol{y}_{a-}+k_3\boldsymbol{z}_a,\ (k \to \tilde{k}, a \to b)\right\}$
A_2	$\phi_2^E\mathbf{0}_a+\phi_1^E\mathbf{0}_b$	$\left\{\tilde{k}_1\boldsymbol{x}_{a+}+\tilde{k}_2\boldsymbol{y}_{a-}+\tilde{k}_3\boldsymbol{z}_a,\ (\tilde{k} \to k, a \to b)\right\}$
E	$(\phi^{A_1}\mathbf{0}_a, -\phi^{A_1}\mathbf{0}_b),$	$\left\{\left(\frac{k_1}{\sqrt{3}}\boldsymbol{x}_{a+}+\frac{k_2}{\sqrt{3}}\boldsymbol{y}_{a-}-\frac{2k_3}{\sqrt{3}}\boldsymbol{z}_a, k_2\boldsymbol{y}_{a-}-k_1\boldsymbol{x}_{a+}\right),\ (k\to\tilde{k}, a \to b)\right\},$
	$(\phi^{A_2}\mathbf{0}_b, \phi^{A_2}\mathbf{0}_a),$	$\left\{\left(\tilde{k}_1\boldsymbol{x}_{a+}-\tilde{k}_2\boldsymbol{y}_{a-}, \frac{\tilde{k}_1}{\sqrt{3}}\boldsymbol{x}_{a+}+\frac{\tilde{k}_2}{\sqrt{3}}\boldsymbol{y}_{a-}-\frac{2\tilde{k}_3}{\sqrt{3}}\boldsymbol{z}_a\right),\ (\tilde{k}\to k, a \to b)\right\}$
	$(\phi_1^E\mathbf{0}_a+\phi_2^E\mathbf{0}_b, -\phi_2^E\mathbf{0}_a+\phi_1^E\mathbf{0}_b)$	

T_1	$(k_1\mathbf{0}_{a+}, k_2\mathbf{0}_{a-}, k_3\mathbf{0}_a)$,	$\Big\{\phi^{A_1}(\boldsymbol{x}_{a+}, \boldsymbol{y}_{a-}, \boldsymbol{z}_a),\ (A_1 \to A_2, a \to b)\Big\}$,
	$(\tilde{k}_1\mathbf{0}_{b+}, \tilde{k}_2\mathbf{0}_{b-}, \tilde{k}_3\mathbf{0}_b)$	$\Big\{(\phi^E_{1+}\boldsymbol{x}_{a+}, \phi^E_{1-}\boldsymbol{y}_{a-}, \phi^E_1\boldsymbol{z}_a),\ (\phi^E_1 \to \phi^E_2, a \to b)\Big\}$,
		$\Big\{(k_2\boldsymbol{z}_a - k_3\boldsymbol{y}_{a-}, k_3\boldsymbol{x}_{a+} - k_1\boldsymbol{z}_a, k_1\boldsymbol{y}_{a-} - k_2\boldsymbol{x}_{a+}),\ (k \to \tilde{k}, a \to b)\Big\}$,
		$\Big\{(\tilde{k}_2\boldsymbol{z}_a + \tilde{k}_3\boldsymbol{y}_{a-}, \tilde{k}_3\boldsymbol{x}_{a+} + \tilde{k}_1\boldsymbol{z}_a, \tilde{k}_1\boldsymbol{y}_{a-} + \tilde{k}_2\boldsymbol{x}_{a+}),\ (\tilde{k} \to k, a \to b)\Big\}$
T_2	$(\tilde{k}_1\mathbf{0}_{a+}, \tilde{k}_2\mathbf{0}_{a-}, \tilde{k}_3\mathbf{0}_a)$,	$\Big\{\phi^{A_1}(\boldsymbol{x}_{b+}, \boldsymbol{y}_{b-}, \boldsymbol{z}_b),\ (A_1 \to A_2, b \to a)\Big\}$,
	$(k_1\mathbf{0}_{b+}, k_2\mathbf{0}_{b-}, k_3\mathbf{0}_b)$	$\Big\{(\phi^E_{1+}\boldsymbol{x}_{b+}, \phi^E_{1-}\boldsymbol{y}_{b-}, \phi^E_1\boldsymbol{z}_b),\ (\phi^E_1 \to \phi^E_2, b \to a)\Big\}$,
		$\Big\{(k_2\boldsymbol{z}_a + k_3\boldsymbol{y}_{a-}, k_3\boldsymbol{x}_{a+} + k_1\boldsymbol{z}_a, k_1\boldsymbol{y}_{a-} + k_2\boldsymbol{x}_{a+}),\ (k \to \tilde{k}, a \to b)\Big\}$,
		$\Big\{(\tilde{k}_2\boldsymbol{z}_a - \tilde{k}_3\boldsymbol{y}_{a-}, \tilde{k}_3\boldsymbol{x}_{a+} - \tilde{k}_1\boldsymbol{z}_a, \tilde{k}_1\boldsymbol{y}_{a-} - \tilde{k}_2\boldsymbol{x}_{a+}),\ (\tilde{k} \to k, a \to b)\Big\}$

IR		$\Gamma_8 \otimes \Gamma_8$
A_1	$\phi^{A_1}\tau^0\mathbf{0}, \phi^{A_2}\tau^y\mathbf{0}$,	$\Big\{k_1\zeta^1\boldsymbol{x} + k_2\zeta^2\boldsymbol{y} + k_3\zeta^3\boldsymbol{z},\ (k \to \tilde{k}, \zeta \to \eta)\Big\}$
	$\phi^E_1\tau^z\mathbf{0} + \phi^E_2\tau^x\mathbf{0}$	
A_2	$\phi^{A_2}\tau^0\mathbf{0}, \phi^{A_1}\tau^y\mathbf{0}$,	$\Big\{\tilde{k}_1\zeta^1\boldsymbol{x} + \tilde{k}_2\zeta^2\boldsymbol{y} + \tilde{k}_3\zeta^3\boldsymbol{z},\ (\tilde{k} \to k, \zeta \to \eta)\Big\}$
	$\phi^E_2\tau^z\mathbf{0} - \phi^E_1\tau^x\mathbf{0}$	
E	$(\phi^{A_1}\tau^z, \phi^{A_1}\tau^x)\mathbf{0}$,	$\Big\{\Big(\frac{k_1}{\sqrt{3}}\zeta^1\boldsymbol{x} + \frac{k_2}{\sqrt{3}}\zeta^2\boldsymbol{y} - \frac{2k_3}{\sqrt{3}}\zeta^3\boldsymbol{z}, k_2\zeta^2\boldsymbol{y} - k_1\zeta^1\boldsymbol{x}\Big),\ (k \to \tilde{k}, \zeta \to \eta)\Big\}$,
	$(\phi^{A_2}\tau^x, -\phi^{A_2}\tau^z)\mathbf{0}$,	$\Big\{\Big(\tilde{k}_1\zeta^1\boldsymbol{x} + \tilde{k}_2\zeta^2\boldsymbol{y}, \frac{\tilde{k}_1}{\sqrt{3}}\zeta^1\boldsymbol{x} + \frac{\tilde{k}_2}{\sqrt{3}}\zeta^2\boldsymbol{y} + \frac{2\tilde{k}_3}{\sqrt{3}}\zeta^3\boldsymbol{z}\Big),\ (\tilde{k} \to k, \zeta \to \eta)\Big\}$
	$(\phi^E_1\tau^z - \phi^E_2\tau^x, -\phi^E_2\tau^z - \phi^E_1\tau^x)\mathbf{0}$,	
	$(\phi^E_1, \phi^E_2)\tau^0\mathbf{0}, (\phi^E_2, -\phi^E_1)\tau^y\mathbf{0}$	
T_1	$(k_1,\ k_2,\ k_3)\tau^0\mathbf{0}$,	$\Big\{\phi^{A_1}(\zeta^1\boldsymbol{x},\ \zeta^2\boldsymbol{y},\ \zeta^3\boldsymbol{z}),\ (A_1 \to A_2, \zeta \to \eta)\Big\}$,
	$(\tilde{k}_1,\ \tilde{k}_2,\ \tilde{k}_3)\tau^y\mathbf{0}$,	$\Big\{(\phi^E_{1+}\zeta^1\boldsymbol{x},\ \phi^E_{1-}\zeta^2\boldsymbol{y},\ \phi^E_1\zeta^3\boldsymbol{z}),\ (\phi^E_1 \to \phi^E_2, \zeta \to \eta)\Big\}$,
	$(k_1\tau^z_-,\ k_2\tau^z_+,\ k_3\tau^z)\mathbf{0}$,	$\Big\{(k_2\zeta^3\boldsymbol{z} - k_3\zeta^2\boldsymbol{y},\ k_3\zeta^1\boldsymbol{x} - k_1\zeta^3\boldsymbol{z},\ k_1\zeta^2\boldsymbol{y} - k_2\zeta^1\boldsymbol{x}),\ (k \to \tilde{k}, \zeta \to \eta)\Big\}$,
	$(\tilde{k}_1\tau^x_-,\ \tilde{k}_2\tau^x_+,\ \tilde{k}_3\tau^x)\mathbf{0}$	$\Big\{(\tilde{k}_2\zeta^3\boldsymbol{z} + \tilde{k}_3\zeta^2\boldsymbol{y},\ \tilde{k}_3\zeta^1\boldsymbol{x} + \tilde{k}_1\zeta^3\boldsymbol{z},\ \tilde{k}_1\zeta^2\boldsymbol{y} + \tilde{k}_2\zeta^1\boldsymbol{x}),\ (\tilde{k} \to k, \zeta \to \eta)\Big\}$
T_2	$(\tilde{k}_1,\ \tilde{k}_2,\ \tilde{k}_3)\tau^0\mathbf{0}$,	$\Big\{\phi^{A_2}(\zeta^1\boldsymbol{x},\ \zeta^2\boldsymbol{y},\ \zeta^3\boldsymbol{z}),\ (A_2 \to A_1, \zeta \to \eta)\Big\}$,
	$(k_1,\ k_2,\ k_3)\tau^y\mathbf{0}$,	$(\phi^E_{2+}\zeta^1\boldsymbol{x},\ \phi^E_{2-}\zeta^2\boldsymbol{y},\ \phi^E_2\zeta^3\boldsymbol{z}),\ (\phi^E_2 \to \phi^E_1, \zeta \to \eta)\Big\}$,
	$(\tilde{k}_1\tau^z_-,\ \tilde{k}_2\tau^z_+,\ \tilde{k}_3\tau^z)\mathbf{0}$,	$\Big\{(\tilde{k}_2\zeta^3\boldsymbol{z} - \tilde{k}_3\zeta^2\boldsymbol{y},\ \tilde{k}_3\zeta^1\boldsymbol{x} - \tilde{k}_1\zeta^3\boldsymbol{z},\ \tilde{k}_1\zeta^2\boldsymbol{y} - \tilde{k}_2\zeta^1\boldsymbol{x}),\ (\tilde{k} \to k, \zeta \to \eta)\Big\}$,
	$(k_1\tau^x_-,\ k_2\tau^x_+,\ k_3\tau^x)\mathbf{0}$	$\Big\{(k_2\zeta^3\boldsymbol{z} + k_3\zeta^2\boldsymbol{y},\ k_3\zeta^1\boldsymbol{x} + k_1\zeta^3\boldsymbol{z},\ k_1\zeta^2\boldsymbol{y} + k_2\zeta^1\boldsymbol{x}),\ (k \to \tilde{k}, \zeta \to \eta)\Big\}$

Table 3.5: Basis functions of irreducible representations in D_4 group.

IR	$\Gamma_6 \otimes \Gamma_6$ / $\Gamma_7 \otimes \Gamma_7$	
A_1	$\phi^{A_1}\mathbf{0}$	$\phi^{A_2}\boldsymbol{z},\ \phi_1^E\boldsymbol{x}+\phi_2^E\boldsymbol{y}$
A_2	$\phi^{A_2}\mathbf{0}$	$\phi^{A_1}\boldsymbol{z},\ \phi_2^E\boldsymbol{x}-\phi_1^E\boldsymbol{y}$
B_1	$\phi^{B_1}\mathbf{0}$	$\phi^{B_2}\boldsymbol{z},\ \phi_1^E\boldsymbol{x}-\phi_2^E\boldsymbol{y}$
B_2	$\phi^{B_2}\mathbf{0}$	$\phi^{B_1}\boldsymbol{z},\ \phi_2^E\boldsymbol{x}+\phi_1^E\boldsymbol{y}$
E	$(\phi_1^E,\phi_2^E)\mathbf{0}$	$\phi^{A_1}(\boldsymbol{x},\boldsymbol{y}),\phi^{A_2}(\boldsymbol{y},-\boldsymbol{x}),\phi^{B_1}(\boldsymbol{x},-\boldsymbol{y}),\phi^{B_2}(\boldsymbol{y},\boldsymbol{x}),(\phi_2^E,-\phi_1^E)\boldsymbol{z}$
IR	$\Gamma_6 \otimes \Gamma_7$	
A_1	$\phi^{B_1}\mathbf{0}$	$\phi^{B_2}\boldsymbol{z},\ \phi_1^E\boldsymbol{x}-\phi_2^E\boldsymbol{y}$
A_2	$\phi^{B_2}\mathbf{0}$	$\phi^{B_1}\boldsymbol{z},\ \phi_2^E\boldsymbol{x}+\phi_1^E\boldsymbol{y}$
B_1	$\phi^{A_1}\mathbf{0}$	$\phi^{A_2}\boldsymbol{z},\ \phi_1^E\boldsymbol{x}+\phi_2^E\boldsymbol{y}$
B_2	$\phi^{A_2}\mathbf{0}$	$\phi^{A_1}\boldsymbol{z},\ \phi_2^E\boldsymbol{x}-\phi_1^E\boldsymbol{y}$
E	$(\phi_1^E,-\phi_2^E)\mathbf{0}$	$\phi^{A_1}(\boldsymbol{x},-\boldsymbol{y}),\ \phi^{A_2}(\boldsymbol{y},\boldsymbol{x}),\phi^{B_1}(\boldsymbol{x},\boldsymbol{y}),\ \phi^{B_2}(\boldsymbol{y},-\boldsymbol{x}),(\phi_2^E,\phi_1^E)\boldsymbol{z}$

Table 3.6: Basis functions of irreducible representations in D_6 group. Expressions for $\Gamma_{7(8)}$ correspond to upper(lower) signs.

IR	$\Gamma_7 \otimes \Gamma_7$(upper) / $\Gamma_8 \otimes \Gamma_8$(lower)	
A_1	$\phi^{A_1}\mathbf{0}$	$\phi^{A_2}\boldsymbol{z},\ \phi_1^{E_1}\boldsymbol{x}\pm\phi_2^{E_1}\boldsymbol{y}$
A_2	$\phi^{A_2}\mathbf{0}$	$\phi^{A_1}\boldsymbol{z},\ \phi_2^{E_1}\boldsymbol{x}\mp\phi_1^{E_1}\boldsymbol{y}$
B_1	$\phi^{B_1}\mathbf{0}$	$\phi^{B_2}\boldsymbol{z},\ \phi_1^{E_2}\boldsymbol{x}\pm\phi_2^{E_2}\boldsymbol{y}$
B_2	$\phi^{B_2}\mathbf{0}$	$\phi^{B_1}\boldsymbol{z},\ \phi_2^{E_2}\boldsymbol{x}\mp\phi_1^{E_2}\boldsymbol{y}$
E_1	$(\phi_1^{E_1},\phi_2^{E_1})\mathbf{0}$	$\phi^{A_1}(\boldsymbol{x},\pm\boldsymbol{y}),\ \phi^{A_2}(\boldsymbol{y},\mp\boldsymbol{x}),$ $(\phi_2^{E_2}\boldsymbol{x}\pm\phi_1^{E_2}\boldsymbol{y},\phi_1^{E_2}\boldsymbol{x}\mp\phi_2^{E_2}\boldsymbol{y}),(\phi_2^{E_1},-\phi_1^{E_1})\boldsymbol{z}$
E_2	$(\phi_1^{E_2},\phi_2^{E_2})\mathbf{0}$	$\phi^{B_1}(\boldsymbol{x},\pm\boldsymbol{y}),\ \phi^{B_2}(\boldsymbol{y},\mp\boldsymbol{x}),$ $(\phi_2^{E_1}\boldsymbol{x}\pm\phi_1^{E_1}\boldsymbol{y},\phi_1^{E_1}\boldsymbol{x}\mp\phi_2^{E_1}\boldsymbol{y}),(\phi_2^{E_2},-\phi_1^{E_2})\boldsymbol{z}$

IR	$\Gamma_9 \otimes \Gamma_9$	
A_1	$\phi^{A_1}\mathbf{0}$	$\phi^{A_2}\boldsymbol{z},\ \phi^{B_1}\boldsymbol{y},\ \phi^{B_2}\boldsymbol{x}$
A_2	$\phi^{A_2}\mathbf{0}$	$\phi^{A_1}\boldsymbol{z},\ \phi^{B_2}\boldsymbol{y},\ \phi^{B_1}\boldsymbol{x}$
B_1	$\phi^{B_1}\mathbf{0}$	$\phi^{B_2}\boldsymbol{z},\ \phi^{A_1}\boldsymbol{y},\ \phi^{A_2}\boldsymbol{x}$
B_2	$\phi^{B_2}\mathbf{0}$	$\phi^{B_1}\boldsymbol{z},\ \phi^{A_2}\boldsymbol{y},\ \phi^{A_1}\boldsymbol{x}$
E_1	$(\phi_1^{E_1}, \phi_2^{E_1})\mathbf{0}$	$(\phi_1^{E_2}, \phi_2^{E_2})\boldsymbol{y},\ (\phi_2^{E_2}, -\phi_1^{E_2})\boldsymbol{x}, (\phi_2^{E_1}, -\phi_1^{E_1})\boldsymbol{z}$
E_2	$(\phi_1^{E_2}, \phi_2^{E_2})\mathbf{0}$	$(\phi_1^{E_1}, \phi_2^{E_1})\boldsymbol{y},\ (\phi_2^{E_1}, -\phi_1^{E_1})\boldsymbol{x}, (\phi_2^{E_2}, -\phi_1^{E_2})\boldsymbol{z}$
IR	$\Gamma_7 \otimes \Gamma_8$	
A_1	$\phi^{B_1}\boldsymbol{y},\ \phi^{B_2}\boldsymbol{x}$	$\phi_1^{E_2}\boldsymbol{z} - i\phi_2^{E_2}\mathbf{0}$
A_2	$\phi^{B_2}\boldsymbol{y},\ \phi^{B_2}\boldsymbol{x}$	$\phi_2^{E_2}\boldsymbol{z} + i\phi_1^{E_2}\mathbf{0}$
B_1	$\phi^{A_1}\boldsymbol{y},\ \phi^{A_2}\boldsymbol{x}$	$\phi_1^{E_1}\boldsymbol{z} - i\phi_2^{E_1}\mathbf{0}$
B_2	$\phi^{A_2}\boldsymbol{y},\ \phi^{A_1}\boldsymbol{x}$	$\phi_2^{E_1}\boldsymbol{z} + i\phi_1^{E_1}\mathbf{0}$
E_1	$(\phi_1^{E_2}, \phi_2^{E_2})\boldsymbol{y}, (\phi_2^{E_2}, -\phi_1^{E_2})\boldsymbol{x}$	$\phi^{B_1}(\boldsymbol{z}, -i\mathbf{0}),\ \phi^{B_2}(i\mathbf{0}, \boldsymbol{z}),$ $(\phi_2^{E_1}\boldsymbol{z} - i\phi_1^{E_1}\mathbf{0}, \phi_1^{E_1}\boldsymbol{z} + i\phi_2^{E_1}\mathbf{0})$
E_2	$(\phi_1^{E_1}, \phi_2^{E_1})\boldsymbol{y}, (\phi_2^{E_1}, -\phi_1^{E_1})\boldsymbol{x}$	$\phi^{A_1}(\boldsymbol{z}, -i\mathbf{0}),\ \phi^{A_2}(i\mathbf{0}, \boldsymbol{z}),$ $(\phi_2^{E_2}\boldsymbol{z} - i\phi_1^{E_2}\mathbf{0}, \phi_1^{E_2}\boldsymbol{z} + i\phi_2^{E_2}\mathbf{0})$
IR	$\Gamma_7 \otimes \Gamma_9$(upper) / $\Gamma_8 \otimes \Gamma_9$(lower)	
A_1	$\phi_1^{E_1}\boldsymbol{x} \mp \phi_2^{E_1}\boldsymbol{y}$	$\phi_1^{E_2}\boldsymbol{z} \pm i\phi_2^{E_2}\mathbf{0}$
A_2	$\phi_2^{E_1}\boldsymbol{x} \pm \phi_1^{E_1}\boldsymbol{y}$	$\phi_2^{E_2}\boldsymbol{z} \mp i\phi_1^{E_2}\mathbf{0}$
B_1	$\phi_1^{E_2}\boldsymbol{x} \mp \phi_2^{E_2}\boldsymbol{y}$	$\phi_1^{E_1}\boldsymbol{z} \pm i\phi_2^{E_1}\mathbf{0}$
B_2	$\phi_2^{E_2}\boldsymbol{x} \pm \phi_1^{E_2}\boldsymbol{y}$	$\phi_2^{E_1}\boldsymbol{z} \mp i\phi_1^{E_1}\mathbf{0}$
E_1	$\phi^{A_1}(\boldsymbol{x}, \mp\boldsymbol{y}), \phi^{A_2}(\boldsymbol{y}, \pm\boldsymbol{x}),$ $(\phi_2^{E_2}\boldsymbol{x} \mp \phi_1^{E_2}\boldsymbol{y}, \phi_1^{E_2}\boldsymbol{x} \pm \phi_2^{E_2}\boldsymbol{y})$	$\phi^{B_1}(\boldsymbol{z}, \pm i\mathbf{0}),\ \phi^{B_2}(i\mathbf{0}, \mp\boldsymbol{z}),$ $(\phi_2^{E_1}\boldsymbol{z} \pm i\phi_1^{E_1}\mathbf{0}, \phi_1^{E_1}\boldsymbol{z} \mp i\phi_2^{E_1}\mathbf{0})$
E_2	$\phi^{B_1}(\boldsymbol{x}, \mp\boldsymbol{y}), \phi^{B_2}(\boldsymbol{y}, \pm\boldsymbol{x}),$ $(\phi_2^{E_1}\boldsymbol{x} \mp \phi_1^{E_1}\boldsymbol{y}, \phi_1^{E_1}\boldsymbol{x} \pm \phi_2^{E_1}\boldsymbol{y})$	$\phi^{A_1}(\boldsymbol{z}, \pm i\mathbf{0}),\ \phi^{A_2}(i\mathbf{0}, \mp\boldsymbol{z}),$ $(\phi_2^{E_2}\boldsymbol{z} \pm i\phi_1^{E_2}\mathbf{0}, \phi_1^{E_2}\boldsymbol{z} \mp i\phi_2^{E_2}\mathbf{0})$

Tables 3.4-3.6 are one of the main results. Even considering systems with two or more orbitals, the present results can be always applied by focusing on the 4×4 submatrix embedded in the entire space. Therefore, the basis functions in Tables 3.4-3.6 are sufficient for any symmorphic systems. Although Tables 3.4-3.6 seem to be rather complicated, they include important physical information about the pairing mechanism. This is because one can deduce what kinds (symmetry) of order parameters are realized when the system shows a characteristic fluctuation, since we have classified the superconducting order parameters in the orbital bases, which is easily related to the form of the characteristic interaction. In Sec. 3.4, we will see this point by discussing several examples.

3.2 General consideration of classification

In the previous section, we have classified superconducting gap functions according to irreducible representations of a given point group P. Before proceeding to the next step, we here show that superconducting order parameters can be characterized by irreducible representations of P in both symmorphic and non-symmorphic systems. Moreover, in symmorphic systems, the form of gap functions can be determined by considering only the spin-orbital coupled degrees of freedom.

3.2.1 Mean field theory under the space group G

Let us consider a BCS type model Hamiltonian, $H = H_0 + H_{\rm int}$, under a space group G,

$$H_0 = \sum_{\boldsymbol{k}} \sum_{12} \left[\hat{h}(\boldsymbol{k})\right]_{12} c_1^\dagger(\boldsymbol{k}) c_2(\boldsymbol{k}), \tag{3.2.1}$$

$$H_{\rm int} = -\frac{1}{2N} \sum_{\boldsymbol{k}\boldsymbol{k}'} \sum_{1234} v_{14,32}(\boldsymbol{k}-\boldsymbol{k}') c_1^\dagger(\boldsymbol{k}) c_2^\dagger(-\boldsymbol{k}) c_3(-\boldsymbol{k}') c_4(\boldsymbol{k}'), \tag{3.2.2}$$

where $\hat{h}(\boldsymbol{k})$ is a Hermitian matrix describing the band structure, and the subscripts $(1 \sim 4)$ symbolically represent the orbital, the spin, and the atomic site (sublattice) degrees of freedom. In this Hamiltonian, H_0 and $H_{\rm int}$ should respectively be invariant under any operation g in the space group G. That is to say, $[H_0, g] = 0$ and $[H_{\rm int}, g] = 0$. The space group element g is denoted as $g = \{p|\boldsymbol{a}\}$ in Seitz notation, where p is an operation of the point group P associated with G, and $\boldsymbol{a}$ is a translation. From $[H_0, g] = 0$, we obtain,

$$\hat{U}(g;\boldsymbol{k}) \hat{h}(\boldsymbol{k}) \hat{U}^\dagger(g;\boldsymbol{k}) = \hat{h}(p\boldsymbol{k}), \tag{3.2.3}$$

using the following relation,

$$g\, c_1^\dagger(\boldsymbol{k})\, g^{-1} = \sum_2 c_2^\dagger(p\boldsymbol{k}) [\hat{U}(g;\boldsymbol{k})]_{21}, \tag{3.2.4}$$

where the matrix $\hat{U}(g;\boldsymbol{k})$ describes the transformation property of $c_1^\dagger(\boldsymbol{k})$, which generally depends on $\boldsymbol{k}$ (see Appendix A.2.3). As for $H_{\rm int}$, one can expand $v_{14,32}(\boldsymbol{k}-\boldsymbol{k}')$ into the following form,

$$v_{14,32}(\boldsymbol{k}-\boldsymbol{k}') = \sum_{\Gamma}\sum_{i} v^{\Gamma}\Big[\hat{\varphi}_i^{\Gamma}(\boldsymbol{k})\Big]_{12}\Big[\hat{\varphi}_i^{\Gamma}(\boldsymbol{k}')\Big]^*_{43}. \tag{3.2.5}$$

Here, the sum of Γ contains non-equivalent irreducible representations of P and the label i denotes degenerate bases in the same Γ. v^{Γ} can be regarded as a pairing interaction in Γ irreducible representation channel, which is a real number due to the Hermitian of $H_{\rm int}$. The matrix $\hat{\varphi}_i^{\Gamma}(\boldsymbol{k})$ is the ith basis function for the Γ irreducible representation of P, which transforms according to,

$$\hat{U}(g;\boldsymbol{k})\hat{\varphi}_i^{\Gamma}(\boldsymbol{k})\hat{U}^T(g;-\boldsymbol{k}) = \sum_j \hat{\varphi}_j^{\Gamma}(p\boldsymbol{k})\mathcal{D}^{(\Gamma)}_{ji}(p), \tag{3.2.6}$$

where $\mathcal{D}^{(\Gamma)}_{ji}(p)$ is the representation matrix of Γ irreducible representation. Equation (3.2.6) can be obtained from a requirement that

$$\Psi^\dagger_{\Gamma i} = \sum_{\boldsymbol{k}}\sum_{12}\Big[\hat{\varphi}_i^{\Gamma}(\boldsymbol{k})\Big]_{12} c_1^\dagger(\boldsymbol{k})c_2^\dagger(-\boldsymbol{k}), \tag{3.2.7}$$

satisfies the following transformation properties,

$$g\,\Psi^\dagger_{\Gamma i}\,g^{-1} = \sum_j \Psi^\dagger_{\Gamma j}\mathcal{D}^{(\Gamma)}_{ji}(p). \tag{3.2.8}$$

Thus, $H_{\rm int}$ is written as follows,

$$H_{\rm int} = -\frac{1}{2N}\sum_{\Gamma}\sum_i v^{\Gamma}\Psi^\dagger_{\Gamma i}\Psi_{\Gamma i}. \tag{3.2.9}$$

This clearly shows that $H_{\rm int}$ is certainly invariant under any operation g.

Now, let us confirm the requirements of basis functions:

$$\hat{\varphi}_i^{\Gamma}(\boldsymbol{k}) = -\Big(\hat{\varphi}_i^{\Gamma}(-\boldsymbol{k})\Big)^T, \tag{3.2.10a}$$

$$\frac{1}{N}\sum_{\boldsymbol{k}}\mathrm{Tr}\Big[\hat{\varphi}_i^{\Gamma}(\boldsymbol{k})\hat{\varphi}_j^{\Gamma'\dagger}(\boldsymbol{k})\Big] = \delta_{ij}\delta_{\Gamma\Gamma'}. \tag{3.2.10b}$$

The first equation (3.2.10a) is evident from Eq. (3.2.5), while the second one (3.2.10b) can be derived by using the grand orthogonal theorem among irreducible representations;

$$\begin{aligned}
\sum_{\boldsymbol{k}}\mathrm{Tr}\Big[\hat{\varphi}_i^{\Gamma}(\boldsymbol{k})\hat{\varphi}_j^{\Gamma'\dagger}(\boldsymbol{k})\Big] &= \frac{1}{m}\sum_{\boldsymbol{k}}\sum_p \mathrm{Tr}\Big[\hat{\varphi}_i^{\Gamma}(p\boldsymbol{k})\hat{\varphi}_j^{\Gamma'\dagger}(p\boldsymbol{k})\Big] \\
&= \frac{1}{m}\sum_{\boldsymbol{k}}\sum_{i'j'}\mathrm{Tr}\Big[\hat{\varphi}_{i'}^{\Gamma}(\boldsymbol{k})\hat{\varphi}_{j'}^{\Gamma'\dagger}(\boldsymbol{k})\Big]\sum_p\Big(\mathcal{D}^{(\Gamma)}_{ii'}(p)\Big)^*\mathcal{D}^{(\Gamma')}_{jj'}(p) \\
&= \frac{1}{d_\Gamma}\delta_{ij}\delta_{\Gamma\Gamma'}\sum_{\boldsymbol{k}}\sum_i\mathrm{Tr}\Big[\hat{\varphi}_i^{\Gamma}(\boldsymbol{k})\hat{\varphi}_i^{\Gamma\dagger}(\boldsymbol{k})\Big],
\end{aligned}$$

where m is the order of P, and d_Γ the dimension of Γ. Thus, with the appropriate normalization, we can choose $\hat{\varphi}_i^\Gamma(\boldsymbol{k})$ to satisfy Eqs. (3.2.10a) and (3.2.10b).

Next, we apply the mean-field theory to Eq. (3.2.2), and introduce the superconducting order parameter,

$$\begin{aligned}\left[\hat{\Delta}(\boldsymbol{k})\right]_{12} &= \frac{1}{N}\sum_{\boldsymbol{k}'}\sum_{34} v_{14,32}(\boldsymbol{k}-\boldsymbol{k}')\langle c_4(\boldsymbol{k}')c_3(-\boldsymbol{k}')\rangle \\ &= \frac{1}{N}\sum_{\boldsymbol{k}'}\sum_{34} v_{14,32}(\boldsymbol{k}-\boldsymbol{k}')F_{43}(\boldsymbol{k}'). \end{aligned} \tag{3.2.11}$$

Substituting Eq. (3.2.5) to (3.2.11), we obtain

$$\hat{\Delta}(\boldsymbol{k}) = \sum_\Gamma\sum_i \Delta_i^\Gamma \hat{\varphi}_i^\Gamma(\boldsymbol{k}), \tag{3.2.12a}$$

$$\Delta_i^\Gamma = v^\Gamma \frac{1}{N}\sum_{\boldsymbol{k}}\sum_{12} F_{12}(\boldsymbol{k})\left[\hat{\varphi}_i^\Gamma(\boldsymbol{k})\right]^*_{12}. \tag{3.2.12b}$$

Just below the transition temperature $T = T_c$, we can linearize $F_{12}(\boldsymbol{k})$ as

$$F_{12}(\boldsymbol{k}) = T\sum_n \left[\hat{G}(\boldsymbol{k}, i\omega_n)\hat{\Delta}(\boldsymbol{k})\hat{G}^*(-\boldsymbol{k}, i\omega_n)\right]_{12}, \tag{3.2.13}$$

with Matsubara frequency $\omega_n = \pi T(2n+1)$. The one-particle normal Green's function $\hat{G}(\boldsymbol{k}, i\omega_n)$ meets a similar relation to Eq. (3.2.3),

$$\hat{U}(g;\boldsymbol{k})\hat{G}(\boldsymbol{k}, i\omega_n)\hat{U}^\dagger(g;\boldsymbol{k}) = \hat{G}(p\boldsymbol{k}, i\omega_n). \tag{3.2.14}$$

Finally, from Eqs. (3.2.12b), (3.2.13), and the grand orthogonal theorem, we obtain the gap equations as follows,

$$\Delta_i^\Gamma = v^\Gamma \Delta_i^\Gamma \frac{1}{d_\Gamma}\frac{T}{N}\sum_{\boldsymbol{k}}\sum_j\sum_n \mathrm{Tr}\left[\hat{G}(\boldsymbol{k}, i\omega_n)\hat{\varphi}_j^\Gamma(\boldsymbol{k})\hat{G}^*(-\boldsymbol{k}, i\omega_n)\hat{\varphi}_j^{\Gamma\dagger}(\boldsymbol{k})\right]. \tag{3.2.15}$$

It should be noted that the gap equation (3.2.15) is decoupled in each Γ, and also does not depend on the label i. This fact means that the gap function just below T_c can be classified according to irreducible representations of P in both symmorphic and non-symmorphic systems. In practice, $\hat{\varphi}_i^\Gamma(\boldsymbol{k})$ may be a linear combination of several basis functions in the same irreducible representation, namely, $\hat{\varphi}_i^\Gamma(\boldsymbol{k}) = \sum_\alpha C_{\Gamma\alpha}\hat{\varphi}_{\alpha,i}^\Gamma(\boldsymbol{k})$. The generalization to such situations is straightforward.

3.2.2 Classification in symmorphic systems

In a symmorphic space group, apart from the lattice translations T, all generating symmetry operations leave at least one common point fixed. The generators consist of the elements

in the semi-direct product of T and the point group P. In this case, for all point group operations $p = \{p|0\} \in P$, we can always set $\hat{U}(p;\boldsymbol{k})$ in Eq. (3.2.4) to be $\boldsymbol{k}$-independent $\hat{U}(p)$. This can be verified by the following discussions.

Let us denote $c^\dagger_{\ell\alpha b}(\boldsymbol{R})$ as the electron creation operator, where ℓ indicates a basis function labeled by an irreducible representation of P, α and b denote the Kramers degrees of freedom and the position of the atom within a unit cell, respectively. $\boldsymbol{R}$ represents the position for the unit cell (lattice vector) and we also define the relative position for the b-atom $\boldsymbol{x}_b$ in a unit cell. In general, space group operations exchange the equivalent atoms in the same or the different unit cells. Considering the Fourier transform,

$$c^\dagger_{\ell\alpha b}(\boldsymbol{k}) = \frac{1}{\sqrt{N}} \sum_{\boldsymbol{R}} e^{i\boldsymbol{k}\cdot(\boldsymbol{R}+\boldsymbol{x}_b)} c^\dagger_{\ell\alpha b}(\boldsymbol{R}), \tag{3.2.16}$$

we can check the symmetry property of $c^\dagger_{\ell\alpha b}(\boldsymbol{k})$ (see Appendix A.2.3),

$$g\, c^\dagger_{\ell\alpha b}(\boldsymbol{k})\, g^{-1} = e^{-ip\boldsymbol{k}\cdot\boldsymbol{a}} \sum_{\alpha' b'} c^\dagger_{\ell\alpha' b'}(p\boldsymbol{k}) D^{\text{site}}_{b'b}(p) D^{(\ell)}_{\alpha'\alpha}(p), \tag{3.2.17}$$

where $g = \{p|\boldsymbol{a}\} \in G$. Here, $D^{\text{site}}(p)$ and $D^{(\ell)}(p)$ are the unitary matrices corresponding to the exchange of equivalent atoms and the rotation of the Kramers degrees of freedom, respectively. Since the phase factor $e^{-ip\boldsymbol{k}\cdot\boldsymbol{a}}$ in Eq. (3.2.17) is irrelevant to the point group operations alone, $\hat{U}(p;\boldsymbol{k})$ appearing in Eq. (3.2.4) becomes $\boldsymbol{k}$-independent.

Equation (3.2.17) also indicates that $c^\dagger_{\ell\alpha b}(\boldsymbol{k})$ is a basis function for a reducible representation of P regarding $c^\dagger_{\ell\alpha b}(\boldsymbol{k}) \overset{p}{\mapsto} p\, c^\dagger_{\ell\alpha b}(p^{-1}\boldsymbol{k}) p^{-1}$ as the action of p. Therefore, in the usual manner, we can construct the basis functions of the irreducible representations of P from $c^\dagger_{\ell\alpha b}(\boldsymbol{k})$, by using the projection method. The obtained basis $c^\dagger_{\Gamma i}(\boldsymbol{k})$ satisfies,

$$p\, c^\dagger_{\Gamma i}(\boldsymbol{k})\, p^{-1} = \sum_j c^\dagger_{\Gamma j}(p\boldsymbol{k}) \left[\hat{D}^{(\Gamma)}(p)\right]_{ji}, \tag{3.2.18}$$

where Γ and i are the irreducible representation of P and its basis, respectively. $\hat{D}^{(\Gamma)}(p)$ is the corresponding representation matrix. Here, we omit the other labels for simplicity. Due to the unitarity of the irreducible decomposition, we can always rewrite the Hamiltonian in the new basis $c^\dagger_{\Gamma i}(\boldsymbol{k})$.

By using $c^\dagger_{\Gamma i}(\boldsymbol{k})$ given above, Eq. (3.2.1) can be divided into each block for irreducible representations of P,

$$H_0 = \sum_{\boldsymbol{k}} \sum_{\Gamma_1\Gamma_2} \sum_{ij} \left[\hat{h}(\boldsymbol{k};\Gamma_1\Gamma_2)\right]_{ij} c^\dagger_{\Gamma_1 i}(\boldsymbol{k}) c_{\Gamma_2 j}(\boldsymbol{k}), \tag{3.2.19}$$

where $\hat{h}(\boldsymbol{k};\Gamma_1\Gamma_2)$ satisfies

$$\hat{h}(p\boldsymbol{k};\Gamma_1\Gamma_2) = \hat{D}^{(\Gamma_1)}(p) \hat{h}(\boldsymbol{k};\Gamma_1\Gamma_2) \hat{D}^{(\Gamma_2)\dagger}(p). \tag{3.2.20}$$

Similarly, Eq. (3.2.7) leads to,

$$\Psi_i^{\Gamma} = \sum_{\boldsymbol{k}} \sum_{\Gamma_1\Gamma_2} \sum_{j_1 j_2} \left[\hat{\varphi}_i^{\Gamma}(\boldsymbol{k}; \Gamma_1\Gamma_2)\right]_{j_1 j_2} c^{\dagger}_{\Gamma_1 j_1}(\boldsymbol{k}) c^{\dagger}_{\Gamma_2 j_2}(-\boldsymbol{k}), \tag{3.2.21}$$

$$\hat{D}^{(\Gamma_1)}(p)\hat{\varphi}_i^{\Gamma}(p^{-1}\boldsymbol{k}; \Gamma_1\Gamma_2)(\hat{D}^{(\Gamma_2)}(p))^T = \sum_j \hat{\varphi}_j^{\Gamma}(\boldsymbol{k}; \Gamma_1\Gamma_2)\mathcal{D}^{(\Gamma)}_{ji}(p). \tag{3.2.22}$$

Equation (3.2.22) indicates that $\hat{\varphi}_i^{\Gamma}(\boldsymbol{k}; \Gamma_1\Gamma_2)$ with Γ irreducible representation can be obtained from the subduction $\Gamma_{\boldsymbol{k}} \otimes (\Gamma_1 \otimes \Gamma_2)\downarrow P$ [See Eq. (3.1.6)], where $\Gamma_{\boldsymbol{k}}$ denotes the irreducible representation of the momentum transform: $\hat{\varphi}_i^{\Gamma}(\boldsymbol{k}) \overset{p}{\mapsto} \hat{\varphi}_i^{\Gamma}(p^{-1}\boldsymbol{k})$.

Note that Eq. (3.2.20) is similar to the case of $\Gamma = A_{1g}$ in Eq. (3.2.22), apart from the irreducible representation for the Kramers sector. It is given by $\Gamma_1 \otimes \Gamma_2$ for (3.2.22), while $\Gamma_1 \otimes \Gamma_2^*$ for (3.2.20). Therefore, the tables derived in this chapter will be helpful also in constructing a generic tight-binding model in multiorbital systems.

Finally, let us comment on non-symmorphic systems. In this case, the above discussion is no longer applicable due to inevitable $\boldsymbol{k}$ dependence in the phase factor of $\hat{U}(g; \boldsymbol{k})$. An available alternative method [138, 139, 3] is the classification based on a little group at a given $\boldsymbol{k}$ point. This is applicable in both symmorphic and non-symmorphic systems and discussed in detail in Chapter 4.

3.3 Band based representations

So far, we have discussed the pair amplitudes and their basis functions in orbital based representations. Here, let us examine the relation between the orbital based and the band based representations, since many observables strongly depend on the (band based) energy gap on the Fermi surfaces.

3.3.1 Nodal structure in band basis

As usual, an intra-band Cooper pair amplitude can be defined by (the band index omitted),

$$\tilde{F}_{\sigma\sigma'}(\boldsymbol{k}) = \left[\Big(\Phi(\boldsymbol{k})\sigma^0 + \boldsymbol{d}(\boldsymbol{k})\cdot\boldsymbol{\sigma}\Big) i\sigma_y\right]_{\sigma\sigma'}, \tag{3.3.1}$$

with *pseudo*-spin-singlet amplitude $\Phi(\boldsymbol{k})$ and triplet $\boldsymbol{d}(\boldsymbol{k})$. Strictly, *pseudo*-spin $\sigma(\sigma') = \uparrow, \downarrow$ is the Kramers index for a given band. From Eqs. (3.1.1) and (3.1.2), one can obtain the relation between the band and the orbital based pair amplitudes,

$$\tilde{F}_{\sigma\sigma'}(\boldsymbol{k}) = \sum_{\ell\alpha,\ell'\alpha'} u^*_{\ell\alpha,\sigma}(\boldsymbol{k}) u^*_{\ell'\alpha',\sigma'}(-\boldsymbol{k}) F_{\ell\alpha,\ell'\alpha'}(\boldsymbol{k}). \tag{3.3.2}$$

Before discussing the details, let us explain our phase convention. We use a convention that the degenerate pair for a given $\boldsymbol{k}$ satisfies

$$(\theta I)c^\dagger_{\ell\pm}(\boldsymbol{k})(\theta I)^{-1} = \mp c^\dagger_{\ell\mp}(\boldsymbol{k}), \tag{3.3.3}$$

under the time reversal (θ) and spatial inversion (I) operations. Using this convention, one obtains

$$u_{\ell+,\uparrow}(\boldsymbol{k}) = (-1)^{P_\ell} u^*_{\ell-,\downarrow}(\boldsymbol{k}), \tag{3.3.4a}$$
$$u_{\ell+,\downarrow}(\boldsymbol{k}) = (-1)^{P_\ell+1} u^*_{\ell-,\uparrow}(\boldsymbol{k}), \tag{3.3.4b}$$

where P_ℓ is the parity of the orbital ℓ. Furthermore, in centrosymmetric systems, one can take

$$u_{\ell\alpha,\sigma}(\boldsymbol{k}) = u_{\ell\alpha,\sigma}(-\boldsymbol{k})(-1)^{\bar{P}_\ell}, \tag{3.3.5}$$

with $\bar{P}_\ell \equiv P_\ell + P_0$, where P_0 is the parity for a reference orbital ℓ_0 of the band electron concerned (See the definition of ℓ_0 below).

Although the sum of $\ell(\ell')$ in Eq. (3.3.2) contains all of orbitals, it is sufficient to consider the case of two orbitals $\ell(\ell') = 1, 2$ in the discussion below. In Eq. (3.1.7), $F_{\ell\alpha,\ell'\alpha'}(\boldsymbol{k})$ is expressed by $d^{\mu\nu}_{\ell\ell'}(\boldsymbol{k})$, which is related to $\Phi(\boldsymbol{k})$ and $\boldsymbol{d}(\boldsymbol{k})$ in the following way,

$$\begin{pmatrix} \Phi(\boldsymbol{k}) \\ \boldsymbol{d}(\boldsymbol{k}) \end{pmatrix} = (-1)^{\bar{P}_\ell} \sum_{s=\pm} \sum_{\nu=0,x,y,z} \mathcal{W}^s_\nu(\boldsymbol{k}) \begin{pmatrix} d^{0\nu}_s(\boldsymbol{k}) \\ \vec{d}^{\,\nu}_s(\boldsymbol{k}) \end{pmatrix}, \tag{3.3.6}$$

with $[\vec{d}^{\,\nu}_s(\boldsymbol{k})]_\mu = d^{\mu\nu}_s(\boldsymbol{k})$, $d^{\mu\nu}_\pm = \frac{1}{2}(d^{\mu\nu}_{12} \pm d^{\mu\nu}_{21})$, and $\mathcal{W}^s_\nu(\boldsymbol{k})$ are transformation matrices defined below. When the two orbitals have the same parity $P_1 = P_2$, due to the fermion antisymmetry, only $\mathcal{W}^+_{0,x,z}$ and $\mathcal{W}^-_y$ are non-vanishing, and the others are zero;

$$\mathcal{W}^+_\nu(\boldsymbol{k}) = \begin{pmatrix} w^0_{0\nu} & 0 & 0 & 0 \\ \vec{0} & -\vec{w}_{x\nu} & \vec{w}_{y\nu} & -\vec{w}_{z\nu} \end{pmatrix}, \tag{3.3.7a}$$

$$\mathcal{W}^-_y(\boldsymbol{k}) = i \begin{pmatrix} 0 & -w^0_{xy} & w^0_{yy} & -w^0_{zy} \\ \vec{w}_{0y} & \vec{0} & \vec{0} & \vec{0} \end{pmatrix}, \tag{3.3.7b}$$

where $\nu = 0, x$, and z. Here, $\vec{0} = (0, 0, 0)^T$ and

$$w^0_{\mu\nu} = (-1)^{P_\ell}(u\sigma^\mu\tau^\nu u^*), \tag{3.3.8a}$$
$$\vec{w}_{\mu\nu} = \left[\mathrm{Re}(u\bar{\sigma}^\mu\tau^\nu u), \mathrm{Im}(u\bar{\sigma}^\mu\tau^\nu u), -w^0_{\mu\nu}\right]^T, \tag{3.3.8b}$$

with

$$(u\sigma^{\mu}\tau^{\nu}u') \equiv \sum_{\alpha\alpha'}^{\pm}\sum_{\ell\ell'}^{1,2} u_{\ell\alpha,\uparrow}(\boldsymbol{k})\sigma^{\mu}_{\alpha\alpha'}\tau^{\nu}_{\ell\ell'}u'_{\ell'\alpha',\uparrow}(\boldsymbol{k}), \tag{3.3.9}$$

and $\sigma^{\mu} \to \bar{\sigma}^{\mu}$. Even when the two parities are different $P_1 \neq P_2$, $\mathcal{W}^{s}_{\nu}$ can be easily obtained by multiplying (-1) and replacing $\mathcal{W}^{\pm}_{\nu} \to \mathcal{W}^{\mp}_{\nu}$ in Eqs. (3.3.7a) and (3.3.7b). Note also that in this case, $\mathcal{W}^{\pm}_{\nu}(\boldsymbol{k}) = -\mathcal{W}^{\pm}_{\nu}(-\boldsymbol{k})$ holds from Eq. (3.3.5).

Equation (3.3.6) indicates that $\tilde{F}_{\sigma\sigma'}(\boldsymbol{k})$ is the product of $\mathcal{W}^{s}_{\nu}(\boldsymbol{k})$ and the orbital based $F_{\ell\alpha,\ell\alpha'}(\boldsymbol{k})$. Thus, the $\boldsymbol{k}$ dependence of $\mathcal{W}^{\pm}_{\nu}(\boldsymbol{k})$ can yield additional nodes in the band based gap functions [140]. We will discuss this aspect in Sec. 3.4, but before that, we need to explain how to fix the phase ambiguity involved in $\mathcal{W}^{\pm}_{\nu}(\boldsymbol{k})$.

Generally, when the time reversal and space inversion symmetries are held, $\mathcal{W}^{\pm}_{\nu}(\boldsymbol{k})$ is accompanied by at least U(2) phase ambiguity for every band and at every $\boldsymbol{k}$ point, due to the U(1) gauge and the Kramers degeneracy. In order to remove such ambiguity, a natural phase fixing procedure is necessary. Here, we consider assigning an irreducible representation of the point group to each band n in such a way that the irreducible representation corresponds to that of the dominant orbital ℓ_0 for the band n. Indeed, the choices of the irreducible representations are arbitrary, but the above choice is one of natural ways as explained below. This can be performed by the following procedure; for the dominant orbital component ℓ_0 in the band n, $u_{\ell_0\pm,n\mp}(\boldsymbol{k})$ are set to zero and $u_{\ell_0\pm,n\pm}(\boldsymbol{k})$ to a real number, respectively (see Sec. 3.3.2). This way of the phase convention naturally connects generic situations to the orbital-diagonal limit, where there exist no hybridizations between different orbitals. With this, the band n and the main orbital ℓ_0 have the same symmetry without ambiguity. Therefore, Tables 3.4-3.6 are still valid in the band based Cooper pairs (see Sec. 3.3.3).

Using the phase-fixed bases, one can discuss the additional nodes through $\mathcal{W}^{\pm}_{\nu}(\boldsymbol{k})$. Information of the irreducible representation in the orbital based Cooper pairs is encoded in $\mathcal{W}^{\pm}_{\nu}(\boldsymbol{k})$, and thus, $\mathcal{W}^{\pm}_{\nu}(\boldsymbol{k})$ can possess nodes if this belongs to an anisotropic irreducible representations. Equation (3.3.6) means that the $\boldsymbol{k}$ dependence of the band based pair amplitudes is determined by a product of $\mathcal{W}^{\pm}_{\nu}(\boldsymbol{k})$ and the orbital based ones. This implies that even local orbital pairs can be transformed into anisotropic ones in the band representation, and also non-A_{1g} inter-orbital pairs can lead to an anisotropic A_{1g} band based pairs in connection with non-A_{1g} $\mathcal{W}^{\pm}_{\nu}(\boldsymbol{k})$. In the following section, we will discuss these mechanisms to realize anisotropic superconductivity in detail.

3.3.2 Phase fixing procedure

Here, we describe a procedure to fix the U(2) phase ambiguity in the band based representation, and demonstrate that the gap structure looks apparently different, depending on the choice of the fixed phase, although the structure of excitations is unchanged.

Let us consider an N-orbital system. If all the orbitals are independent and not hybridized with each other, then any electron in the band representation consists of single orbital; a unitary matrix $u(\boldsymbol{k})$ is an identity matrix. No matter how complicated the band structure is, we can line up orbital indices in such a way that the dominant orbital in each band is arranged in a diagonal position of the matrix $u(\boldsymbol{k})$. After this procedure, we now fix the U(2) gauge.

Under the presence of the space inversion and time reversal symmetries, the following relation holds

$$(\theta I)\, c^{\dagger}_{n\sigma}(\boldsymbol{k})\, (\theta I)^{-1} = \sum_{\sigma'} c^{\dagger}_{n\sigma'}(\boldsymbol{k})(i\sigma^y)_{\sigma'\sigma}. \tag{3.3.10}$$

Substituting Eq. (3.1.1) into the both sides of Eq. (3.3.10), we obtain,

$$u_{\ell\alpha,n\sigma}(\boldsymbol{k}) = (-1)^{P_\ell} \sum_{\alpha'\sigma'} (i\sigma^y)_{\alpha\alpha'} u^*_{\ell\alpha',n\sigma'}(\boldsymbol{k})(i\sigma^y)^{\dagger}_{\sigma'\sigma}, \tag{3.3.11}$$

where P_ℓ is the parity of the orbital ℓ. In what follows, we focus on the 2×2 submatrix $\hat{u}(\boldsymbol{k}; \ell n)$, where $\left[\hat{u}(\boldsymbol{k}; \ell n)\right]_{\alpha\sigma} \equiv u_{\ell\alpha,n\sigma}(\boldsymbol{k})$. From Eq. (3.3.11), we find that each submatrix $\hat{u}(\boldsymbol{k}; \ell n)$ satisfies,

$$\hat{u}(\boldsymbol{k}; \ell n)\hat{u}^{\dagger}(\boldsymbol{k}; \ell n) = |\det \hat{u}(\boldsymbol{k}; \ell n)| I_{2\times 2}, \tag{3.3.12}$$

which is independent of P_ℓ. Here, $I_{2\times 2}$ is the 2×2 identity matrix. Let us consider the following matrix,

$$\hat{K}_n(\boldsymbol{k}) = \frac{1}{\sqrt{|\det \hat{u}(\boldsymbol{k}; nn)|}} \hat{u}(\boldsymbol{k}; nn). \tag{3.3.13}$$

Then, the U(2) phase ambiguity can be fixed by redefining the unitary matrix as follows,

$$\tilde{u}_{\ell\alpha,n\sigma}(\boldsymbol{k}) = \left[\hat{u}(\boldsymbol{k}; \ell n)\hat{K}^{\dagger}_n(\boldsymbol{k})\right]_{\alpha\sigma}. \tag{3.3.14}$$

Indeed, this matrix diagonalizes H_0, and the phase for $\ell = n$ component is fixed to be positive real as,

$$\tilde{u}_{n\alpha,n\sigma}(\boldsymbol{k}) = \sqrt{|\det \hat{u}(\boldsymbol{k}; nn)|}\delta_{\alpha\sigma}. \tag{3.3.15}$$

In the following sections, $u(\boldsymbol{k})$ means this $\tilde{u}(\boldsymbol{k})$, unless otherwise noted. It should be noted that the unitary matrix preserves the Kramers label α for each orbital. In other words, if the nth orbital belongs to a Γ irreducible representation, the corresponding band electron also belongs to the same Γ irreducible representation. It is useful to discuss the nodal positions in the band based gap functions as will be shown in Secs. 3.3.3 and 3.3.4. In addition, the unitary matrix obtained in the above way smoothly connects to the $2N \times 2N$ identity

matrix in the limit where there is no hybridization between different orbitals, which is one of desirable properties as a diagonalizing matrix.

Note that the gap structure in the multiorbital systems strongly depends on the way of the phase fixing, although observable quantities are unchanged. Depending on the way, meaningless complicated structure can appear in the obtained gap structure. We will demonstrate this point in Sec. 3.3.4.

3.3.3 Symmetry of unitary matrix and band based pair amplitude

Here, let us study the symmetry of the unitary matrix $u_{\ell\alpha,n\sigma}(\boldsymbol{k})$. In our case, due to the phase fixing mentioned in Sec. 3.3.2, we can explicitly discuss the symmetry. In actual calculations, we first diagonalize H_0 in the irreducible Brillouin zone. At this stage, the obtained unitary matrix still has an arbitrary phase. Then, we fix the phase, following the procedure explained in Sec. 3.3.2. The unitary matrix in the whole first Brillouin zone can be obtained by the following transformation,

$$\hat{u}(p\boldsymbol{k};\ell n) = \hat{D}^{(\Gamma_\ell)}(p)\hat{u}(\boldsymbol{k};\ell n)\hat{D}^{(\Gamma_n)\dagger}(p), \tag{3.3.16}$$

where $\Gamma_\ell(\Gamma_n)$ denotes irreducible representations of $\ell(n)$, and $\boldsymbol{k}$ is in the irreducible Brillouin zone. Note that Eq. (3.3.16) is similar to Eq. (3.2.20). This indicates that our unitary matrix has the same structure as $\hat{h}(\boldsymbol{k})$ with respect to the symmetry. From this property, the symmetry of the band based gap functions is readily available from that of orbital based ones.

Indeed, using Eqs. (3.2.18) and (3.3.16), we obtain

$$\begin{aligned} p\,\tilde{c}^\dagger_{n\sigma}(\boldsymbol{k})\,p^{-1} &= \sum_{\ell\alpha\alpha'} c^\dagger_{\ell\alpha}(p\boldsymbol{k})\Big[\hat{D}^{(\Gamma_\ell)}(p)\Big]_{\alpha\alpha'} u_{\ell\alpha',n\sigma}(\boldsymbol{k}) \\ &= \sum_{\ell\alpha\sigma'} c^\dagger_{\ell\alpha}(p\boldsymbol{k}) u_{\ell\alpha,n\sigma'}(p\boldsymbol{k})\Big[\hat{D}^{(\Gamma_n)}(p)\Big]_{\sigma'\sigma} \\ &= \sum_{\sigma'} \tilde{c}^\dagger_{n\sigma'}(p\boldsymbol{k})\Big[\hat{D}^{(\Gamma_n)}(p)\Big]_{\sigma'\sigma}. \end{aligned} \tag{3.3.17}$$

This transformation property for the band n is the same as the orbital based case in Eq. (3.2.18). Therefore, when we consider the band based pair amplitude,

$$\tilde{F}_{n\sigma,n'\sigma'}(\boldsymbol{k}) \equiv \langle \tilde{c}_{n\sigma}(\boldsymbol{k})\tilde{c}_{n'\sigma'}(-\boldsymbol{k})\rangle, \tag{3.3.18}$$

the symmetry arguments in Sec. 3.1 hold for this band based gap functions. Also it is evident that Tables 3.4-3.6 are valid. However, such band based arguments are insufficient to understand a variety of multiorbital superconductivity, because the pairing interactions can be more clearly defined in the orbital based representation. Indeed, in the band based representation, we will miss the presence of additional nodes as discussed in Sec. 3.4, which

are not symmetry protected but inevitable from the orbital based viewpoint. Thus, it is clear that the unitary matrix $u_{\ell\alpha,n\sigma}(\boldsymbol{k})$ can possess significant information about $\boldsymbol{k}$ dependence of gap functions.

3.3.4 Efficacy of the phase fixing

Finally, let us demonstrate an advantage of our phase fixing method. We consider a two-orbital model constructed from Γ_{7g} and Γ_{9g} orbitals in D_{6h} group. The general form of $\hat{h}(\boldsymbol{k})$ in Eq. (3.2.1) is given as

$$\begin{aligned}\hat{h}(\boldsymbol{k}) = h_1^{A_{1g}}\tau^0\sigma^0 + h_2^{A_{1g}}\tau^z\sigma^0 + h_1^{E_{1g}}\tau^y\sigma^x \\ - h_2^{E_{1g}}\tau^x\sigma^y + h_1^{E_{2g}}\tau^y\sigma^z + h_2^{E_{2g}}\tau^x\sigma^0,\end{aligned} \tag{3.3.19}$$

where $h_{1,2}^{\Gamma}$ consists of basis functions of Γ irreducible representations:

$$\begin{aligned}h_1^{A_{1g}} &= -t_0\Big(\cos\sqrt{3}k_x + 2\cos\frac{\sqrt{3}k_x}{2}\cos\frac{3k_y}{2}\Big) - \mu, \\ h_2^{A_{1g}} &= -t_1, \quad h_1^{E_{1g}} = t_2 s'_x \sin k_z, \quad h_2^{E_{1g}} = t_2 s'_y \sin k_z, \\ h_1^{E_{2g}} &= 2t_3 s'_x s'_y, \quad h_2^{E_{1g}} = t_3(s'^2_x - s'^2_y),\end{aligned}$$

with

$$\begin{aligned}s'_x &= \sin\sqrt{3}k_x + \sin\frac{\sqrt{3}k_x}{2}\cos\frac{3k_y}{2}, \\ s'_y &= \sqrt{3}\sin\frac{3k_y}{2}\cos\frac{\sqrt{3}k_x}{2}.\end{aligned}$$

Here, we set t_0 to the unit of energy and $(t_1, t_2, t_3) = (0.25, 0.05, 0.05)$ and $\mu = -1.20$. With these parameters, the dominant component of the lower (upper) band is almost composed of $\Gamma_{7g}(\Gamma_{9g})$ orbital. Below, we will focus on the band mainly composed of Γ_{9g} and will not discuss the other band for simplicity.

For example, let us consider one of E_{2u} pairing states in Γ_{9g} orbital, i.e., $\phi_1^{E_{1u}}\boldsymbol{y}$ for $\Gamma_9 \otimes \Gamma_9$ pairs in Table 3.6:

$$\hat{\varphi}^{E_{2u}}(\boldsymbol{k}) = \phi_1^{E_{1u}}(\boldsymbol{k})(\tau^0 - \tau^z)\boldsymbol{y}, \tag{3.3.20}$$

with $\phi_1^{E_{1u}}(\boldsymbol{k}) = s'_x$. Here, $\tau^0 - \tau^z$ represents the pair in $\Gamma_9 \otimes \Gamma_9$. In Fig. 3.1, we illustrate the band based gap function for the lower band, which is evaluated via Eq. (3.3.2). Figures 3.1(a), (b) and (c) depict, respectively, d_x, d_y, and d_z components with our phase fixing method, where the upper (lower) band is smoothly connected with the $\Gamma_{7g}\,(\Gamma_{9g})$ orbital. Through the unitary matrix, d_x and d_z components are induced, but the magnitude is very small. d_y component is almost the same as $\phi_1^{E_{1u}}(\boldsymbol{k})$ given in Eq. (3.3.20). In contrast, one can see the

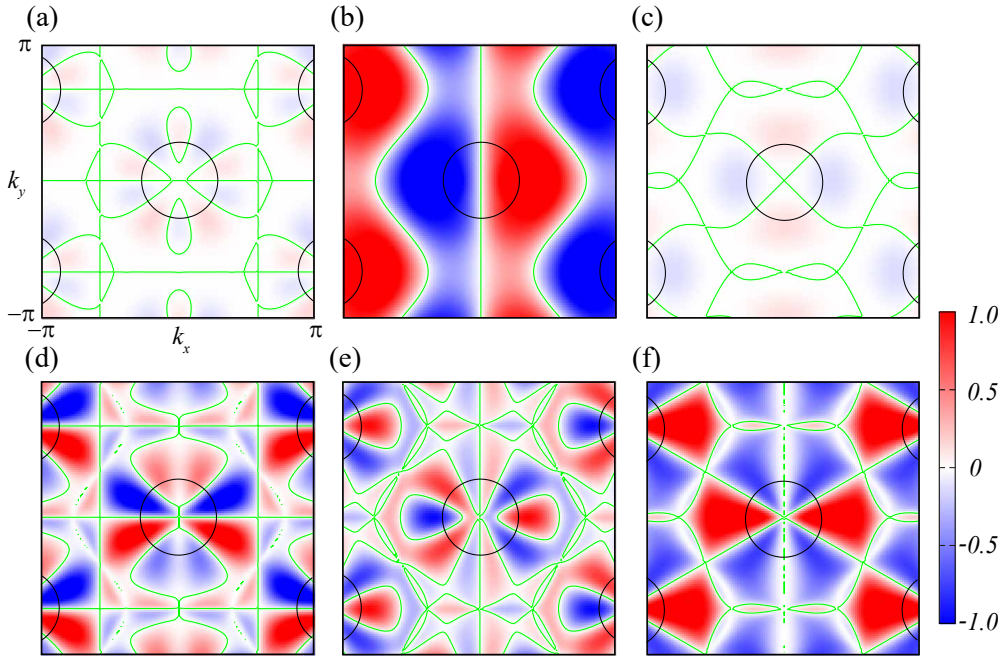

Figure 3.1: Band-based gap functions of the lower band in $k_z = \pi$ plane. (a) d_x, (b) d_y, and (c) d_z components of the band based gap functions are obtained by our phase fixing procedure, where the Kramers index is labeled by that of the major Γ_{9g} orbital. (d) d_x, (e) d_y, and (f) d_z components of the gap functions, labeled by the Kramers index of the minor Γ_{7g} orbital. Green dashed lines denote gap nodes.

complicated gap structures in Figs. 3.1(d)-(f), the magnitudes of which are comparable to each other. Here, the Kramers index for the lower band is labeled by that for the minor Γ_{7g} orbital. At a glance, there seem to exist complicated additional nodes. The gap amplitude $\sqrt{|\boldsymbol{d}|}$, however, is identical to that shown in Figs. 3.1(a)-(c), and is independent of the way of the phase fixing. This demonstrates that our phase fixing method is effective and useful in the discussion about the gap structures in the multiorbital systems.

3.4 Applications : Superconductivity mediated by multipole fluctuations

In this section, we discuss (i) the pairing states emerging in close proximity to (anti-)ferroic quadrupole ordering, (ii) a mechanism of anisotropic s-wave (A_{1g}) pairing state, and (iii) anisotropic pairing states mediated by local fluctuations. The case (i) is a generalization of spin-fluctuation mechanism; d-wave pairing state [9, 10] next to antiferromagnetic phases, or p-wave to ferromagnetic phases. We will discuss these features unique to multiorbital

superconductors. Here, we focus on gap functions rather than the Cooper pair amplitudes, since the former can be more easily obtained in actual calculations.

3.4.1 Γ_8 model in a cubic lattice

First, let us consider a model with non-Kramers doublet Γ_{8u} on a simple-cubic lattice. It may be related to recently discovered superconductivity in Pr-based 1-2-20 compounds [141, 142]. Local bases $|\Gamma_{8a,b};\pm\rangle$ are fourfold degenerate with the orbital a, b and the Kramers degeneracy $\pm$. For simplicity, as a pairing interaction $H_{\rm int}$, we take the nearest-neighbor E_g-orbital (quadrupole) fluctuations,

$$H_{\rm int} = \frac{1}{N}\sum_{\boldsymbol{q}}\sum_{i} v(\boldsymbol{q})\mathcal{M}_{E_g^i}(-\boldsymbol{q})\mathcal{M}_{E_g^i}(\boldsymbol{q}), \tag{3.4.1}$$

$$\mathcal{M}_{E_g^i}(\boldsymbol{q}) = \sum_{\boldsymbol{k}}\sum_{12}\left[\hat{M}_{E_g^i}\right]_{12} c_1^\dagger(\boldsymbol{k})c_2(\boldsymbol{k}+\boldsymbol{q}), \tag{3.4.2}$$

where the sum of 1(2) symbolically represents the sum of the fourfold local bases $|\Gamma_{8a,b};\pm\rangle$, and the matrices of the multipole part $\hat{M}_{E_g^i}$ are defined by

$$\hat{M}_{E_g^1} = \frac{\tau^z\sigma^0}{2}, \qquad \hat{M}_{E_g^2} = \frac{\tau^x\sigma^0}{2}. \tag{3.4.3}$$

Thus, $[\tau^\nu\sigma^\mu]_{12} = \tau^\nu_{a_1a_2}\sigma^\mu_{\sigma_1\sigma_2}$ with $a_j = a$ or b and $\sigma_j = \pm$. The momentum dependence of the pairing interaction is $v(\boldsymbol{q}) = 2v(c_x + c_y + c_z)$, where v is a constant, $c_\mu = \cos q_\mu$ $(\mu = x, y, z)$ and the lattice constant is set to unity. Note that the normalization condition $\mathrm{Tr}\left[\hat{M}_{E_g^i}\hat{M}^\dagger_{E_g^j}\right] = \delta_{ij}$ is satisfied, where Tr is taken for both the orbital and the Kramers indices.

Now, let us solve a superconducting gap equation within the mean field theory. It is convenient to decouple Eq. (3.4.1) into each Cooper channel. To this end, we rewrite $v(\boldsymbol{q})$ as follows,

$$v(\boldsymbol{k}-\boldsymbol{k}') = v\sum_{\Gamma}\sum_{i}\phi_i^\Gamma(\boldsymbol{k})\phi_i^\Gamma(\boldsymbol{k}'), \tag{3.4.4}$$

where Γ runs over A_{1g}, E_g, and T_{2g} irreducible representations, and i is the label for different bases in E_g and T_{2g}. The basis functions $\phi_i^\Gamma(\boldsymbol{k})$ are defined as follows,

$$\phi^{A_{1g}} = \sqrt{\tfrac{2}{3}}\left(c_x + c_y + c_z\right), \tag{3.4.5a}$$

$$\phi_1^{E_g} = \tfrac{1}{\sqrt{3}}\left(2c_z - c_x - c_y\right), \tag{3.4.5b}$$

$$\phi_2^{E_g} = c_x - c_y, \tag{3.4.5c}$$

$$\phi_\mu^{T_{1u}} = \sqrt{2}s_\mu, \qquad (\mu = x, y, z) \tag{3.4.5d}$$

with $s_\mu = \sin k_\mu$. These basis functions meet the orthonormality condition:

$$\frac{1}{N}\sum_{\boldsymbol{k}} \phi_i^{\Gamma}(\boldsymbol{k})\Big(\phi_j^{\Gamma'}(\boldsymbol{k})\Big)^* = \delta_{ij}\delta_{\Gamma\Gamma'}. \tag{3.4.6}$$

Then, we can decompose the pairing interaction into the zero-momentum Cooper channels,

$$H_{\rm int} = -\frac{1}{2N}\sum_{\Gamma\alpha}\sum_{i} v_\alpha^{\Gamma}\ \Psi^\dagger_{\Gamma i,\alpha}\Psi_{\Gamma i,\alpha}, \tag{3.4.7}$$

$$\Psi^\dagger_{\Gamma i,\alpha} = \sum_{\boldsymbol{k}}\sum_{12}\Big[\hat{\varphi}^{\Gamma}_{\alpha,i}(\boldsymbol{k})\Big]_{12} c_1^\dagger(\boldsymbol{k})c_2^\dagger(-\boldsymbol{k}). \tag{3.4.8}$$

Here, the form factor $\hat{\varphi}^{\Gamma}_{\alpha,i}(\boldsymbol{k})$, which will be calculated below and shown in Eqs. (3.4.11) and (3.4.12), is regarded as a basis function of the Cooper channel labeled by Γ, i, and α. The $\boldsymbol{k}$ dependence of gap functions is determined by one or a linear combination of $\hat{\varphi}^{\Gamma}_{\alpha,i}(\boldsymbol{k})$.

For the decomposition into the Cooper channels, it is convenient to use the following identity

$$2\sigma^0_{14}\sigma^0_{23} = \sum_\mu \bar{\sigma}^\mu_{12}\bar{\sigma}^{\mu *}_{43}, \tag{3.4.9}$$

and similar ones for the orbital components. Signs arising from these decomposition are summarized in Table 4.3, which is also useful to understand what kinds of Cooper channel are attractive. In the present case, we obtain the following decomposition,

$$\sum_{i=z,x}[\tau^i\sigma^0]_{14}[\tau^i\sigma^0]_{23} = \frac{1}{2}\sum_\mu\Big([\tau^0\bar{\sigma}^\mu]_{12}[\tau^0\bar{\sigma}^\mu]^*_{43} - [\tau^y\bar{\sigma}^\mu]_{12}[\tau^y\bar{\sigma}^\mu]^*_{43}\Big). \tag{3.4.10}$$

This indicates that the pairing interaction is v for o-singlet, and $-v$ for o-triplet.

Now, let us illustrate a possible phase diagram. In the case of $v > 0$ (antiferroic E_g fluctuations), the o-singlet channels $\tau^y\bar{\sigma}^\mu$ in Eq. (3.4.10) is attractive. Thus, the gap functions for the following channels can be realized;

$$\phi^{A_{1g}}\eta^\nu\boldsymbol{\mu},\ \phi^{E_g}_{1,2}\eta^\nu\boldsymbol{\mu},\ \phi^{T_{1u}}_\mu\tau^y\mathbf{0}, \tag{3.4.11}$$

which belong to, respectively, T_{2g}, $T_{2g,1g}$, and T_{2u} irreducible representations in Table 3.4. Following the symmetrization procedure in Sec. 3.1.3, we find that $\boldsymbol{\mu} = \mathbf{0}$ components in Eq. (3.4.11) are forbidden due to the fermion antisymmetry, since $\phi^{A_{1g}}(\boldsymbol{k})$ and $\phi^{E_g}(\boldsymbol{k})$ are even functions in $\boldsymbol{k}$. Thus, it is natural that the superconducting states in close proximity to an antiferroic quadrupole ordered phase belong to three-dimensional representations. In this regards, it is very interesting to explore what kinds of superconducting state are realized in Pr-based 1-2-20 compounds under high pressures, where the quadrupole order is suppressed.

Next, in the case of $v < 0$ (ferroic quadrupole fluctuations), o-triplet channels $\tau^0\bar{\sigma}^\mu$ in Eq. (3.4.10) are favored. The gap functions in attractive channels are

$$\phi^{A_{1g}}\tau^0\mathbf{0},\ \phi^{E_g}_{1,2}\tau^0\mathbf{0},\ \phi^{T_{1u}}_\mu\zeta^\nu\boldsymbol{\mu}, \tag{3.4.12}$$

Table 3.7: Signs $c^i_{\mu\nu}$ involved in the decomposition from particle-hole (ph) to the Cooper channels: $2\tau^{\mu}_{a_1a_4}\tau^{\mu}_{a_2a_3} = \sum_\nu c^1_{\mu\nu}\tau^{\nu}_{a_1a_2}\tau^{\nu*}_{a_4a_3}$ for the orbital sector, and $2\sigma^{\mu}_{\sigma_1\sigma_4}\sigma^{\mu}_{\sigma_2\sigma_3} = \sum_\nu c^2_{\mu\nu}\bar{\sigma}^{\nu}_{\sigma_1\sigma_2}\bar{\sigma}^{\nu*}_{\sigma_4\sigma_3}$ for the spin sector.

ph-channels	Cooper channels			
	$\tau^0\tau^{0*}$	$\tau^x\tau^{x*}$	$\tau^y\tau^{y*}$	$\tau^z\tau^{z*}$
$2\tau^0\tau^0$	1	1	1	1
$2\tau^x\tau^x$	1	1	-1	-1
$2\tau^y\tau^y$	-1	1	-1	1
$2\tau^z\tau^z$	1	-1	-1	1
	$\bar{\sigma}^0\bar{\sigma}^{0*}$	$\bar{\sigma}^x\bar{\sigma}^{x*}$	$\bar{\sigma}^y\bar{\sigma}^{y*}$	$\bar{\sigma}^z\bar{\sigma}^{z*}$
$2\sigma^0\sigma^0$	1	1	1	1
$2\sigma^x\sigma^x$	-1	-1	1	1
$2\sigma^y\sigma^y$	-1	1	-1	1
$2\sigma^z\sigma^z$	-1	1	1	-1

which belong to, respectively, A_{1g}, E_g, and $\{A_{1u},\ E_u,\ T_{1u,2u}\}$ irreducible representations. Again, the fermion antisymmetry requires $\boldsymbol{\mu \neq 0}$ in Eq. (3.4.12). It should be noted that the intersite fluctuations can lead to an A_{1g} pairing state.

Finally, let us illustrate schematic phase diagrams expected for antiferroic fluctuations in Fig. 3.2(a) and for ferroic ones in Fig. 3.2(b). The superconducting states in Fig. 3.2(a) are expected to be three dimensional representations, while, in Fig. 3.2(b), there are several candidates for the superconductivity within the present analysis. Fluctuations beyond the mean field approximation may favor some of the gap functions. Elaborated calculations are needed to clarify this. Note that the present results are based on a simple model, and the details depend on the electronic structures in actual materials.

It is often hard to observe quadrupole orderings experimentally. Several materials have been reported to exhibit quadrupole orders; CeB_6 [134, 143], $PrPb_3$ [144, 145], Pr-based 1-2-20 compounds [146] and so on. As far as we know, among these systems, superconductivity is observed only in Pr-based 1-2-20 compounds [141, 142]. Strictly speaking, as Pr-based 1-2-20 compounds are non-symmorphic systems, our theory is not directly applicable. However, the pressure-temperature phase diagram for PrV_2Al_{20} is similar to Fig. 3.2(a). We can expect the emergence of unconventional three-dimensional superconductivity mentioned above.

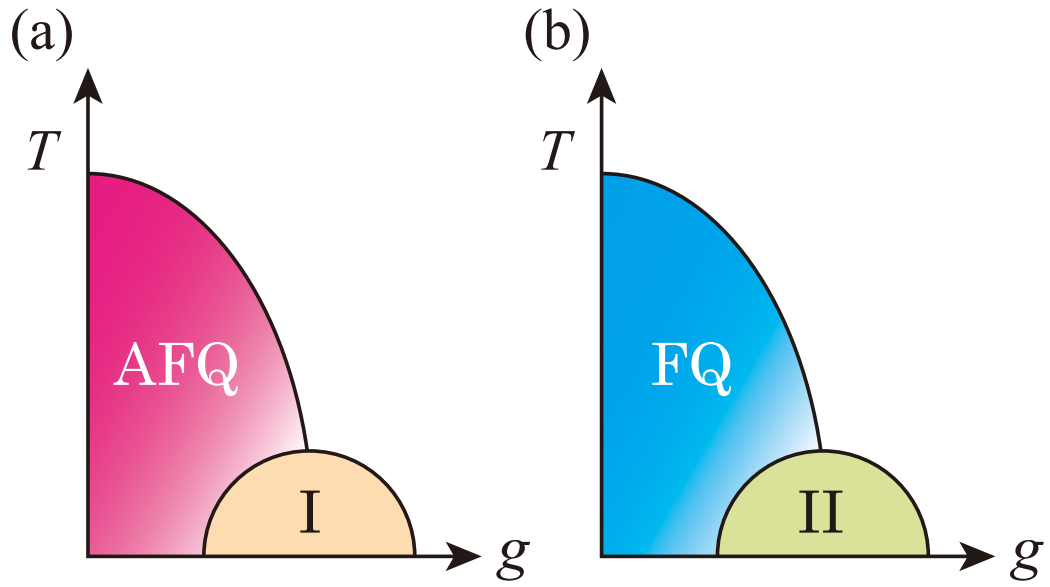

Figure 3.2: Schematic phase diagram near (a) antiferroic and (b) ferroic quadrupole (E_g) ordered phase as a function of temperature T and a control parameter g, such as pressures. irreducible representations of the obtained superconductivity belong to $T_{1g}, 2T_{2g}$, and T_{2u} in the region I, while $A_{1g}, A_{1u}, E_g, E_u, T_{1u}$, and T_{2u} in the region II.

3.4.2 Γ_{6u} and Γ_{7u} model in a tetragonal lattice

The second example is a two-orbital model with p_x/p_y orbitals in a two dimensional square lattice with D_{4h} symmetry. This corresponds to a model for BiS_2-layered superconductors, $LaO_{1-x}F_xBiS_2$ [147]. Under D_{4h} symmetry, p_x and p_y orbitals are classified into Γ_{6u} and Γ_{7u};

$$c^\dagger_{\Gamma_{6u},\pm} = \frac{1}{\sqrt{2}}\left(ic^\dagger_{p_x,\mp} \mp c^\dagger_{p_y,\mp}\right), \tag{3.4.13a}$$

$$c^\dagger_{\Gamma_{7u},\pm} = \frac{1}{\sqrt{2}}\left(ic^\dagger_{p_x,\mp} \pm c^\dagger_{p_y,\mp}\right). \tag{3.4.13b}$$

Here, $c^\dagger_{p_{x,y},\sigma}$ is the creation operator for the $p_{x,y}$ orbital with the *pure*-spin $\sigma = \pm$, while $c^\dagger_{\Gamma_{6u,7u},\alpha}$ is that for the $\Gamma_{6u,7u}$ orbital with the Kramers degrees of freedom $\pm$. In terms of $c^\dagger_{\Gamma_{6u,7u},\alpha}$, we define the non-interacting Hamiltonian by

$$H_0 = \sum_{\boldsymbol{k}}\sum_{12}\left[\hat{h}(\boldsymbol{k})\right]_{12} c^\dagger_1(\boldsymbol{k})c_2(\boldsymbol{k}), \tag{3.4.14}$$

with

$$\hat{h}(\boldsymbol{k}) = \Big(h_0(\boldsymbol{k})\tau^0 + \Delta\tau^z + h_x(\boldsymbol{k})\tau^x\Big)\sigma^0 + h_y(\boldsymbol{k})\tau^y\sigma^z. \tag{3.4.15}$$

Following Ref. [148], we set,

$$h_0(\boldsymbol{k}) = t_1(c_x + c_y) + t_2 c_x c_y + t_3(c'_x c_y + c_x c'_y) - \mu, \tag{3.4.16a}$$
$$h_x(\boldsymbol{k}) = t_4(c_x - c_y), \tag{3.4.16b}$$
$$h_y(\boldsymbol{k}) = [t_5 + t_6(c_x + c_y)]s_x s_y, \tag{3.4.16c}$$

where $c'_{x,y} = \cos 2k_{x,y}$ and $(t_1, t_2, t_3, t_4, t_5, t_6, \mu) = (-0.334, 1.948, 0.166, -0.214, -1.572, -0.220, -1.40)$ in the unit of eV. The additional Δ term in Eq. (3.4.15) simply comes from the atomic spin-orbit coupling for the Bi p-electrons, and we set $\Delta = -0.15$. Note that the model (3.4.14) holds D_{4h} symmetry, although the actual material $LaO_{1-x}F_xBiS_2$ belongs to non-symmorphic space group. Hereafter, by using the model (3.4.14), we discuss unconventional superconductivity due to two kinds of pairing mechanisms: (A) an inter-site orbital density wave fluctuations [149, 150], and (B) a local fluctuation, *e.g.*, driven by electron-phonon interactions.

First, let us consider fourfold-symmetry breaking orbital fluctuations. For simplicity, we consider B_{1g} and B_{2g} type orbital fluctuations, which are respectively described by $\hat{M}_{B_{1g}} = \tau^x\sigma^0/2$ and $\hat{M}_{B_{2g}} = \tau^y\sigma^z/2$ in $\Gamma_{6u}\otimes\Gamma_{7u}$ space. The corresponding pairing interaction is given by

$$H_{\rm int} = \frac{1}{N}\sum_{\boldsymbol{q}}\sum_{\Gamma=B_{1g},B_{2g}} v^{\Gamma}(\boldsymbol{q})\mathcal{M}_{\Gamma}(-\boldsymbol{q})\mathcal{M}_{\Gamma}(\boldsymbol{q}), \tag{3.4.17}$$

with $v^{\Gamma}(\boldsymbol{q}) = 2v^{\Gamma}(c_x + c_y)$. For $\boldsymbol{q} = \boldsymbol{k} - \boldsymbol{k}'$, $v^{\Gamma}(\boldsymbol{k} - \boldsymbol{k}')$ can be decomposed into A_{1g}, B_{1g}, and E_u irreducible representations:

$$\phi^{A_{1g}} = c_x + c_y, \tag{3.4.18a}$$
$$\phi^{B_{1g}} = c_x - c_y, \tag{3.4.18b}$$
$$(\phi^{E_u}_1, \phi^{E_u}_2) = \sqrt{2}(s_x, s_y). \tag{3.4.18c}$$

Thus, Eq. (3.4.17) simply reads

$$\begin{aligned} H_{\rm int} = -\frac{1}{4N}\sum_{\mu\nu} v^{\mu\nu} \sum_{1234} \left[\tau^{\nu}\bar{\sigma}^{\mu}\right]_{12}\left[\tau^{\nu}\bar{\sigma}^{\mu}\right]^*_{43} \\ \times \sum_{\boldsymbol{k}\boldsymbol{k}'}\sum_{\Gamma i} \phi^{\Gamma}_i(\boldsymbol{k})\phi^{\Gamma}_i(\boldsymbol{k}')c^{\dagger}_1(\boldsymbol{k})c^{\dagger}_2(-\boldsymbol{k})c_3(-\boldsymbol{k}')c_4(\boldsymbol{k}'), \end{aligned} \tag{3.4.19}$$

with $\Gamma = A_{1g}, B_{1g}$, or E_u. Here, $v^{\mu\nu}$ are given as follows,

$$4v^{\rm I} = -(v^{B_{1g}} + v^{B_{2g}}), \tag{3.4.20a}$$
$$4v^{\rm II} = -(v^{B_{1g}} - v^{B_{2g}}), \tag{3.4.20b}$$
$$4v^{\rm III} = \ (v^{B_{1g}} - v^{B_{2g}}), \tag{3.4.20c}$$
$$4v^{\rm IV} = \ (v^{B_{1g}} + v^{B_{2g}}), \tag{3.4.20d}$$

where the indices I $\sim$ IV indicate the following sets of (μ, ν):

$$\mathrm{I}: (0,0),\ (z,0),\ (x,x),\ (y,x), \tag{3.4.21a}$$
$$\mathrm{II}: (x,0),\ (y,0),\ (0,x),\ (z,x), \tag{3.4.21b}$$
$$\mathrm{III}: (0,y),\ (z,y),\ (x,z),\ (y,z), \tag{3.4.21c}$$
$$\mathrm{IV}: (x,y),\ (y,y),\ (0,z),\ (z,z). \tag{3.4.21d}$$

From the same analysis as in Sec. 3.4.1, for example, $\phi(\boldsymbol{k})\tau^0\mathbf{0}$ is favored for the ferroic B_{1g}/B_{2g} fluctuations, while $\phi(\boldsymbol{k})\tau^0\boldsymbol{x}$ for the ferroic B_{1g} and the antiferroic B_{2g} fluctuations, and so on. When we focus on even-parity pairing states, the gap functions favored by the present interactions are listed as follows:

$$\mathrm{I}: \quad \hat{\varphi}_1^{A_{1g}} = \phi^{A_{1g}}\tau^0\mathbf{0}, \quad \hat{\varphi}_1^{B_{1g}} = \phi^{B_{1g}}\tau^0\mathbf{0}, \tag{3.4.22a}$$
$$\mathrm{II}: \quad \hat{\varphi}_2^{A_{1g}} = \phi^{B_{1g}}\tau^x\mathbf{0}, \quad \hat{\varphi}_2^{B_{1g}} = \phi^{A_{1g}}\tau^x\mathbf{0}, \tag{3.4.22b}$$
$$\mathrm{III}: \quad \hat{\varphi}^{A_{2g}} = \phi^{B_{1g}}\tau^y\boldsymbol{z}, \quad \hat{\varphi}^{B_{2g}} = \phi^{A_{1g}}\tau^y\boldsymbol{z}, \tag{3.4.22c}$$
$$\mathrm{IV}: \quad \hat{\varphi}_3^{A_{1g}} = \phi^{A_{1g}}\tau^z\mathbf{0}, \quad \hat{\varphi}_3^{B_{1g}} = \phi^{B_{1g}}\tau^z\mathbf{0},$$
$$(\hat{\varphi}_{1,1}^{E_g}, \hat{\varphi}_{1,2}^{E_g}) = \phi^{A_{1g}}\tau^y(-\boldsymbol{x}, \boldsymbol{y}), \quad (\hat{\varphi}_{2,1}^{E_g}, \hat{\varphi}_{2,2}^{E_g}) = \phi^{B_{1g}}\tau^y(\boldsymbol{x}, \boldsymbol{y}). \tag{3.4.22d}$$

These orbital based gap functions $\hat{\varphi}_i^{\Gamma}$ are transformed into the band based ones $\tilde{\varphi}_i^{\Gamma}$ via unitary transformations as discussed in Sec. 3.3. It should be noted that the band based $\tilde{\varphi}_i^{\Gamma}$ is crucially important in low-energy excitations observed experimentally. In what follows, let us elucidate the nodal structure of $\tilde{\varphi}_i^{\Gamma}$.

For the case I, the nodal structures of $\tilde{\varphi}$'s solely come from those in $\hat{\varphi}_1^{A_{1g}}$ or $\hat{\varphi}_1^{B_{1g}}$, since $\tau^0\mathbf{0}$ is A_{1g}. In contrast, in the case II, due to a unique property of multiorbital systems, both $\tilde{\varphi}_2^{A_{1g}}$ and $\tilde{\varphi}_2^{B_{1g}}$ possess nontrivial nodal structure along $k_x \pm k_y = 0$ lines. In the orbital based $\hat{\varphi}_2^{B_{1g}}$, since the $\boldsymbol{k}$ dependence of $\phi^{A_{1g}}$ belongs to A_{1g}, the nodal structures of $\tilde{\varphi}_2^{B_{1g}}$ come from the unitary matrix through Eq. (3.3.6). Indeed, $\tau^x\mathbf{0}$ is B_{1g} irreducible representation in Table 3.2. The elements of the unitary matrix, which transform into the band mainly composed of Γ_{6u} orbital, are given by

$$(u_{\Gamma_{6u}+,\uparrow},\ u_{\Gamma_{6u}-,\uparrow}) \sim (1,0)\,,$$
$$(u_{\Gamma_{7u}+,\uparrow},\ u_{\Gamma_{7u}-,\uparrow}) \sim \left(e^{2i\theta_{\boldsymbol{k}}}, e^{-i\theta_{\boldsymbol{k}}}\right),$$

with $\theta_{\boldsymbol{k}}$ being the angle in the k_x-k_y plane. Then,

$$[\mathcal{W}_x^+(\boldsymbol{k})]_{11} \sim \cos 2\theta_{\boldsymbol{k}} \sim k_x^2 - k_y^2, \tag{3.4.23}$$

which has, indeed, B_{1g} symmetry (see Sec. 3.3.3). As for the gap function with A_{1g} symmetry, it is commonly considered that it does not have symmetry protected nodes. However, for $\hat{\varphi}_2^{A_{1g}}$ in Eq. (3.4.22b), since both $\phi^{B_{1g}}$ and Eq. (3.4.23) have line nodes along $k_x \pm k_y = 0$, $\tilde{\varphi}_2^{A_{1g}}$

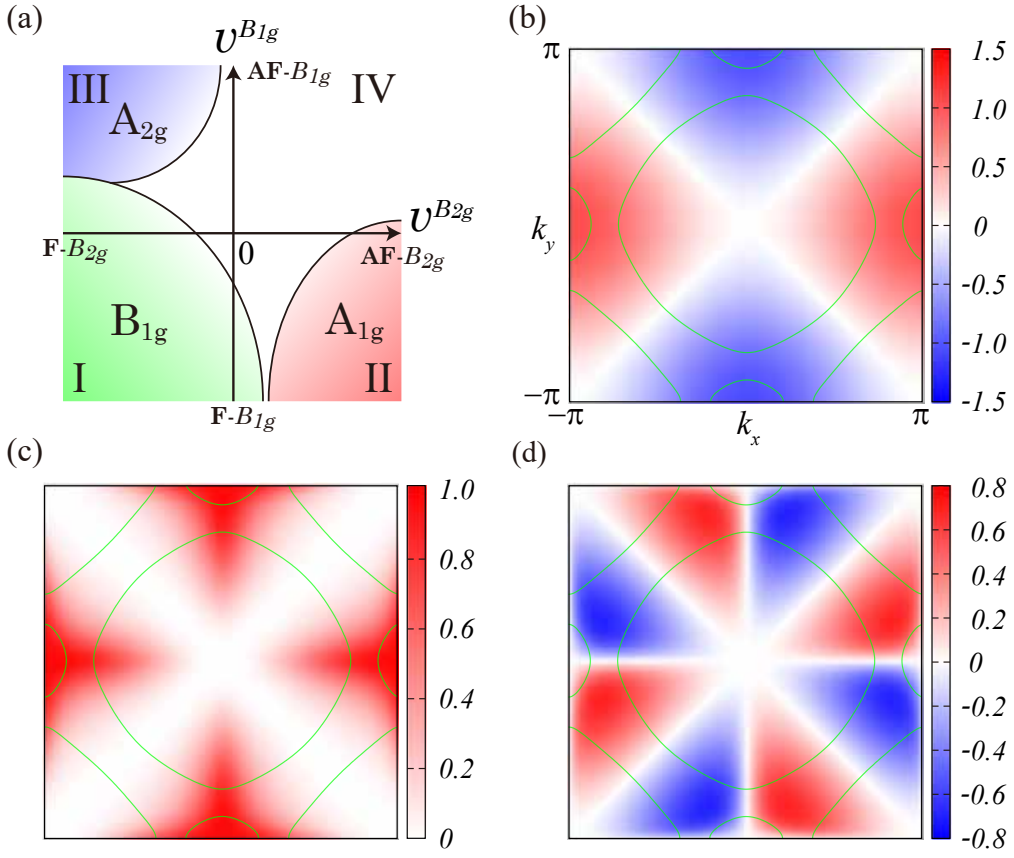

Figure 3.3: (a) Schematic phase diagram of the simple two-orbital model for BiS_2 layered superconductors. B_{1g} and B_{2g} type ferroic(F)/antiferroic(AF) orbital fluctuations have been considered. A typical band based gap structure $\tilde{\varphi}^{\Gamma}(\boldsymbol{k})$ is illustrated in (b) $\Gamma = B_{1g}$, (c) A_{1g}, and (d) A_{2g} states. The (green) solid lines indicate the Fermi surface in this model.

possesses B_{1g}-like gap nodes [Fig. 3.3(c)]. Although these nodes are not symmetry protected, one can expect that a specific fluctuation leads to such accidental nodes in A_{1g} gap functions.

Figure 3.3(a) depicts the schematic phase diagram for the even parity sector obtained by numerical calculations. The corresponding nodal structures are summarized in Figs. 3.3(b)-(d). The region around IV is regarded as a normal state, because the corresponding T_c is very low due to the fact that the attractive pairs are in inter-band pairing rather than intra-band pairing. Figure 3.3(c) clearly shows that the A_{1g} gap function is strongly anisotropic as discussed above. It should be emphasized that this orbital-driven anisotropic A_{1g} gap is not specific to the present model, but can commonly appear in any multiorbital superconductors. This mechanism may provide a clue to understanding gap anisotropies in, *e.g.*, $CeRu_2$ [151] and $PrOs_4Sb_{12}$ [152, 153]. Furthermore, the appearance of the A_{2g} gap structure can be also

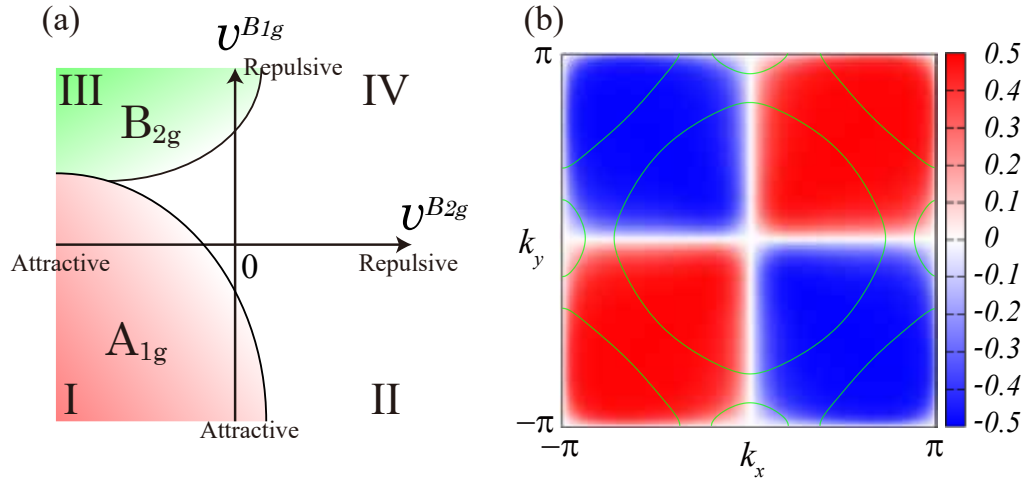

Figure 3.4: (a) Schematic phase diagram for local (on-site) B_{1g} and B_{2g} fluctuations in the same model as in Fig. 3.3. (b) The momentum dependence of the band based gap function for B_{2g} state appearing around the region Ⅲ .

regarded as a characteristic property of multiorbital systems, because if the $\boldsymbol{k}$ dependence of the gap function comes only from $\phi^{A_{2g}}(\boldsymbol{k})$, $\phi^{A_{2g}}(\boldsymbol{k})$ must take the form of $\phi^{A_{2g}}(\boldsymbol{k}) \sim \sin k_x \sin k_y(\cos k_x - \cos k_y)$. To realize such gap function in a single orbital system, there need much longer-range interactions than in the present nearest-neighbor model.

3.4.3 Nodal gap derived from local fluctuations

Next, we focus on local fluctuations with no $\boldsymbol{k}$ dependence. First, we show that only the local fluctuations can induce anisotropic and nodal superconductivity [140] in sharp contrast to a naive expectation. As in Sec. 3.4.2, we consider B_{1g} and B_{2g} fluctuations, setting a constant $v^{\Gamma}(\boldsymbol{q}) = v^{\Gamma}$ in Eq. (3.4.17). In this case, the basis functions in the orbital basis are also independent of $\boldsymbol{k}$. Therefore, the possible gap functions in attractive channels are:

$$\text{I}: \quad \hat{\varphi}_1^{A_{1g}} = \tau^0 \mathbf{0}, \tag{3.4.24a}$$

$$\text{Ⅱ}: \quad \hat{\varphi}^{B_{1g}} = \tau^x \mathbf{0}, \tag{3.4.24b}$$

$$\text{Ⅲ}: \quad \hat{\varphi}^{B_{2g}} = \tau^y \boldsymbol{z}, \tag{3.4.24c}$$

$$\text{Ⅳ}: \quad \hat{\varphi}_2^{A_{1g}} = \tau^z \mathbf{0}, \ (\hat{\varphi}_1^{E_g}, \hat{\varphi}_2^{E_g}) = \tau^y(-\boldsymbol{x}, \boldsymbol{y}), \tag{3.4.24d}$$

where I $\sim$ Ⅳ represent the regions specified in Eqs. (3.4.21a)-(3.4.21d). Note that any odd parity $\hat{\varphi}^{\Gamma_u}$ is not allowed in stark contrast to the cases in Sec. 3.4.2. As typical examples, we focus on the $\tilde{\varphi}^{B_{1g}}$ and $\tilde{\varphi}^{B_{2g}}$. As mentioned in Sec. 3.4.2, $\tilde{\varphi}^{B_{1g}}$ and $\tilde{\varphi}^{B_{2g}}$ in the band representation must have nodes. The $\boldsymbol{k}$ dependence of $\tilde{\varphi}^{B_{1g}}(\tilde{\varphi}^{B_{2g}})$ come from $u(\boldsymbol{k})$ and shows line nodes along $k_x \pm k_y = 0$ $(k_x k_y = 0)$.

Figure 3.4(a) depicts the $v^{B_{2g}}$-$v^{B_{1g}}$ phase diagram. We find that, due to only local fluctuations, anisotropic B_{2g} gap structure can emerge in the region around Ⅲ. The obtained B_{2g} nodal structure is illustrated in Fig. 3.4(b). In particular, for large repulsion of $v^{B_{1g}}$, the nodal superconductivity with B_{1g} symmetry can be induced by only repulsive local interactions. This can be understood via Table 4.3; the repulsion in B_{1g}-channel leads to the attractive interaction in B_{2g} channel. Thus, in multiorbital systems, anisotropic gap structure can be also realized in the BCS approximation of purely local (on-site) interactions. This indicates that anisotropic pairing states can emerge without characteristic momentum dependent fluctuations in multiorbital systems, which differs from the case of single-orbital systems. It also implies that in multiorbital systems, the electron-phonon interaction can lead to anisotropic superconductivity. In what follows, let us elucidate local fluctuations arising from electron-phonon couplings.

In general, a specific phonon mode couples to electronic multipoles with the same irreducible representation. Local nonmagnetic multipoles in the present two-orbital model with Γ_{6u} and Γ_{7u} are written as

$$\mathcal{M}_\Gamma(\boldsymbol{r}) = \sum_{12} \left[\hat{M}_\Gamma\right]_{12} c_1^\dagger(\boldsymbol{r}) c_2(\boldsymbol{r}), \tag{3.4.25}$$

with $\Gamma = A_{1g}, B_{1g}$, or B_{2g}, and $\hat{M}_\Gamma$'s are given by

$$\hat{M}_{A_{1g}} = \frac{\tau^0\sigma^0}{2}, \quad \hat{M}_{B_{1g}} = \frac{\tau^x\sigma^0}{2}, \quad \hat{M}_{B_{2g}} = \frac{\tau^y\sigma^z}{2}. \tag{3.4.26}$$

Integrating out the phonon degrees of freedom, we obtain an effective interaction,

$$H_{\rm int} = -\sum_\Gamma \frac{g_\Gamma^2}{\Omega^\Gamma} \sum_{\boldsymbol{r}} \mathcal{M}_\Gamma(\boldsymbol{r}) \mathcal{M}_\Gamma(\boldsymbol{r}), \tag{3.4.27}$$

where g_Γ is the local electron-phonon couplings and Ω^Γ is the local phonon frequency for $\Gamma = A_{1g}$, B_{1g}, and B_{2g} mode. Following the procedure in Secs. 3.4.2 and 3.4.3, Eq. (3.4.27) can be decomposed in the same way as in Eq. (3.4.19) with appropriate $v^{\mu\nu}$. Using Table 4.3, we obtain *e.g.,* $4v^{0x} = v^{A_{1g}} + v^{B_{1g}} - v^{B_{2g}}$, and so on. Note that such interactions $v^\Gamma = g_\Gamma^2/\Omega^\Gamma$ are always positive, different from the electron-electron interactions. Therefore, since A_{1g} pairing channel $\tau^0\mathbf{0}$ is always attractive in all the phonon modes, namely, $4v^{00} = \sum_\Gamma v^\Gamma$, we re-realize that a fully gapped A_{1g} state is the most favorable.

One possibility of electron-phonon mediated anisotropic superconductivity arises when the Hund's coupling and the pair hopping term of on-site Coulomb repulsions are taken into account. For example, local interactions are $4v^{00} = U + J$ for $\tau^0\mathbf{0}$ pairing, and $4v^{0x} = 4v^{zy} = U - J$ for $\tau^x\mathbf{0}$ and $\tau^y\boldsymbol{z}$, with the intra-orbital repulsion U and the Hund's coupling J. Thus, the presence of the on-site Coulomb repulsions works against the isotropic pairing state as is well known. Another possibility is the $\boldsymbol{k}$-dependent interaction via the electron-phonon

coupling, but here we do not go into detail. Instead, let us focus on the fact that *e.g.*, $\tau^0\tau^0 \times \sigma^z\sigma^z = -1$ in Table 4.3, which indicates that time reversal symmetry-breaking mode can suppress A_{1g} pairing states. It implies that the electron-phonon interaction may lead to anisotropic pairing states in a magnetically-ordered state. These mechanisms for electron-phonon driven anisotropic superconductivity in combinations with other degrees of freedom are fascinating issues and we leave the detailed analysis in our future works.

3.5 Conclusion

We have constructed a complete table of irreducible representations of superconducting gap functions in symmorphic multiorbital systems. Classification in the orbital based pairing functions offers novel entries in the classification tables. The Cooper pairs in multiorbital systems can be regarded as ones with multipole degrees of freedom, and we have called it multipole superconductivity. From this viewpoint, we find that unconventional superconductivity can be realized not only by the momentum dependence of the pairing interactions, but also by the orbital degrees of freedom.

One of the nontrivial results appears in the system composed of $\Gamma_9 \otimes \Gamma_9$ orbitals in D_6 group. The transformation properties of the Cooper pairs are not explained by those for the *pure*-spin 1/2 in the conventional classification. This is an important consequence of orbital degrees of freedom.

We have also clarified how the superconducting gap nodes appear in multiorbital systems. We have explained the relation between the gap functions in the orbital bases and those in the band ones. The momentum dependence of the band based gap functions depends on that of the orbital based ones and the unitary matrix transforming the two bases. The latter depends on the irreducible representation for the corresponding Kramers degrees of freedom in the orbital bases, which include both the *pure*-spin and the orbital angular momentum and are generally not only the *pure*-spin 1/2.

On the basis of the present group theoretical analysis, we have discussed a cubic Γ_{8u} model and tetragonal $\Gamma_{6u} + \Gamma_{7u}$ models. In the former model, superconductivity with anisotropic three-dimensional representations emerges in the vicinity of an antiferroic quadrupole ordered phase. In the latter, we have discussed the formation of anisotropic gap functions including anisotropic s-wave (A_{1g}) type functions induced by various orbital fluctuations. We have also proposed nodal/anisotropic superconductivity mediated by local fluctuations, which can be realized only in the multiorbital systems. Our findings imply that fluctuations arising from electron-phonon couplings also may induce anisotropic superconductivity with the help of the time reversal symmetry-breaking and the local Coulomb interactions, although the conventional local electron-phonon interactions favor isotropic s-wave pairing. We hope that the present study provides a renewed interest in multiorbital systems and encourages experimental research for new superconducting materials.

Chapter 4

Nodal structure in non-symmorphic magnetic superconductors

Micklitz and Norman demonstrated in the pioneering work [3] that, in systems with *non-symmorphic* space groups, new types of symmetry protected nodes can appear at the Brillouin zone boundary. This can be shown by the classification scheme based on the representation theory of the *space group*. In contrast to the conventional classifications, which are based on the *point group* symmetry, this gives us the correct way to take into account a non-trivial phase due to a non-primitive translation in a space group operation, which arises in the small representation at the Brillouin zone boundary. In this chapter, we extend the classification into non-symmorphic *magnetic* space groups, which has been less understood in spite of the growing interest in superconductors coexisting with a magnetic order. The results are applied to the analysis of the superconductivity in UPd_2Al_3 and UCoGe as examples.

The organization of this chapter is as follows. First, in Sec. 4.1, we introduce the superconductivity in two heavy fermion compounds with a magnetic order UPd_2Al_3 and UCoGe especially focusing on their nodal structure. Then, in Sec. 4.2, we provide the minimal space groups describing the magnetic structure of each compound and discuss emergent symmetry protected line nodes by the group theoretical argument based on the space group approach [3]. The details of the methods are summarized in Appendix A.3.5. The relations to experimental observations are discussed in Sec. 4.3. Finally, in Sec. 4.4, the limits of its validity are discussed with the help of specific model calculations. Here, the importance of the band splitting on the Brillouin zone boundary is pointed out. In Sec. 4.5, we summarize the present study.

4.1 Introduction to the superconductivity in UPd_2Al_3 and UCoGe

In the research field of superconductivity, its coexistence of magnetism is a very interesting topic. The microscopic coexistence between superconductivity and magnetism is often discovered in the strongly correlated electron systems. For example, it is known that the 122 family of iron-pnictide superconductors, such as $BaFe_2(As_{1-x}P_x)_2$ and $Ba(Fe_{1-x}Co_x)_2As_2$, shows superconductivity coexisting with an antiferromagnetic order, which is associated with the quantum critical behavior of the spin density wave transition [154]. As for heavy fermion compounds, the centrosymmetric $CePd_2Si_2$ [155], $CeIn_3$ [155, 156], and $CeRhIn_5$ [157, 158], and also the non-centrosymmetric $CeRhSi_3$ [159] and $CeIrSi_3$ [160] exhibit such superconductivity with an antiferromagnetism under high pressure. However, observing the coexistence without any tuning is still a rare event. In this point of view, the U-based heavy fermion superconductors UPd_2Al_3 [74] and UNi_2Al_3 [75] were unique candidates to show such coexistence, as well as the subsequently discovered non-centrosymmetric superconductor $CePt_3Si$ [28]. Although UNi_2Al_3 is considered a spin-triplet superconductor, as is indicated by the absence of Knight shift [161] and the anisotropy of H_{c2} [162], it is still controversial because the paramagnetic suppression in the thin film sample [163] and the indication of line nodes [164] are naively incompatible with the spin-triplet scenario. On the other hand, the superconducting property in UPd_2Al_3, including not only the gap structure but also the pairing mechanism, is well-established by various experiments. Here, we summarize basic features of this material.

4.1.1 Superconductivity in UPd_2Al_3

UPd_2Al_3 is known as a heavy fermion compound with symmorphic hexagonal lattice structure in a paramagnetic phase (see the left panel of Fig. 4.1). At the transition temperature $T_N = 14$K, this enters into an antiferromagnetic phase, and then coexists with unconventional superconductivity below $T_c = 2$K [74]. In the antiferromagnetic phase, the magnetic moments are lying in the basal plane and ordering with the propagating vector $\boldsymbol{Q} = (0, 0, \pi/c)$, as is revealed by the neutron diffraction study [165]. Moreover, it is believed that the antiferromagnetism occurs in a different electronic subsystem to the main superconducting band, i.e., one of the three U 5f-electrons is itinerant and contributes the superconductivity while the others are localized and form the magnetic order with a relative large magnetic moment about $0.85\mu_B$ per U atom. Such a dual nature has been confirmed by comparing the Fermi surfaces determined in the de Hass-van Alphen measurements [166, 167, 168] with those obtained in the band calculations with the duality model [169]. Indeed, this is considered to play a key role for its pairing mechanism. Namely, inelastic neutron scattering measurements detect broad peak structure at $\boldsymbol{Q} = (0, 0, \pi/c)$ corresponding to the virtual exchange of magnetic excitons [170, 171], and the tunneling junction experiments imply the pairing

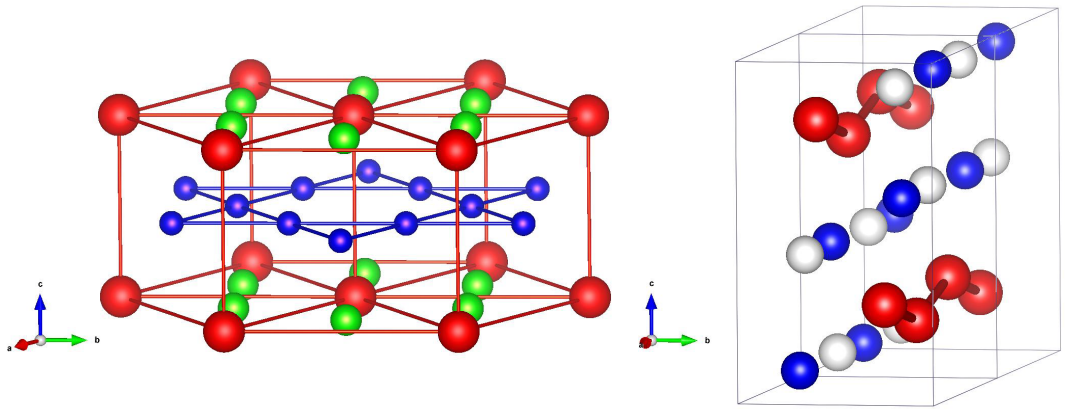

Figure 4.1: (Left) Crystal structure of UPd_2Al_3. Red, green and blue spheres indicate U, Pd, and Al atoms, respectively. The space group is symmorphic $P6/mmm$. (Right) Crystal structure of UCoGe. Red, blue and white spheres indicate U, Co, and Ge atoms, respectively. The space group is non-symmorphic $Pnma$.

states mediated by its excitations [172]. Here, the magnetic exciton is a Frankel type exciton propagating among the local crystalline electric filed states, and thus, the presence of localized U 5f-electrons is essential for the emergence of its unconventional superconductivity. As for gap structure, there seems to exist a horizontal line node at the magnetic Brillouin zone boundary perpendicular to the c-axis, because this should be compatible with the magnetic exciton excitations. Such nodal structure is also consistent with the power law behavior of the spin-relaxation ratio $1/T_1 \sim T^3$ observed in the NMR measurements [173, 174]. Moreover, recently performed field-angle resolved thermal conductivity [175] and specific heat [176] measurements support this scenario.

Theoretically, the relations between superconductivity and antiferromagnetism has been attracted much attentions since many of the unconventional superconductivity appear in the vicinity of an antiferromagnetic phase boundary [9, 10]. However, in spite of extensive studies on the pairing mechanism, there is little progress about the gap structure in the coexisting phase. In UPd_2Al_3, the emergence of line nodes in the magnetic Brillouin zone boundary was studied based on the microscopic theory in Ref. [177]. They demonstrated that a on-site spin-singlet gap function yields line node like excitations when the exchange coupling with the antiferromagnetic moments is sufficiently larger than the gap amplitude. Although this seems to be consistent with the observations, it is not so clear whether or not such a nodal feature should appear in a realistic model or a material with multiorbital or sublattice degrees of freedom.

4.1.2 Superconductivity in UCoGe

The superconductivity coexisting with a ferromagnetic order is also hardly observed in nature. For example, several rare-earth compounds, such as $ErRh_4B_4$ and $HoMo_6S_8$, show magnetic transitions deep inside superconducting phases [178], however, their coexisting phases possess complex magnetic structures called a cryptoferromagnetism, including magnetic domains or spiral spin textures. Moreover, the superconductivity finally disappears at low temperatures with growing of the ferromagnetic moments, which is due to the ordinary paramagnetic effect on the spin-singlet superconductivity. Recently, the series of U-based superconductors, including UGe_2 [76], URhGe [77], UIr [29], and UCoGe [78], has been attracted much attention as a promising system of the spin-triplet superconductivity coexisting with ferromagnetism. These compounds encounter a superconducting transition in a ferromagnetic phase at high or ambient pressure. Moreover, a rare reentrant superconductivity has been discovered under the magnetic field in URhGe [179]. Among these compounds, UCoGe has the lowest ferromagnetic and the highest superconducting transition temperatures, and thus, is suited to study the cooperation between superconductivity and ferromagnetism. Therefore, in the following, we focus on UCoGe and briefly summarize its basic properties.

UCoGe possesses TiNiSi type crystal structure (space group $Pnma$) with zigzag chains composed of U atoms (see the right panel of Fig. 4.1). This shows the ferromagnetic transition at $T_C = 3.0$K with the magnetic moments lying along the c-axis. The superconductivity then appears below $T_c = 0.8$K. In this compound, it has been considered that the Ising-like ferromagnetic fluctuation leads to a spin-triplet equal spin pairing state [180, 181], and many fascinating phenomena including the peculiar H-T phase diagram have been studied so far [182, 183, 184, 185, 186, 187]. However, in spite of the growing interest, the properties characteristic of the coexisting phase are less well understood systematically. For example, with respect to the gap structure, the power law behavior of the spin-relaxation ratio $1/T_1 \sim T^3$ observed in Co-NQR measurements [188, 189] seems to indicate the presence of line nodes. However, the analysis of the H-T phase diagram in various field directions implies that the point nodal states are the most compatible with the observations [181]. In this situation, the group theoreical classification, which provides definite statements independent of the details of materials, plays an important role in general. Indeed, the gap classification in ferromagnetic superconductors has been performed by several groups [79, 80, 182]. According to the results for UCoGe [182], there are two types of possible gap symmetries, A_u and B_u, within the weak coupling BCS theory. The former possesses only point nodes, which are considered as Weyl nodes [190], while the latter possesses only a horizontal line node. Therefore, the nodal structures expected by the spin-relaxation and the H-T phase diagram are incompatible with each other. Note that the recently performed thermal conductivity measurements will be compatible with both nodal structures [191].

Here, we should remark that the classification given in Ref. [182] is based on the usual

point group symmetry. Today, however, it is known that there is another gap classification based on the space group symmetry [138, 139, 3], which provide the correct nodal structure at the Brillouin zone boundary even in the non-symmorphic systems [59, 192]. Since the coexisting phase of UCoGe belongs to the non-symmorphic space group, it is unclear, for instance, whether the existence of both point and line nodes is really forbidden. The results in Ref. [3] cannot directly apply to the superconductivity in magnetic crystals because the time reversal symmetry assumed in Ref. [3] no longer holds. Thus, the extension to the coexisting phase is necessary.

Motivated by the above observations, in this study, we extend the gap classification into non-symmorphic magnetic space groups, which can be applied to the analysis of superconductivity in UCoGe and UPd_2Al_3. In these compounds, the magnetic ordered phase belongs to the type III or IV Shubnikov space groups due to the presence of time reversal symmetry with a point group operation and/or a non-primitive translation (see Appendix A.1.3). Based on the classification, we obtain the following nontrivial consequences within the weak-coupling BCS theory.

1. The UCoGe-type ferromagnetic superconductors have horizontal line nodes on either the $k_z = 0$ or the $k_z = \pm\pi/c$ plane. In addition, it is likely that additional Weyl point nodes exist along the $k_x = k_y = 0$ line.

2. In UPd_2Al_3-type antiferromagnetic superconductors, A_g gap functions always have line nodes on the $k_z = \pm\pi/c$ plane (i.e., the magnetic Brillouin zone face), in other words, the conventional fully gapped s-wave superconductivity is forbidden.

Needless to say, in both cases, it is necessary that the Fermi surface crosses nodal planes. The obtained symmetry protected nodal structures are fully consistent with the various observations both of the cases in UPd_2Al_3 and UCoGe. Thus, we conclude that UPd_2Al_3 and UCoGe are candidate unconventional superconductors possessing hidden symmetry protected line nodes, peculiar to non-symmorphic magnetic space groups.

4.2 Classification based on space group approach

Here, we consider minimal space groups describing the crystal structure in the magnetic phase of UPd_2Al_3 and UCoGe. First, we focus on a space group G_0 that is given as a coset decomposition

$$G_0 = \{E|\boldsymbol{0}\}T + \{2_z|\boldsymbol{t}_z\}T + \{I|\boldsymbol{0}\}T + \{\sigma_h|\boldsymbol{t}_z\}T, \tag{4.2.1}$$

where the translation group T defines a Bravais Lattice, and $\boldsymbol{t}_z = \frac{c}{2}\boldsymbol{e}_c$ is a non-primitive translation along the c-axis (for details, see Appendix A.1.1). The notation $\{p|\boldsymbol{a}\}$ is a conventional Seitz space group symbol with a point-group operation p and a translation $\boldsymbol{a}$. E

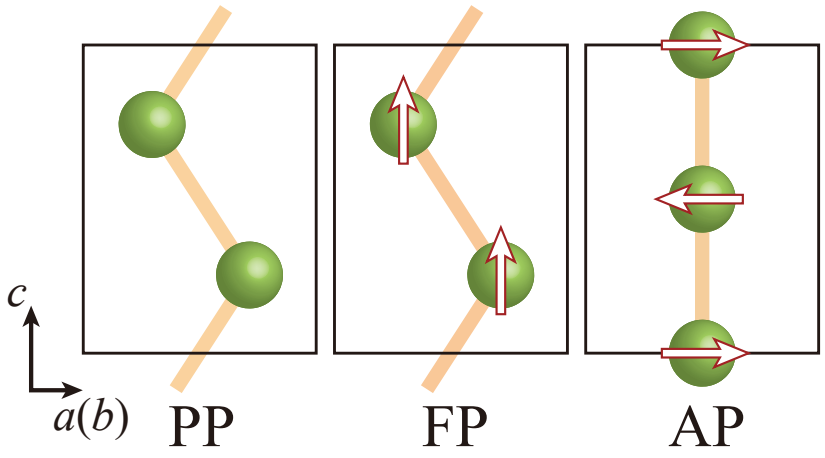

Figure 4.2: A side view of the unit cell in the typical structures with three types of space groups considered in this study. PP and FP contain a zigzag structure, and AP possesses staggered ordered moments along the c-axis, in which the orientations are in the ab-plane.

denotes an identity operation, 2_z a π-rotation around c-axis, I a space inversion, and σ_h a mirror about ab-plane. Taking into account the magnetism order, we here consider the three types of systems given as follows,

$$\begin{aligned} G &= G_0 + \{\theta|\mathbf{0}\}G_0 \quad : \text{PP} \\ G &= G_0 \qquad\qquad\quad : \text{FP} \\ G &= G_0 + \{\theta|\boldsymbol{t}_z\}G_0 \quad : \text{AP} \end{aligned} \tag{4.2.2}$$

where θ denotes a time reversal operation. We can easily see that PP, FP, and AP correspond to paramagnetic, ferromagnetic, and antiferromagnetic phase of matter, respectively. Typical crystal structures for corresponding space groups are shown in Fig. 4.2. Unless otherwise assigned, the spin-orbit coupling is included in all systems. Note that the space group G of PP is the same as discussed in Ref. [3].

Let $\gamma_{\boldsymbol{k}}$ be a small representation of a little group $K_{\boldsymbol{k}}$, which represents the Bloch state with the crystal momentum $\boldsymbol{k}$. Through this chapter, we have used the word "representation" both as a representation of a unitary group and a corepresentation of a non-unitary group. We should note that the (zero-momentum) Cooper pairs have to be formed between the degenerate states present at $\boldsymbol{k}$ and $-\boldsymbol{k}$ within the BCS theory. Therefore, these two states should be connected by some symmetry operations except for an accidentally degenerate case. As a result, the representation of Cooper pair wave functions, which we denote by $P_{\boldsymbol{k}}$, can be constructed from $\gamma_{\boldsymbol{k}}$ as summarized in Refs. [138, 139, 3]. Here, we do not repeat the details of the prescription, and instead, indicate the practical procedure step by step. For

Table 4.1: The characters of $\bar{\gamma}_{\boldsymbol{k}}$ in the case of PP, FP, and AP. Upper and lower expressions in PP and FP correspond to the two non-equivalent irreducible representations.

Basal plane			Zone face		
$\bar{K}_{\boldsymbol{k}}$	$\{E\|\mathbf{0}\}$	$\{\sigma_h\|\boldsymbol{t}_z\}$	$\bar{K}_{\boldsymbol{k}}$	$\{E\|\mathbf{0}\}$	$\{\sigma_h\|\boldsymbol{t}_z\}$
PP	2	0	PP	2	$\pm 2i$
FP	1	$\pm i$	FP	1	$\pm i$
AP	2	0	AP	2	0

details of the formulation, see also Appendix A.3

Here, we only consider the Cooper pairs in the basal plane ($k_z = 0$) and the zone face ($k_z = \pm\pi/c$) for simplicity. It should be noted that the discussions given below may not be applicable for non primitive lattice systems, such as base, body, or face centered lattice systems, since the $k_z = \pm\pi/c$ plane may not be the Brillouin zone boundary in such cases. Indeed, the present arguments cannot be simply applied to eight of the fourteen Bravais lattices.

Focusing on the both planes in the primitive lattice systems, the little groups $K_{\boldsymbol{k}}$ are given by the following coset decompositions,

$$K_{\boldsymbol{k}} = \begin{cases} \{E|\mathbf{0}\}T + \{\sigma_h|\boldsymbol{t}_z\}T + \{\theta I|\mathbf{0}\}T + \{\theta 2_z|\boldsymbol{t}_z\}T & : \text{PP} \\ \{E|\mathbf{0}\}T + \{\sigma_h|\boldsymbol{t}_z\}T & : \text{FP} \\ \{E|\mathbf{0}\}T + \{\sigma_h|\boldsymbol{t}_z\}T + \{\theta I|\boldsymbol{t}_z\}T + \{\theta 2_z|\mathbf{0}\}T & : \text{AP} \end{cases} \tag{4.2.3}$$

To obtain the small representations, it is sufficient to see the (projective) irreducible representations of the corresponding little co-groups $\bar{K}_{\boldsymbol{k}} = K_{\boldsymbol{k}}/T$ with the appropriate factor systems [59, 192] (see also Appendix A.3). We denote them by $\bar{\gamma}_{\boldsymbol{k}}$. Here, we specifies the elements of $\bar{K}_{\boldsymbol{k}}$ as the representatives $r = \{p|\boldsymbol{a}\}$ of the decompositions (4.2.3) $\bar{\gamma}_{\boldsymbol{k}}$ can be obtained by calculating the irreducible representations for the unitary part of $\bar{K}_{\boldsymbol{k}}$, and then inducing them by an anti-unitary operation [193]. In Table 4.4, we summarize the characters of $\bar{\gamma}_{\boldsymbol{k}}$ for the unitary operations in $\bar{K}_{\boldsymbol{k}}$. Now, the corresponding small representations are given by $\gamma_{\boldsymbol{k}}(g) = \bar{\gamma}_{\boldsymbol{k}}(r)F_{\boldsymbol{k}}(t)$ where $g = rt$ for $g \in K_{\boldsymbol{k}}$ and $t \in T$. $F_{\boldsymbol{k}}$ is the irreducible representation of T defined by $F_{\boldsymbol{k}}(t) = e^{-i\boldsymbol{k}\cdot\boldsymbol{t}}$ for $t = \{E|\boldsymbol{t}\}$. From Table 4.4, we can see that the irreducible representations of $\bar{K}_{\boldsymbol{k}}$ in PP and AP become two-dimensional, which reflect the Kramers degeneracy for the anti-unitary operations $\{\theta I|\mathbf{0}\}$ and $\{\theta I|\boldsymbol{t}_z\}$. In the case of AP, since the non-primitive translation included in $\{\theta I|\boldsymbol{t}_z\}$ cancels out the phase factor arising from that in $\{\sigma_h|\boldsymbol{t}_z\}$, $\bar{\gamma}_{\boldsymbol{k}}(\{\sigma_h|\boldsymbol{t}_z\})$ in the zone face is the same in the basal plane. This situation is in sharp contrast to the case of PP.

Table 4.2: The characters of $\bar{P}_{\boldsymbol{k}}$ in PP, FP, and AP.

Basal plane

$M_{\boldsymbol{k}}/T$	$\{E\|\mathbf{0}\}$	$\{2_z\|\boldsymbol{t}_z\}$	$\{I\|\mathbf{0}\}$	$\{\sigma_h\|\boldsymbol{t}_z\}$
PP	4	2	-2	0
FP	1	1	-1	-1
AP	4	2	-2	0

Zone face

$M_{\boldsymbol{k}}/T$	$\{E\|\mathbf{0}\}$	$\{2_z\|\boldsymbol{t}_z\}$	$\{I\|\mathbf{0}\}$	$\{\sigma_h\|\boldsymbol{t}_z\}$
PP	4	-2	-2	4
FP	1	-1	-1	1
AP	4	-2	-2	0

Next, we consider the representation of the Cooper pairs $P_{\boldsymbol{k}}$. In the space group operation d connecting two states of the paired electrons, its rotation/inversion part p_d satisfies $p_d\boldsymbol{k} = -\boldsymbol{k}$ modulo a reciprocal lattice vector. In the present cases, $\{I|\mathbf{0}\}$ and $\{2_z|\boldsymbol{t}_z\}$ are the candidates for the operator d in FP, while $\{\theta|\mathbf{0}\}$ ($\{\theta|\boldsymbol{t}_z\}$) is also in PP (AP). Regardless of the choice of d, $M_{\boldsymbol{k}} = K_{\boldsymbol{k}} + dK_{\boldsymbol{k}}$ is identical to the space group G. Taking into account the antisymmetry of the Cooper pairs and the degeneracy of the two states, we can regard $P_{\boldsymbol{k}}$ as an antisymmetrized Kronecker square [59], with zero total momentum, of the induced representation $\gamma_{\boldsymbol{k}} \uparrow M_{\boldsymbol{k}}$. In practice, this is obtained by using the following formula,

$$\chi^{P_{\boldsymbol{k}}}(g) = \chi^{\gamma_{\boldsymbol{k}}}(g)\chi^{\gamma_{\boldsymbol{k}}}(d^{-1}gd), \tag{4.2.4}$$

$$\chi^{P_{\boldsymbol{k}}}(dg) = -\chi^{\gamma_{\boldsymbol{k}}}(dgdg), \tag{4.2.5}$$

where $\chi^{P_{\boldsymbol{k}}}(g)$ ($\chi^{\gamma_{\boldsymbol{k}}}(g)$) is a character of $P_{\boldsymbol{k}}$ ($\gamma_{\boldsymbol{k}}$) for $g \in K_{\boldsymbol{k}}$. These are special cases of Mackey-Bradley theorem [194, 195]. For details, see Appendix A.3.5. The obtained results are summarized in Table 4.2. Here, $\bar{P}_{\boldsymbol{k}}$ is the representation of $M_{\boldsymbol{k}}/T$ satisfying $P_{\boldsymbol{k}}(g) = \bar{P}_{\boldsymbol{k}}(r)$ where $g = rt$ for $g \in M_{\boldsymbol{k}}$, $r \in M_{\boldsymbol{k}}/T$, and $t \in T$. In the case of AP, $\chi^{P_{\boldsymbol{k}}}(\{\sigma_h|\boldsymbol{t}_z\})$ is equal to zero even in the zone face, different from the case of PP. This comes from the difference of $\bar{\gamma}_{\boldsymbol{k}}(\{\sigma_h|\boldsymbol{t}_z\})$ in Table 4.4. On the other hand, since $\bar{P}_{\boldsymbol{k}}$ in FP is one-dimensional representation, only one irreducible representation is allowed both in the basal plane and the zone face.

Finally, we reduce the representation $\bar{P}_{\boldsymbol{k}}$ into the irreducible representations. In both planes, there are four irreducible representations, A_g, B_g, A_u, and B_u since the coset group $M_{\boldsymbol{k}}/T$ is isomorphic to the point group $\mathrm{C_{2h}}$. Note that, strictly, $M_{\boldsymbol{k}}/T$ is isomorphic to the

Table 4.3: The reduction of $\bar{P}(\boldsymbol{k})$ to the irreducible representations of C_{2h} in the case of PP, FP, and AP.

Basal plane		Zone face	
PP	$A_g + 2A_u + B_u$	PP	$A_g + 3B_u$
FP	A_u	FP	B_u
AP	$A_g + 2A_u + B_u$	AP	$B_g + A_u + 2B_u$

gray point group of C_{2h} in PP and AP. However, its corepresentations are trivial because the anti-unitary operations do not cause the extra degeneracy. The results are summarized in Table 4.3. Note that the gap functions should be zero, which means the appearance of gap nodes, if the corresponding irreducible representations do not exist in the reduction of $\bar{P}_{\boldsymbol{k}}$. The absence of A_u in PP corresponds to the emergent horizontal line node of the recently proposed E_{2u} state in UPt_3 superconductors [3, 2, 132, 196]. On the other hand, in the case of AP, we find that A_g does not appear in the zone face, in other words, A_g possesses horizontal line nodes in the zone face (i.e., the magnetic Brillouin zone boundary). This means that the conventional fully gapped s-wave superconductivity is forbidden, if the Fermi surfaces cross $k_z = \pm\pi/c$ plane. On the other hand, in the case of FP, only odd-parity pairing is allowed in both planes, due to the absence of Kramers degeneracy. A_u is forbidden in the zone face, and B_u is forbidden in the basal plane. Therefore, the line nodes always appear, as for as the Fermi surface crosses $k_z = 0$ and $k_z = \pm\pi/c$ planes. It should be noted that the emergence of such nodal structure does not depend on the pairing mechanism. These are the main results of this study. Note that these results are applicable to not only conventional magnetic dipole ordered states, but also magnetic multipole ordered states.

4.3 Relation to the experiments

Here, we discuss several U-based materials in non-symmorphic magnetic space groups. First, we focus on the case of AP. The space group $G = G_0 + \{\theta|\boldsymbol{t}_z\}G_0$ corresponds to P_b2_1/m (the unique axis is chosen to be c-axis). As mentioned in Sec. 4.1, its typical example is the antiferromagnetic phase of UPd_2Al_3, in which the ordering vector is $\boldsymbol{Q} = (0, 0, \pi/c)$ and the orientations of moments are in the basal plane [165]. Many experimental observations [170, 172, 197, 175, 176] imply the presence of horizontal line nodes at the magnetic Brillouin zone boundary perpendicular to the c-axis. Moreover, it has been expected that the gap function belongs to even parity irreducible representations [173, 174, 198, 199] and the Fermi surfaces cross $k_z = \pm\pi/c$ plane [166, 167, 200, 168]. These findings are also supported in the self-consistent calculations based on the microscopic electronic structure obtained by the

first principles calculations [201]. Following our results, the expected horizontal line nodes are symmetry protected nodes in the non-symmorphic magnetic space groups.

Next, let us consider the case of FP. Its candidates are hotly-debated ferromagnetic superconductors, UCoGe, URhGe and UGe_2. In the paramagnetic phase, the space group of UCoGe and URhGe is $Pnma1'$, while UGe_2 possesses symmorphic $Cmmm1'$. In the ferromagnetic phase, the former two belong to FP as shown below, while the latter does not meet the condition. In the former two, since the ordered moments align parallel to c-axis in the ferromagnetic phase, the space group is reduced from $Pnma1'$ into $Pn'm'a$. This group is given explicitly by $G = G_0' + \{\theta 2_y|\boldsymbol{t}_y\}G_0'$ where $G_0' = \{E|\boldsymbol{0}\}T + \{2_z|\boldsymbol{t}_n\}T + \{I|\boldsymbol{0}\}T + \{\sigma_h|\boldsymbol{t}_n\}T$ with $\boldsymbol{t}_y = \frac{b}{2}\boldsymbol{e}_y$ and $\boldsymbol{t}_n = \frac{a}{2}\boldsymbol{e}_x + \frac{c}{2}\boldsymbol{e}_z$. Here, a, b, and c are the lattice parameters and 2_y represents the π-rotation around b-axis. At first glance, this seems rather different from that of FP. However, considering a general point in the basal plane and the zone face, we can ignore the anti-unitary part because this is not the element of the little groups. Therefore, the only difference is that the non-primitive translation becomes $\boldsymbol{t}_n$ instead of $\boldsymbol{t}_z$. As a result, $\bar{\gamma}_{\boldsymbol{k}}(\{\sigma_h|\boldsymbol{t}_z\})$ in the zone face changes from $\pm i$ to $\pm ie^{-ik_x/2}$. We can easily confirm that this change does not affect the final results given in Table 4.2 and 4.3. Therefore, any superconductivity in these materials have line nodes in either the basal plane or the zone face.

Now, let us consider the nodal structure of superconductivity in UCoGe in details. Unfortunately, the Fermi surfaces of this compound have not been established in experiments [202, 203, 204], however, the first-principles calculations show the existence of many complicated Fermi surfaces, some of which cross the $k_z = 0$ and $k_z = \pm\pi/c$ planes [202]. Therefore, our results suggest the existence of horizontal line nodes in the coexistent phase of UCoGe. Both power law behaviors of the spin-lattice relaxation rate $1/T_1 \sim T^3$ [188, 189] and the behavior of the residual thermal conductivity [191] are consistent with our prediction. Note that in the pressure-temperature phase diagram, the ferromagnetic transition seems to have little effect on the superconductivity [205, 206]. In the absence of magnetism, the straightforward calculation shows that the space group $Pnma1'$ leads to the same nodal structure as the case of PP in Table 4.3, by regarding the irreducible representations of D_{2h} as those of C_{2h} with the compatibility relation. Therefore, the line nodes in the basal plane of B_u irreducible representation (B_{2u} and B_{3u} irreducible representations of D_{2h} group) are forbidden in the paramagnetic phase, which is consistent with the Blount's theorem of the triplet superconductors [60, 61]. Therefore, we may expect that the realized gap function belongs to A_u irreducible representation (A_{1u} or B_{1u} in the paramagnetic phase) and has the line nodes at $k_z = \pm\pi/c$ plane. As for the A_u gap functions in the coexistent phase, there should be an additional point node at $k_x = k_y = 0$, which is regarded as Weyl nodes [79, 190]. Thus, the hybrid gap structure of line and point nodes would be realized such as proposed in URu_2Si_2 [27] and UPt_3 [19].

4.4 Numerical results for minimal models

Finally, we demonstrate the above-mentioned group theoretical arguments by using a specific model, and discuss the stability of horizontal line nodes on the zone face. We consider a Bogoliubov-de Gennes (BdG) Hamiltonian of an AP (FP) superconductivity A_g (A_u) with the given gap structure, which is regarded as a minimal model of UPd_2Al_3 (UCoGe).

4.4.1 Minimal models

In this subsection, we briefly show our model Hamiltonians, which mimic UPd_2Al_3 or UCoGe superconductors. For simplicity, we set the lattice constant to unity, and consider a single orbital on each U site.

The antiferromagnetic phase of UPd_2Al_3 belongs to the magnetic space group P_b2_1/m (the unique axis is chosen to be c-axis). In the unit cell, two U atoms are placed at $\boldsymbol{x}_1 = (0, 0, 0)$ and $\boldsymbol{x}_2 = (0, 0, \frac{1}{2})$. A minimal tight-binding Hamiltonian contains four orbitals, corresponding to two atoms (sublattice) and the spin-1/2 degrees of freedom. The Hamiltonian $\mathcal{H}$ is defined by,

$$\mathcal{H} = \sum_{\boldsymbol{k}} \sum_{\alpha\beta} \sum_{\sigma\sigma'} h_{\alpha\sigma,\beta\sigma'}(\boldsymbol{k}) c^\dagger_{\alpha\sigma}(\boldsymbol{k}) c_{\beta\sigma'}(\boldsymbol{k}), \tag{4.4.1}$$

where $c^\dagger_{\alpha\sigma}(\boldsymbol{k})$ ($c_{\beta\sigma'}(\boldsymbol{k})$) is a creation (annihilation) operator of electrons with spin σ (σ') $=\uparrow, \downarrow$ on an atom α (β) $= 1, 2$. Here, we have used the sublattice dependent Fourier transformation defined as,

$$c^\dagger_{\alpha\sigma}(\boldsymbol{k}) = \frac{1}{\sqrt{N}} \sum_{\boldsymbol{R}} e^{i\boldsymbol{k}\cdot(\boldsymbol{R}+\boldsymbol{x}_\alpha)} c^\dagger_{\alpha\sigma}(\boldsymbol{R}), \tag{4.4.2}$$

where N is a total number of unit cell, $\boldsymbol{R}$ is a lattice vector, and $\boldsymbol{x}_\alpha$ is a relative position for the site α in the unit cell. In this case, $h_{\alpha\sigma,\beta\sigma'}(\boldsymbol{k})$ in the matrix form is given by,

$$h(\boldsymbol{k}) = \varepsilon_0(\boldsymbol{k})\tau^0 \otimes \sigma^0 + \varepsilon_1(\boldsymbol{k})\tau^x \otimes \sigma^0 + \delta_M \tau^z \otimes \sigma^x, \tag{4.4.3}$$

where $\varepsilon_0(\boldsymbol{k}) = -2t_{xy}(\cos k_x + \cos k_y) - 2t'_z \cos k_z - \mu$ and $\varepsilon_1(\boldsymbol{k}) = -2t_z \cos\frac{k_z}{2}$. τ^μ and σ^μ ($\mu = 0, x, y,$ and z) are the Pauli matrices acting on the sublattice and the spin degrees of freedom, respectively. The third term of Eq. (4.4.3) tunes the magnitude of the staggered magnetic moment along a-axis in the antiferromagnetic phase.

In the superconducting state, the anomalous part Ψ^Γ given by

$$\Psi^\Gamma = \sum_{\boldsymbol{k}} \sum_{\alpha\beta} \varphi^\Gamma_{\alpha\sigma,\beta\sigma'}(\boldsymbol{k}) c^\dagger_{\alpha\sigma}(\boldsymbol{k}) c^\dagger_{\beta\sigma'}(-\boldsymbol{k}) \tag{4.4.4}$$

should be added in the Hamiltonian $\mathcal{H}$. Here, $\varphi^\Gamma_{\alpha\sigma,\beta\sigma'}(\boldsymbol{k})$ is the corresponding order parameter. The superscript Γ denotes an irreducible representation of the point group C_{2h}. For the A_g

spin-singlet pairing state discussed in Fig. 1, we can take momentum-independent (constant) order parameter,

$$\varphi^{A_g}(\boldsymbol{k}) = \Delta\tau^0 \otimes (i\sigma^y), \tag{4.4.5}$$

where Δ is the gap amplitude.

On the other hand, the ferromagnetic phase of UCoGe belongs to the magnetic space group $Pn'm'a$. U atoms are placed at $\boldsymbol{x}_1 = (x, \frac{1}{4}, z), \boldsymbol{x}_2 = (\frac{1}{2}-x, \frac{3}{4}, z-\frac{1}{2}), \boldsymbol{x}_3 = (1-x, \frac{3}{4}, 1-z)$, and $\boldsymbol{x}_4 = (\frac{1}{2}+x, \frac{1}{4}, \frac{3}{2}-z)$ in the unit cell, where $x = 0.0101, z = 0.7075$. The ferromagnetic moments are aligned along c-axis. In this case, $h(\boldsymbol{k})$ in Eq. (4.4.1) is given by,

$$h(\boldsymbol{k}) = h_0(\boldsymbol{k}) + h_S(\boldsymbol{k}) + h_M, \tag{4.4.6}$$

where $h_0(\boldsymbol{k})$, $h_S(\boldsymbol{k})$, and h_M represent the hopping integral, the spin-orbit coupling, and the exchange interaction with the magnetic moments, respectively. These are given by,

$$h_0(\boldsymbol{k}) = \begin{pmatrix} \varepsilon_0(\boldsymbol{k}) & \varepsilon_{12}(\boldsymbol{k}) & \varepsilon_{13,-}(\boldsymbol{k}) & \varepsilon_{14}(\boldsymbol{k}) \\ \varepsilon_{12}^*(\boldsymbol{k}) & \varepsilon_0(\boldsymbol{k}) & \varepsilon_{14}(\boldsymbol{k}) & \varepsilon_{13,+}(\boldsymbol{k}) \\ \varepsilon_{13,-}^*(\boldsymbol{k}) & \varepsilon_{14}^*(\boldsymbol{k}) & \varepsilon_0(\boldsymbol{k}) & \varepsilon_{12}^*(\boldsymbol{k}) \\ \varepsilon_{14}^*(\boldsymbol{k}) & \varepsilon_{13,+}^*(\boldsymbol{k}) & \varepsilon_{12}(\boldsymbol{k}) & \varepsilon_0(\boldsymbol{k}) \end{pmatrix} \otimes \sigma^0, \tag{4.4.7a}$$

$$h_S(\boldsymbol{k}) = \delta_S \sin k_y \,\mathrm{diag}(1,-1,-1,1) \otimes \sigma^z, \tag{4.4.7b}$$

$$h_M = \delta_M \,\mathrm{diag}(1,1,1,1) \otimes \sigma^z. \tag{4.4.7c}$$

Here, we only consider a simple spin-orbit coupling term, which lifts the band degeneracy on the zone face. Each element of the hopping matrix $\varepsilon_0(\boldsymbol{k})$, $\varepsilon_{12}(\boldsymbol{k})$, $\varepsilon_{13,\pm}(\boldsymbol{k})$, and $\varepsilon_{14}(\boldsymbol{k})$ is given by,

$$\varepsilon_0(\boldsymbol{k}) = -2t_y \cos k_y - \mu \tag{4.4.8a}$$

$$\varepsilon_{12}(\boldsymbol{k}) = 4t_{12} \cos\frac{k_y}{2} \cos\frac{k_z}{2} (e^{-(4x-1)k_x/2i} + \lambda_1 e^{-(4x+1)k_x/2i}), \tag{4.4.8b}$$

$$\varepsilon_{13,\pm}(\boldsymbol{k}) = 2t_{13} \cos\frac{k_y}{2} (e^{-(2z-1)k_z i} + \lambda_2 e^{-(2z-2)k_z i}) e^{\pm 2xk_x i}, \tag{4.4.8c}$$

$$\varepsilon_{14}(\boldsymbol{k}) = 2t_{14} \cos\frac{k_x}{2} e^{-(4z-3)k_z/2i}. \tag{4.4.8d}$$

In the superconducting phase, we set a typical A_u-type gap function,

$$\varphi^{A_u}(\boldsymbol{k}) = \Delta \,\mathrm{diag}(1,1,1,1) \otimes (\sin k_x i\sigma^x\sigma^y + \sin k_y i\sigma^y\sigma^y), \tag{4.4.9}$$

where Δ is the gap amplitude. Note that each element of the (magnetic) point group P is given by $P = \{E, 2_z, \theta 2_y, \theta 2_x, I, \sigma_h, \theta I 2_y, \theta I 2_x\}$, whose irreducible representations are summarized in TABLE 4.4 [182]. Since the unitary transformation to the basis functions can

Table 4.4: The character table of point group P in UCoGe. ω is an arbitrary phase factor.

IRs	E	2_z	$\theta 2_y$	$\theta 2_x$	I	σ_h	$\theta I 2_y$	$\theta I 2_x$
A_g	1	1	ω	ω	1	1	ω	ω
B_g	1	-1	ω	$-\omega$	1	-1	ω	$-\omega$
A_u	1	1	ω	ω	1	1	ω	ω
B_u	1	-1	ω	$-\omega$	-1	1	$-\omega$	ω

connect the representations with different ω in TABLE 4.4, these representations are equivalent in the sense of corepresentations. Eq. (4.4.9) corresponds to the case of $\omega = 1$. Gap functions of finite $\omega \neq 1$ can be simply obtained by the transformation $\varphi^{\Gamma}(\boldsymbol{k}) \mapsto \omega^{-\frac{1}{2}}\varphi^{\Gamma}(\boldsymbol{k})$ without any change of the nodal structure.

Note that the band structure in Fig. 4.3(a) is the result for the parameters

$$(t_{xy}, t_z, t'_z, \delta_M, \Delta, \mu) = (1.0, 0.4, 0.1, 0.4, 0.1, -2.0).$$

Figures 4.3(c) and 4.4(a) were obtained by changing Δ and δ_M, respectively. And also, the band structure in Fig. 4.3(b) is the result for the parameters,

$$(t_y, t_{12}, t_{13}, t_{14}, \lambda_1, \lambda_2, \delta_M, \delta_S, \Delta, \mu) = (0.1, 0.4, 1.0, 0.8, 0.8, 0.8, 0.2, 0.2, 0.02, -1.9).$$

Figures 4.3(d) and 4.4(b) were obtained by changing Δ and δ_S, respectively.

4.4.2 Numerical results

Here, we discuss the nodal structure in our model Hamiltonians. Figure 4.3(a) depicts the band structure along the high-symmetry line $(0, 0, \pi)$-$(0, \pi, \pi)$ in the AP model of UPd_2Al_3, and its inset shows the Fermi surface. Figure 4.3(b) is the case of UCoGe. In both Figs. 4.3(a) and (b), we can find that the superconducting gap remains closed at the Fermi level in the particle-hole symmetric Bogoliubov band (red arrows), while a gap is open at the inter-band crossing point far from the Fermi level (blue arrows). The emergence of gap zero on the zone face is fully consistent with the group theoretical arguments. On the other hand, the group theory does not say anything about the inter-band gap opening, since the above-mentioned arguments are based on the intra-band pairs. As readily understood, if the inter-band gap is sufficiently large, then the symmetry protected intra-band gap nodes can be lost. In our models, the emergence of gap nodes is controlled by three parameters, Δ, δ_M, and δ_S, which correspond to respectively the gap amplitude, the strength of the magnetic order and the spin-orbit coupling. δ_M and/or δ_S lift the band degeneracy on the zone face.

Note that, in order to lift the band degeneracy on the face, we require both the spin-orbit coupling and the exchange interaction with the magnetic moments in UCoGe, while only

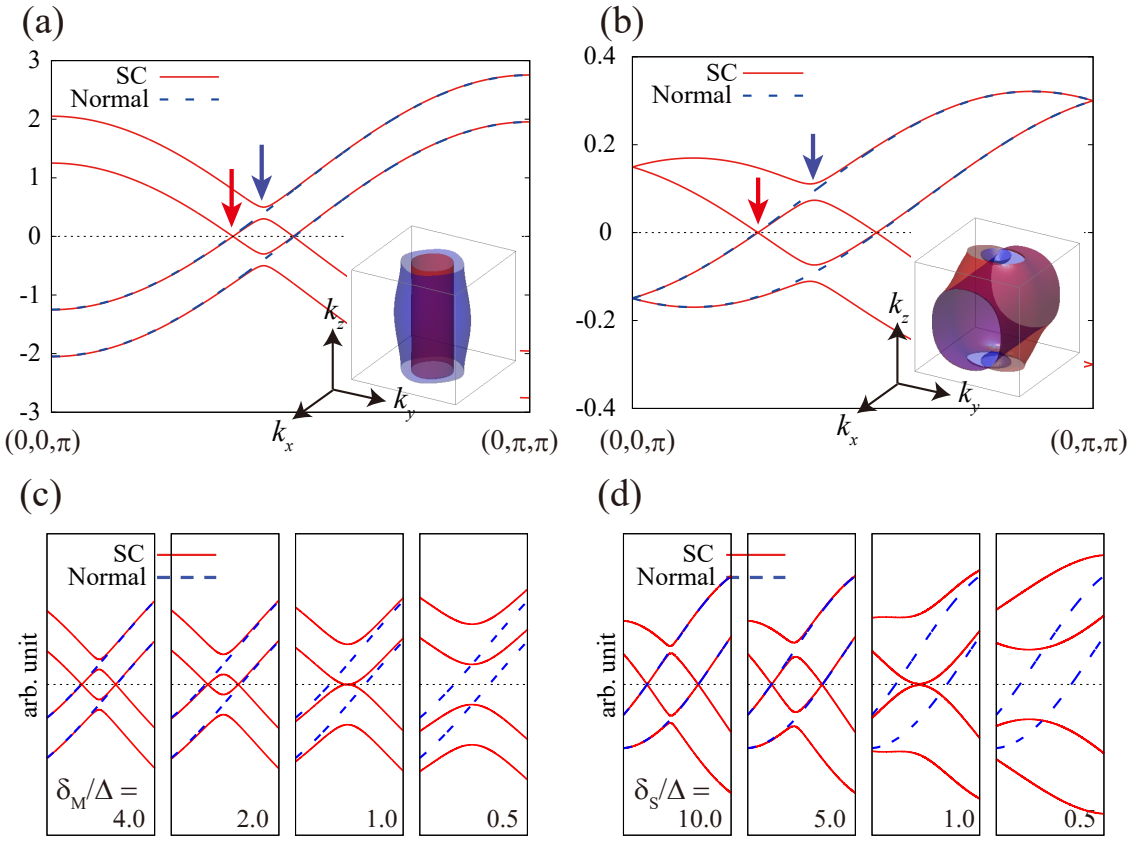

Figure 4.3: Typical band structure of the BdG Hamiltonian assuming (a) the A_g gap function in the AP model of UPd_2Al_3 and (b) the A_u gap function in the FP model of UCoGe. The lattice constants are set to be unity. The measure of energy is the unit of the nearest neighbor hopping integral. Blue dashed lines correspond to the original band in the normal state. The inset shows the corresponding Fermi surface. (c) and (d) Enlarged figure of the Bogoliubov band for several Δ.

latter is necessary in UPd_2Al_3. This comes from the following reasons. Without the spin-orbit coupling, the direction of the magnetic moments can be freely chosen, and then, the extended time reversal symmetry $\{\theta 2_z|\boldsymbol{t}_z\}$ is restored in UCoGe. As a result, there remains twofold degeneracy on the zone face due to the corresponding Kramers theorem, even in the presence of ferromagnetism. Note also that, in UCoGe, the spin-orbit coupling vanishes along $k_y = 0$ line on the zone face, which is also protected by the Kramers theorem for the anti-unitary operation $\{\theta 2_y \sigma_h|\boldsymbol{t}_y + \boldsymbol{t}_n\}$. This implies that the present line nodes also disappear along $k_y = 0$ line, which can be directly confirmed by the present group theoretical arguments, and become arc line nodes similar to ones discussed in Ref. [33].

Figures 4.3(c) and (d) are the Bogoliubov band structure for several Δ. As expected, we can find the vanishing of gap nodes for larger Δ via a kind of Lifshitz transition. Figures 4.4(a)

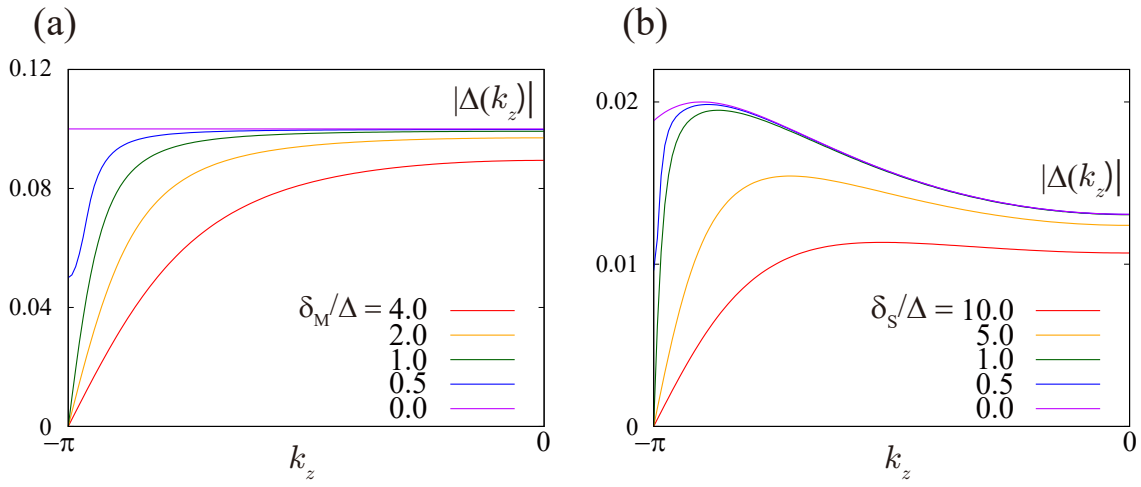

Figure 4.4: k_z dependence of the excitation gap amplitude $|\Delta(k_z)|$ on the Fermi surface at $k_x = 0$ for several (a) δ_M in the AP model and (b) δ_S in the FP model.

and (b) show k_z dependence of the excitation gap amplitude $|\Delta(k_z)|$ on the Fermi surface at $k_x = 0$ for several δ_M and δ_S. For relatively large $\delta_M(\delta_S)$, $\Delta(k_z)$ behaves like $\Delta(k_z) \sim \cos(k_z/2)$. In the AP model, such nodal structure is similar to the self-consistent solution in the previous study of UPd_2Al_3 [201]. On the other hand, for relatively small $\delta_M(\delta_S)$, the gap amplitude sharply changes around the nodes on the zone face, which was also discussed in Ref. [132]. In the limit of $\delta_M(\delta_S) = 0$, the nodal structure is completely lost. Note that, in the FP model, the Weyl point nodes emerging along the $k_x = k_y = 0$ line are insensitive to the ratio δ_S/Δ. These nodes exist unless the pair amplitude of antiparallel spin components exceeds the magnitude of a ferromagnetic exchange splitting. Also, in an antiferromagnetic state, generally, a singlet pairing may induce a staggered pairing. [207, 208] However, it does not affect the present nodal structure.

In our model, such k_z dependence originates only from the unitary matrix diagonalizing the BdG Hamiltonian. It implies that even the BCS approximation of purely local (on-site) interactions, such as the conventional electron-phonon interactions, can induce the anisotropic gap structure in the non-symmorphic magnetic superconductors. In the realistic situations, the band splittings on the zone face will be sufficiently larger than the gap amplitude. Therefore, it is expected that the present nodal structure can be observed as the usual power-law behavior in thermodynamic and/or transport properties at low temperatures. Consequently, nontrivial symmetry protected line nodes in the non-symmorphic magnetic space groups will be observed in magnetic superconductors UCoGe and UPd_2Al_3.

4.5 Conclusion

In this chapter, we investigate the nodal structure in superconductors with a non-symmorphic magnetic space group symmetry. Within the weak-coupling BCS theory, we show that UCoGe-type ferromagnetic superconductors must have horizontal line nodes on either the $k_z = 0$ or $k_z = \pm\pi/c$ plane. Moreover, it is likely that additional Weyl point nodes exist along the $k_x = k_y = 0$ line. On the other hand, in UPd_2Al_3-type antiferromagnetic superconductors, gap functions with A_g symmetry possess horizontal line nodes in the antiferromagnetic Brillouin zone boundary perpendicular to the c-axis. In other words, the conventional fully gapped s-wave superconductivity is forbidden in this type of antiferromagnetic superconductors, regardless of the pairing mechanism, as long as the Fermi surface crosses a zone boundary. In both cases, the emergence of the non-trivial line nodes requires the sufficiently larger band splitting than the gap amplitude at the Brillouin zone boundary. The obtained nodal structures are fully consistent with the various observations both of the cases in UPd_2Al_3 and UCoGe. Thus, we conclude that UPd_2Al_3 and UCoGe are candidate unconventional superconductors possessing hidden symmetry protected line nodes, peculiar to non-symmorphic magnetic space groups.

Chapter 5

Conclusion

In this thesis, we investigate the superconducting symmetry and the gap structure in various unconventional superconductors with spin-orbit coupling and multi-degrees of freedom.

In Chapter 2, we present an exotic multi-gap structure in the heavy fermion superconductor UPt_3, from the gap analysis based on the first-principles calculations [2]. The obtained E_{2u} pairing state has in-plane twofold vertical line nodes, axial point and horizontal line nodes on each Fermi surface, which is completely different from the previous phenomenological models. In particular, the twofold vertical line nodes in the small Fermi surface can consistently explain the field-angle resolved measurements in both the thermal conductivity and the specific heat. This nodal structure is well consistent with the group theoretical consideration of the Cooper pairs in the $j = 5/2$ space, instead of in the (pseudo) spin 1/2 space. In addition, the obtained gap structure can be naturally explained by the mixture of p and f-wave components with different $\boldsymbol{d}$-vectors. These peculiar features may provide a clue to understand the remaining problems of the Pauli limiting of the upper critical field and the anomalous behavior of the Knight shift and so on.

In Chapter 3, we perform the group theoretical classification of various unconventional superconductivity emerging in multiorbital systems with spin-orbit coupling. [4]. The order parameters are classified by introducing generalized Cooper pairs, which possess spin-orbital coupled (multipole) degrees of freedom instead of the conventional spin singlet/triplet in single orbital systems. In systems with the symmorphic space group symmetry, the atomic site (sublattice) degrees of freedom can always be reduced to such multipole degrees of freedom. Thus, the classification tables obtained here include all the possible gap functions in any symmorphic superconductor that belongs to O, D_4, or D_6 point group symmetry. The results can easily be extended to the other point groups. From the classification, we obtain the following key consequences: (1) A superconducting gap function with $\Gamma_9 \otimes \Gamma_9$ in D_6 possesses nontrivial momentum dependence, which is different from the usual spin 1/2 classification. (2) Unconventional gap structure can be realized in the BCS approximation of purely local interactions irrespective of attraction/repulsion. (3) Reflecting symmetry of orbital basis

functions, there appear not symmetry protected but inevitable line nodes/gap minima, and thus, anisotropic s-wave superconductivity can be naturally explained even in the absence of competing fluctuations.

In Chapter 4, we extend the gap classification in non-symmorphic space groups to the magnetic crystals [5]. This is performed based on the representation theory of space group symmetry, which gives us the correct way to take into account the non-symmorphic property of the space group. The results are applied to the analysis of superconductivity in UCoGe and UPd_2Al_3. We show that the UCoGe-type ferromagnetic superconductors have horizontal line nodes on either the $k_z = 0$ or $k_z = \pm\pi/c$ plane. In addition, in UPd_2Al_3-type antiferromagnetic superconductors, A_g gap functions always have line nodes on $k_z = \pm\pi/c$ plane, in other words, the conventional fully gapped s-wave superconductivity is forbidden. Thus, we conclude that UCoGe and UPd_2Al_3 are candidate unconventional superconductors possessing hidden symmetry protected line nodes, peculiar to non-symmorphic magnetic space groups. Note that although we here investigate the nodal structure in UCoGe and UPd_2Al_3, the obtained results are generally applicable in various non-symmorphic superconductors. The extension to more complicated situations such as interface and FFLO superconductivity is a interesting problem in future.

Appendix A

Space groups and their representations

In the appendix, we summarize fundamentals of the space groups and their representations used in this thesis. First, we define several groups specifying the crystal structure, and then introduce two representations, which we denote by *orbital-based* and *band-based* representations respectively. The symmetry of the Cooper pair wave functions in the orbital-based representation, which explicitly deals with all internal degrees of freedom in electrons, is a main subject discussed in Chapter 3. On the other hand, the band-based representation is necessary for the investigation of nodal structure protected by the non-symmorphic space group symmetry, which is extended in Chapter 4. Part of the contents given below overlap with the usual band theory, for example, as seen in Ref. [192].

A.1 Space groups

Let C be a given crystalline structure. The crystal C determines the *space group* G, the *point group* P, and the *lattice translation group* T. The space group G is defined as the symmetry group that does not change the crystal C. Any element of $g \in G$ consists of point group operation p and translation $\boldsymbol{a}$. The point group P is defined as the projection from G by forgetting the translations. Here, $p \in P$ describes a space rotation or a space inversion operation. The lattice translation group T is defined as the set of translations $t \in G$ that is invariant under the point group operations. Namely, if $t \in T$, then $pt \in T$ for any $p \in P$. In three-dimensional crystals, it is known that there are 230 types of crystallographic space groups and 32 types of point groups. The point group is also classified into one of 7 *crystal systems* by its rotational symmetry. The 14 types of Bravais lattices are specified by the crystal system and the centering pattern, which are identical with the types of T.

A.1.1 Seitz notation

Any element of the space group $g \in G$ consists of point group operation $p \in P$ and translation $\boldsymbol{a}$. It is convenient to specify $g \in G$ by use of the Seitz space group symbol $g = \{p|\boldsymbol{a}\}$, which represents the following transformation,

$$\{p|\boldsymbol{a}\}\boldsymbol{x} = a\boldsymbol{x} + \boldsymbol{a}, \tag{A.1.1}$$

for a three-dimensional vector $\boldsymbol{x}$. Note that the center of point group operations is fixed once the crystal C is given. According to Eq. (A.1.1), the product of two space group elements $\{p_1|\boldsymbol{a}_1\}$ and $\{p_2|\boldsymbol{a}_2\}$ is given by,

$$\{p_1|\boldsymbol{a}_1\}\{p_2|\boldsymbol{a}_2\} = \{p_1p_2|p_1\boldsymbol{a}_1 + \boldsymbol{a}_2\}. \tag{A.1.2}$$

Then, the inverse $\{p|\boldsymbol{a}\}^{-1}$ can be naturally defined to satisfy $\{p|\boldsymbol{a}\}\{p|\boldsymbol{a}\}^{-1} = \{p|\boldsymbol{a}\}^{-1}\{p|\boldsymbol{a}\} = \{E|\boldsymbol{0}\}$ where E is the identity operation of P (and of course $\{E|\boldsymbol{0}\}$ is of G), thus,

$$\{p|\boldsymbol{a}\}^{-1} = \{p^{-1}| - p^{-1}\boldsymbol{a}\}. \tag{A.1.3}$$

Eqs. (A.1.2) and (A.1.3) defines the group structure of G.

A.1.2 Symmorphic and non-symmorphic space groups

The lattice translation group T is an invariant abelian subgroup of G, which is immediately seen from $pt \in T$ for all $t \in T$ and $p \in P$. Therefore, if we decompose G as left cosets,

$$G = \sum_{p \in P} \{p|\boldsymbol{a}\}T, \tag{A.1.4}$$

then the cosets $\{p|\boldsymbol{a}\}T$ form a quotient group G/T. In the following, the coset representatives $\{p|\boldsymbol{a}\}$ are fixed once the decomposition Eq. (A.1.4) is chosen. The set of the representatives $r = \{p|\boldsymbol{a}\}$ for all $p \in P$ is denoted by R. An element of the quotient group G/T, which corresponds to the coset $r_\alpha T$, is denoted by α.

Here, if we can choose R to form a group, which is isomorphic with P, then G is called a *symmorphic* space group. If not, G is called a *non-symmorphic* space group and R no longer forms a group. This means that the symmorphic space groups G can be represented as the semi-direct product of T and P as $G = T \rtimes P$ while the non-symmorphic ones cannot be. As was shown by Fedorov, there are 230 types of space groups, which often called Fedorov groups to distinguish from Shubnikov groups in magnetic crystals. Among them, 73 space groups are symmorphic and 157 space groups are non-symmorphic. Note that, in either case, one can see that any element of $g \in G$ has a unique decomposition of the form $g = rt$ with $r \in R$ and $t \in T$.

A.1.3 Magnetic space groups

In the description of magnetic crystals, it is necessary to consider a time reversal operation θ as well as the other space group operations. θ is defined as the operation that inverses magnetic moments, arranged in some symmetrical way, with no change of the lattice structure. Namely, θ commutes any elements of space groups,

$$\theta\{p|\boldsymbol{a}\}\theta^{-1} = \{p|\boldsymbol{a}\} \quad \text{for all} \;\; g = \{p|\boldsymbol{a}\} \in G, \tag{A.1.5}$$

and flips the internal degree of freedom describing the magnetic moments on the atomic sites. According to the well-known result in quantum mechanics, θ should be regarded as an *anti-unitary* operator. In general, any non-unitary group M can be divided into a set of unitary operators G and of anti-unitary operators aG where a is an anti-unitary operation. Then, G is an invariant subgroup of M whose order is $|M/G| = 2$, and thus, we can always write down M as the form of $M = G + aG$.

The space groups describing general magnetic crystals are called Shubnikov groups. It is known that there are 1651 Shubnikov groups, 230 (type I) correspond to the classical Fedorov space groups, (type II) 230 to these groups together with time reversal, and the remaining (type III and type IV) 1191 to groups in which time reversal occurs only in combination with other operations and not by itself. These Shubnikov space groups M are given by,

$$\text{Type I} : M = G, \tag{A.1.6}$$
$$\text{Type II} : M = G + \{\theta|\mathbf{0}\}G, \tag{A.1.7}$$
$$\text{Type III} : M = H + \{\theta|\mathbf{0}\}(G - H), \tag{A.1.8}$$
$$\text{Type IV} : M = G + \{\theta|\boldsymbol{a}\}G, \tag{A.1.9}$$

where G is any Fedorov group, H a halving subgroup of G which $G - H$ contains no pure translation. Type III and IV Shubnikov groups represent the crystal structure with finite magnetic moments, and thus, are called *magnetic* space groups.

In addition, we can consider the time reversal operator θ also in the point group P. Then, similar to the space group, any point group is classified into one of three Shubnikov point groups, which are given by,

$$\text{Type I} : P = G, \tag{A.1.10}$$
$$\text{Type II} : P = G + \theta G, \tag{A.1.11}$$
$$\text{Type III} : P = H + \theta(G - H), \tag{A.1.12}$$

where G is any Fedorov point group and H is a subgroup of G. Note that the Shubnikov point groups corresponding to type IV Shubnikov groups belong to type II, as the same as of type II Shubnikov groups describing paramagnetic crystals.

A.1.4 Representations of space groups

According to the quantum mechanics, the eigenstate of the Hamiltonian can be regarded as the basis of the irreducible representation of the symmetry group, whose elements leave the Hamiltonian invariant. In the solids, the Hamiltonian possesses the same symmetry as the crystal, i.e., the space group symmetry. Thus, the representation theory of the space group symmetry often is the main subject of the symmetry consideration of the quantum states or the Hamiltonian.

In practice, depending on the purpose, it is convenient to use several representations to describe the Hamiltonian, which will be connected by the unitary transformations. In particular, since the crystal momentum $\boldsymbol{k}$ of each one-particle state is preserved in the non-interacting electron systems, it is convenient to extend the discussion on the Hamiltonian in the momentum space. In the rest of the appendix, we introduce two types of such representations, which we call orbital-based and band-based representations, used in this thesis.

More concretely, a representation Γ of the space group G is defined as the homomorphic projection $\Gamma : G \to \mathrm{GL(m)}$, which holds the group structure,

$$D^{(\Gamma)}(g_1)D^{(\Gamma)}(g_2) = D^{(\Gamma)}(g_1 g_2), \tag{A.1.13}$$

for all $g_1, g_2 \in G$. Here, $D^{(\Gamma)} \in \mathrm{GL(m)}$ is called the representation matrix of Γ and m is the dimension of $D^{(\Gamma)}$. Then, the basis of the representation $f_i^{(\Gamma)}$ is defined to be satisfied,

$$g f_i^{(\Gamma)} = \sum_j f_j^{(\Gamma)} D_{ji}^{(\Gamma)}(g). \tag{A.1.14}$$

On the other hand, the representation Γ of the magnetic space group $M = G + aG$ is defined by the following relations,

$$D^{(\Gamma)}(g_1)D^{(\Gamma)}(g_2) = D^{(\Gamma)}(g_1 g_2) \tag{A.1.15}$$
$$D^{(\Gamma)}(g_1)D^{(\Gamma)}(a_2) = D^{(\Gamma)}(g_1 a_2) \tag{A.1.16}$$
$$D^{(\Gamma)}(a_1)(D^{(\Gamma)}(g_2))^* = D^{(\Gamma)}(a_1 g_2) \tag{A.1.17}$$
$$D^{(\Gamma)}(a_1)(D^{(\Gamma)}(a_2))^* = D^{(\Gamma)}(a_1 a_2) \tag{A.1.18}$$

for the unitary $g_1, g_2 \in G$ and the anti-unitary operations $a_1, a_2 \in aG$. The representation of the non-unitary group often is called a *corepresentation*. In this thesis, we only deal with the unitary representation, whose representation matrix is an element of U(m).

A.2 Orbital-based representations

The Hamiltonian on the Fock space describing the electrons in the solids can be expressed in terms of the Wannier state, which approximately represents an atomic or a molecule orbital tightly localized at some site. In the Wannier basis, a quadratic term of the Hamiltonian can be written as follows,

$$H = \sum_{\boldsymbol{R}\boldsymbol{R}'} \sum_{\alpha\beta} \sum_{ij} h_{\alpha i,\beta j}(\boldsymbol{R},\boldsymbol{R}') c^\dagger_{\alpha i}(\boldsymbol{R}) c_{\beta j}(\boldsymbol{R}'), \tag{A.2.1}$$

where $c^\dagger_{\alpha i}(\boldsymbol{R})$ ($c_{\alpha i}(\boldsymbol{R})$) is a creation (annihilation) operator of the electron in the Wannier basis. Here, the lattice vector $\boldsymbol{R} \in T$ represents a center of unit cells, which is an element of the lattice translation symmetry group, namely, $\boldsymbol{R} = \sum_{i=1}^{3} n_i \boldsymbol{t}_i$ where n_i is an integer and $\boldsymbol{t}_i$ is the fundamental translation. α labels an atom located at $\boldsymbol{R} + \boldsymbol{x}_\alpha$, i denotes the other internal degrees of freedom, such as spin and orbital. In this thesis, we denote by the orbital-based Hamiltonian the Fourier transformation of Eq. (A.2.1),

$$H = \sum_{\boldsymbol{k}} \sum_{\alpha\beta} \sum_{ij} h_{\alpha i,\beta j}(\boldsymbol{k}) c^\dagger_{\alpha i}(\boldsymbol{k}) c_{\beta j}(\boldsymbol{k}). \tag{A.2.2}$$

In the following, we will investigate the transformation property of the creation operator $c^\dagger_{\alpha i}(\boldsymbol{k})$ and find that the set of $c^\dagger_{\alpha i}(\boldsymbol{k})$ forms a (reducible) representation of G. First, we focus on a transformation property of the internal degrees of freedom.

A.2.1 Representations of point groups

Let us focus on the point group symmetry P, which contains the real R_r and the spin R_s space rotations, the space inversion I, and the time reversal θ operations. Taking into account the double-valuedness of the electron spin for SO(3) group, it is convenient to deal with both the space rotations as the elements of SU(2) group, and regard the orbital and the spin degrees of freedom as its integer and half-integer irreducible representations, respectively. Let $l \in \mathcal{N}$ and $s \in \mathcal{N} + \frac{1}{2}$ be such representations corresponding to the orbital and the spin. Then, the transformations of their basis functions, $|l, l_z\rangle$ and $|s, s_z\rangle$, are given as follows,

$$R_r(|l,l_z\rangle \otimes |s,s_z\rangle) = \sum_{l'_z} (|l,l'_z\rangle \otimes |s,s_z\rangle) D^{(l)}_{l'_z l_z}(R_r), \tag{A.2.3}$$

$$R_s(|l,l_z\rangle \otimes |s,s_z\rangle) = \sum_{s'_z} (|l,l_z\rangle \otimes |s,s'_z\rangle) D^{(s)}_{s'_z s_z}(R_s), \tag{A.2.4}$$

where $D^{(l)}(R_r)$ and $D^{(s)}(R_s)$ are the representation matrices of l and s, respectively. In the presence of spin-orbit coupling, the system is invariant only under the simultaneous rotation $R = R_r R_s$. Thus, it is convenient to introduce a following representation j and its basis

$|(ls)j, j_z\rangle$, which holds,

$$R\,|(ls)j, j_z\rangle = \sum_{j'_z} |(ls)j, j_z\rangle\, D^{(j)}_{j'_z j_z}(R), \tag{A.2.5}$$

where $|(ls)j, j_z\rangle = \sum_{l_z s_z}(|l, l_z\rangle\otimes|s, s_z\rangle)\,\langle ll_z ss_z|jj_z\rangle$. Here $\langle ll_z ss_z|jj_z\rangle := (\langle l, l_z|\otimes\langle s, s_z|)\,|(ls)j, j_z\rangle$ is known as a Clebsch-Gordan coefficient, which is obtained by reducing the direct product representation $l \otimes s$ into the irreducible representations of SU(2) group. Due to the electron spin, j is also the double-valued representation for SO(3) group.

Since the space inversion I and the time reversal θ are not the elements of SU(2) group, the representation of those have to be defined by the physical insight. In this thesis, we used the following definitions,

$$I(|l, l_z\rangle \otimes |s, s_z\rangle) = (-1)^l(|l, l_z\rangle \otimes |s, s_z\rangle), \tag{A.2.6}$$
$$\theta(|l, l_z\rangle \otimes |s, s_z\rangle) = (-1)^{l+l_z}(-1)^{s+s_z}(|l, \bar{l}_z\rangle \otimes |s, \bar{s}_z\rangle), \tag{A.2.7}$$

then we get,

$$I\,|(ls)j, j_z\rangle = (-1)^l\,|(ls)j, j_z\rangle\,, \tag{A.2.8}$$
$$\theta\,|(ls)j, j_z\rangle = (-1)^{j+j_z}\,|(ls)j, \bar{j}_z\rangle\,, \tag{A.2.9}$$

where $\bar{l}_z = -l_z, \bar{s}_z = -s_z$, and $\bar{j}_z = -j_z$. This is obtained as follows,

$$\begin{aligned}
\theta\,|(ls)j, j_z\rangle &= \sum_{l_z s_z}(-1)^{l+l_z}(-1)^{s+s_z}(|l, \bar{l}_z\rangle \otimes |s, \bar{s}_z\rangle)\,\langle ll_z ss_z|jj_z\rangle \\
&= \sum_{l_z s_z}(-1)^{j-l_z-s_z}(|l, l_z\rangle \otimes |s, s_z\rangle)\,\langle ll_z ss_z|j\bar{j}_z\rangle \\
&= (-1)^{j+j_z}\,\langle (ls)j, \bar{j}_z\rangle\,.
\end{aligned}$$

Here, we have used the following identities, $\langle ll_z ss_z|jj_z\rangle = (-1)^{l+s-j}\,\langle l\bar{l}_z s\bar{s}_z|j\bar{j}_z\rangle$ and $\langle ll_z ss_z|jj_z\rangle = \delta_{l_z+s_z,j_z}\,\langle ll_z ss_z|jj_z\rangle$. In this definition, the representation matrices $D^{(j)}(R)$ and $D^{(j)}(\theta)$ do not depend on both l and s. (Note that the definition that θ satisfies $\theta(|l, l_z\rangle \otimes |s, s_z\rangle) = (-1)^{l_z+s_z}(|l, \bar{l}_z\rangle \otimes |s, \bar{s}_z\rangle)$ so that $\theta\,|(ls)jj_z\rangle = (-1)^{j+j_z-l-s}\,|(ls)j\bar{j}_z\rangle$ is also often used in some literature.) In the following, we neglect the index ls in $|(ls)j, j_z\rangle$ and write simply by $|j, j_z\rangle$.

In practice, the representation matrices of SU(2) group can be obtained with the help of extended Euler's angle [209]. Namely, $R \in$ SU(2) can be assigned by the rotation axis $\boldsymbol{n}$ and the angle $\phi \in [0, 4\pi)$, and thus, we make $(\boldsymbol{n}, \phi)$ correspond to the Euler's angle (α, β, γ) which are defined in $\alpha \in [0, 2\pi), \beta \in [0, \pi]$, and $\gamma \in [0, 4\pi)$ using the convention $\alpha = 0$ when $\beta = 0$ or π. By use of such (α, β, γ), an irreducible representation j or its representation matrix $D^{(j)}(R)$ is given by,

$$\begin{aligned}
D^{(j)}_{j_z j'_z}(R(\boldsymbol{n}, \phi)) &= D^{(j)}_{j_z j'_z}(R(\alpha, \beta, \gamma)) \\
&= e^{-ij_z\alpha}(e^{-i\beta j^{(j)}_y})_{j_z j'_z} e^{-ij'_z\gamma}.
\end{aligned} \tag{A.2.10}$$

Here, $j_y^{(j)}$ is a representation matrix of the operator j_y, which is defined as the generator of anti-clockwise rotation along y axis, of the representation j (*e.g.*, $j_y^{(1/2)} = \sigma^y/2$). Physically, j means a total angular momentum of the electron. Note that, when $\tilde{\gamma} \in [0, 2\pi)$ is used, the set $(\alpha, \beta, \tilde{\gamma})$ becomes usual Euler's angle for the SO(3) group rotations.

A.2.2 Basis functions in O, D_4, and D_6 point groups

In general, P is composed of the (finite number of) rotations R, the space inversion I, and the time reversal θ operations. Thus, the irreducible representations of P can be obtained by restricting j of SU(2) into its subgroup $\tilde{P} = P \cap \mathrm{SU}(2)$, and then inducing by I and θ. Here, we list basis functions of double-valued irreducible representations in O, D_4 and D_6 point groups, which are constructed with $j = 5/2$ states, $|j, j_z\rangle$.

- O group

$$
\begin{aligned}
|\Gamma_7, \pm\rangle &= \sqrt{\frac{1}{6}}\left|\frac{5}{2}, \pm\frac{5}{2}\right\rangle - \sqrt{\frac{5}{6}}\left|\frac{5}{2}, \mp\frac{3}{2}\right\rangle, \\
|\Gamma_{8a}, \pm\rangle &= \sqrt{\frac{5}{6}}\left|\frac{5}{2}, \pm\frac{5}{2}\right\rangle + \sqrt{\frac{1}{6}}\left|\frac{5}{2}, \mp\frac{3}{2}\right\rangle, \\
|\Gamma_{8b}, \pm\rangle &= \left|\frac{5}{2}, \pm\frac{1}{2}\right\rangle,
\end{aligned}
\tag{A.2.11}
$$

$$
\begin{aligned}
|\Gamma_{8a}, \pm\rangle &= \pm\left|\frac{3}{2}, \mp\frac{3}{2}\right\rangle, \\
|\Gamma_{8b}, \pm\rangle &= \pm\left|\frac{3}{2}, \pm\frac{1}{2}\right\rangle.
\end{aligned}
\tag{A.2.12}
$$

- D_4 group

$$
\begin{aligned}
|\Gamma_6, \pm\rangle &= \left|\frac{5}{2}, \pm\frac{1}{2}\right\rangle, \\
|\Gamma_7, \pm\rangle &= \cos\theta\left|\frac{5}{2}, \pm\frac{5}{2}\right\rangle + \sin\theta\left|\frac{5}{2}, \mp\frac{3}{2}\right\rangle,
\end{aligned}
\tag{A.2.13}
$$

$$
\begin{aligned}
|\Gamma_6, \pm\rangle &= \mp\left|\frac{3}{2}, \pm\frac{1}{2}\right\rangle, \\
|\Gamma_7, \pm\rangle &= \mp\left|\frac{3}{2}, \mp\frac{3}{2}\right\rangle.
\end{aligned}
\tag{A.2.14}
$$

- D_6 group

$$
\begin{aligned}
|\Gamma_7,\pm\rangle &= \left|\frac{5}{2},\pm\frac{1}{2}\right\rangle, \\
|\Gamma_8,\pm\rangle &= \left|\frac{5}{2},\pm\frac{5}{2}\right\rangle, \\
|\Gamma_9,\pm\rangle &= \left|\frac{5}{2},\mp\frac{3}{2}\right\rangle,
\end{aligned}
\tag{A.2.15}
$$

$$
\begin{aligned}
|\Gamma_7,\pm\rangle &= \mp\left|\frac{3}{2},\pm\frac{1}{2}\right\rangle, \\
|\Gamma_9,\pm\rangle &= \mp\left|\frac{3}{2},\mp\frac{3}{2}\right\rangle.
\end{aligned}
\tag{A.2.16}
$$

In space inversion invariant systems, these basis functions are classified into even or odd parity, following the orbital angular momentum $l = j \mp s$ with the spin $s = 1/2$. Under our convention, the basis functions defined above satisfy $\theta\,|\Gamma,\pm\rangle = \mp\,|\Gamma,\mp\rangle$ for any Γ.

A.2.3 Symmetry property of orbital-based representation

Next, let us consider the atomic site (sublattice) as well as the other internal degrees of freedom. Let $w_{\alpha i}^{(\Gamma)}(\boldsymbol{x}-\boldsymbol{R}-\boldsymbol{x}_\alpha) = \langle \boldsymbol{x}-\boldsymbol{R}-\boldsymbol{x}_\alpha | w_{\alpha i}^{(\Gamma)}\rangle$ be a Wannier state describing the ith basis orbital of Γ representation in α-atom located at $\boldsymbol{R}+\boldsymbol{x}_\alpha$. This satisfies

$$
w_{\alpha i}^{(\Gamma)}(p^{-1}(\boldsymbol{x}-\boldsymbol{R}-\boldsymbol{x}_\alpha)) = \sum_j w_{\alpha j}^{(\Gamma)}(\boldsymbol{x}-\boldsymbol{R}-\boldsymbol{x}_\alpha) D_{ji}^{(\Gamma)}(p), \tag{A.2.17}
$$

for the point group operation p around $\boldsymbol{r}_0 = \boldsymbol{R}+\boldsymbol{x}_\alpha$. Then, we introduce two states $\psi_{\alpha i}^{(\Gamma)}(\boldsymbol{k})$ and $\tilde{\psi}_{\alpha i}^{(\Gamma)}(\boldsymbol{k})$ constructed from $w_{\alpha i}^{(\Gamma)}(\boldsymbol{x})$ by the Fourier transformations,

$$
\psi_{\alpha i}^{(\Gamma)}(\boldsymbol{k};\boldsymbol{x}) = \sum_{\boldsymbol{R}} e^{i\boldsymbol{k}\cdot\boldsymbol{R}} w_{\alpha i}^{(\Gamma)}(\boldsymbol{x}-\boldsymbol{R}-\boldsymbol{x}_\alpha), \tag{A.2.18}
$$

$$
\tilde{\psi}_{\alpha i}^{(\Gamma)}(\boldsymbol{k};\boldsymbol{x}) = \sum_{\boldsymbol{R}} e^{i\boldsymbol{k}\cdot(\boldsymbol{R}+\boldsymbol{x}_\alpha)} w_{\alpha i}^{(\Gamma)}(\boldsymbol{x}-\boldsymbol{R}-\boldsymbol{x}_\alpha), \tag{A.2.19}
$$

Thus, for the space group operation $g = \{p|\boldsymbol{a}\}$, these transform like following ways,

$$
g\psi_{\alpha i}^{(\Gamma)}(\boldsymbol{k}) = e^{-i\boldsymbol{k}\cdot(p\boldsymbol{x}_\alpha - \boldsymbol{x}_{g\alpha}+\boldsymbol{a})} \sum_j \psi_{g\alpha j}^{(\Gamma)}(p\boldsymbol{k}) D_{ji}^{(\Gamma)}(p), \tag{A.2.20}
$$

$$
g\tilde{\psi}_{\alpha i}^{(\Gamma)}(\boldsymbol{k}) = e^{-i\boldsymbol{k}\cdot\boldsymbol{a}} \sum_j \tilde{\psi}_{g\alpha j}^{(\Gamma)}(p\boldsymbol{k}) D_{ji}^{(\Gamma)}(p), \tag{A.2.21}
$$

when the α-atom transforms to the (equivalent) $g\alpha$-atom. This is obtained by,

$$\begin{aligned} g\psi_{\alpha i}^{(\Gamma)}(\boldsymbol{k}) &= \sum_{\boldsymbol{R}} e^{i\boldsymbol{k}\cdot\boldsymbol{R}} w_{\alpha i}^{(\Gamma)}(g^{-1}\boldsymbol{x} - \boldsymbol{R} - \boldsymbol{x}_\alpha) \\ &= \sum_{\boldsymbol{R}'} e^{i\boldsymbol{k}\cdot(\boldsymbol{R}' - p\boldsymbol{x}_\alpha + \boldsymbol{x}_{g\boldsymbol{x}} - \boldsymbol{a})} w_{\alpha i}^{(\Gamma)}(p^{-1}(\boldsymbol{x} - \boldsymbol{R}' - \boldsymbol{x}_{g\alpha})) \\ &= e^{-i\boldsymbol{k}\cdot(p\boldsymbol{x}_\alpha - \boldsymbol{x}_{g\alpha} + \boldsymbol{a})} \sum_j \psi_{g\alpha j}^{(\Gamma)}(p\boldsymbol{k}) D_{ji}^{(\Gamma)}(p), \end{aligned}$$

and the similar relations for $\tilde{\psi}_{\alpha i}^{(\Gamma)}(\boldsymbol{k})$. Here, we have used $g(\boldsymbol{R} + \boldsymbol{x}_\alpha) = \boldsymbol{R}' + \boldsymbol{x}_{g\alpha}$ with the uniquely determined $\boldsymbol{R}'$. Thus, the corresponding creation operations, $c_{\alpha i}^{(\Gamma)\dagger}(\boldsymbol{k})$ and $\tilde{c}_{\alpha i}^{(\Gamma)\dagger}(\boldsymbol{k})$, meet following relations,

$$g c_{\alpha i}^{(\Gamma)\dagger}(\boldsymbol{k}) g^{-1} = e^{-i\boldsymbol{k}\cdot(p\boldsymbol{x}_\alpha - \boldsymbol{x}_{g\alpha} + \boldsymbol{a})} \sum_j c_{g\alpha j}^{(\Gamma)\dagger}(p\boldsymbol{k}) D_{ji}^{(\Gamma)}(p), \tag{A.2.22}$$

$$g \tilde{c}_{\alpha i}^{(\Gamma)\dagger}(\boldsymbol{k}) g^{-1} = e^{-i\boldsymbol{k}\cdot\boldsymbol{a}} \sum_j \tilde{c}_{g\alpha j}^{(\Gamma)\dagger}(p\boldsymbol{k}) D_{ji}^{(\Gamma)}(p). \tag{A.2.23}$$

We can write Eqs. (A.2.22) and (A.2.23) as $g c^\dagger(\boldsymbol{k}) g^{-1} = c^\dagger(p\boldsymbol{k}) U(g;\boldsymbol{k})$ and $g \tilde{c}^\dagger(\boldsymbol{k}) g^{-1} = \tilde{c}^\dagger(p\boldsymbol{k}) \tilde{U}(g;\boldsymbol{k})$ respectively, by use of the momentum dependent unitary matrix $U(g;\boldsymbol{k})$ and $\tilde{U}(g;\boldsymbol{k})$ in the symbolic manner.

Note that $c^\dagger(\boldsymbol{k})$ is periodic under the transformation $\boldsymbol{k} \to \boldsymbol{k} + \boldsymbol{g}$ with the reciprocal vectors $\boldsymbol{g}$ while $\tilde{c}^\dagger(\boldsymbol{k})$ is not. Thus, $c^\dagger(\boldsymbol{k})$ representation is useful for the numerical calculation using the fast Fourier transformation, and used in Chapter 2. On the other hand, since the phase factor arising in Eq. (A.2.23) does not depend on the atomic positions, $\tilde{c}^\dagger(\boldsymbol{k})$ representation is more convenient for the symmetry based arguments discussed in Chapter 3. In the model calculations in Chapter 4, we have used $\tilde{c}^\dagger(\boldsymbol{k})$.

A.3 Band-based representations

In the following, we discuss another type of representation, which we call a *band-based* representation. The band-based Hamiltonian can be obtained by diagonalizing the orbital-based one, which can be written as,

$$H = \sum_{\boldsymbol{k}} \sum_{n} h_n(\boldsymbol{k}) c_n^\dagger(\boldsymbol{k}) c_n(\boldsymbol{k}), \tag{A.3.1}$$

where n is the band index including the degenerate states. Here, $c_n^\dagger(\boldsymbol{k})$ ($c_n(\boldsymbol{k})$) is a creation (annihilation) operator corresponding to the Bloch state with the momentum $\boldsymbol{k}$. As is seen in Chapter 3, for operations connecting $c_n^\dagger(\boldsymbol{k})$ with different $\boldsymbol{k}$ points, its transformation property can be freely chosen by use of an arbitrary unitary transformation among the degenerate bands. However, for the operations leaving $\boldsymbol{k}$ invariant, we can uniquely determine its transformation property. In contrast to the orbital-based one, such band-based representation is an irreducible representation of a subgroup of the space group, and thus, can be obtained with the help of the usual band theory. For our purpose, it is sufficient to find the eigenstates of a quadratic part of the Hamiltonian labeled by $\boldsymbol{k}$. The subgroup of the space group to leave $\boldsymbol{k}$ invariant is called a *little group* of $\boldsymbol{k}$, and the corresponding eigenstates are identical with the Bloch states. In the following, we summarize the little groups and their representations, and then discuss the representations of Cooper pairs in the basis of them, which is used in Chapter 4.

A.3.1 Little groups

Since the lattice translation group T is an abelian group, its irreducible representations are all one-dimensional, labeled by the crystal momentum $\boldsymbol{k}$. Let $F_{\boldsymbol{k}}$ be the irreducible representation of T, which meets,

$$F_{\boldsymbol{k}}(t) = e^{-i\boldsymbol{k}\cdot\boldsymbol{t}}, \quad \text{for} \quad t = \{E|\boldsymbol{t}\} \in T. \tag{A.3.2}$$

Then, the set $\alpha \in G/T$ for which $F_{\boldsymbol{k}}(t) = F_{\boldsymbol{k}}(r_\alpha^{-1} t r_\alpha)$ for all $t \in T$ forms a subgroup of G/T. This is called a *little co-group* of $F_{\boldsymbol{k}}$ in G, which we denote by $\bar{K}_{\boldsymbol{k}}$. By use of $\bar{K}_{\boldsymbol{k}}$, the subgroup $K_{\boldsymbol{k}}$ of G defined by,

$$K_{\boldsymbol{k}} = \sum_{\alpha \in \bar{K}_{\boldsymbol{k}}} r_\alpha T, \tag{A.3.3}$$

is called a *little group* of $F_{\boldsymbol{k}}$ in G. Note that the requirement $F_{\boldsymbol{k}}(t) = F_{\boldsymbol{k}}(r_\alpha^{-1} t r_\alpha)$ for $r_\alpha = \{p|\boldsymbol{a}\}$ is identical with the following relation,

$$e^{-i\boldsymbol{k}\cdot\boldsymbol{t}} = e^{-ip\boldsymbol{k}\cdot\boldsymbol{t}} \quad \leftrightarrow \quad p\boldsymbol{k} = \boldsymbol{k} + \boldsymbol{g} \tag{A.3.4}$$

where $\boldsymbol{g}$ meets $e^{-i\boldsymbol{g}\cdot\boldsymbol{t}} = 1$ for all $t = \{E|\boldsymbol{t}\} \in T$ and is a reciprocal lattice vector. Thus, in other words, the little group $K_{\boldsymbol{k}}$ can be regarded as the subgroup of G whose point group operations leave $\boldsymbol{k}$ invariant modulo reciprocal lattice vectors.

A.3.2 Magnetic little groups

In analogy with the little group $K_{\boldsymbol{k}}$ in the space group G, we can define a *magnetic little group* $Q_{\boldsymbol{k}}$ in the magnetic space group M. Similar to Eq. (A.1.4), M can be decomposed as left cosets,

$$M = \sum_{p \in P} \{p|\boldsymbol{a}\}T, \tag{A.3.5}$$

where $p \in P$ runs over not only unitary operations but also anti-unitary operations. Then the cosets $\{p|\boldsymbol{a}\}T$ form quotient group M/T. The *magnetic little co-group* $\bar{Q}_{\boldsymbol{k}}$ is defined as follows; $\bar{Q}_{\boldsymbol{k}} = \bar{Q}^u_{\boldsymbol{k}} + \bar{Q}^a_{\boldsymbol{k}}$ where $\bar{Q}^u_{\boldsymbol{k}}$ is the set of unitary cosets $\alpha \in M/T$ for which $F_{\boldsymbol{k}}(t) = F_{\boldsymbol{k}}(r_\alpha^{-1} t r_\alpha)$ for all $t \in T$ and $\bar{Q}^a_{\boldsymbol{k}}$ is the set of anti-unitary cosets $\alpha \in M/T$ for which $F_{\boldsymbol{k}}(t) = F^*_{\boldsymbol{k}}(r_\alpha^{-1} t r_\alpha)$ for all $t \in T$. Then the *magnetic little group* $Q_{\boldsymbol{k}}$ is given by,

$$Q_{\boldsymbol{k}} = \sum_{\alpha \in \bar{Q}^u_{\boldsymbol{k}}} r_\alpha T + \sum_{\alpha \in \bar{Q}^a_{\boldsymbol{k}}} r_\alpha T. \tag{A.3.6}$$

Here, the requirement $F_{\boldsymbol{k}}(t) = F^*_{\boldsymbol{k}}(r_\alpha^{-1} t r_\alpha)$ for $\bar{Q}^a_{\boldsymbol{k}}$ comes from the relation $\theta e^{-i\boldsymbol{k}\cdot\boldsymbol{t}}\theta^{-1} = e^{i\boldsymbol{k}\cdot\boldsymbol{t}}$, which indicates that θ reverses the crystal momentum $\boldsymbol{k}$.

A.3.3 Small representations

In the paramagnetic crystals, any Bloch state is a basis of an irreducible representation in a little group $K_{\boldsymbol{k}}$. This is called a *small representation*. More concretely, a small representation $\gamma_{\boldsymbol{k}}$ is defined as an irreducible representation of $K_{\boldsymbol{k}}$, whose subduction to T yields an integral multiple $\hat{1}$ of $F_{\boldsymbol{k}}$. Here, $\hat{1}$ is the identity matrix with the dimension of $\gamma_{\boldsymbol{k}}$, and thus, $\gamma_{\boldsymbol{k}} \downarrow T = \hat{1}F_{\boldsymbol{k}}$. Note that $\gamma_{\boldsymbol{k}}$ is a usual *vector* (or linear) representation if we consider SU(2) rotations as the space rotations, namely, the double space group.

In order to obtain $\gamma_{\boldsymbol{k}}$, let us focus on that the relation

$$\gamma_{\boldsymbol{k}}(r_i)\gamma_{\boldsymbol{k}}(r_j) = \gamma_{\boldsymbol{k}}(r_k t_{ij}) = F_{\boldsymbol{k}}(t_{ij})\gamma_{\boldsymbol{k}}(r_k), \tag{A.3.7}$$

holds for $r_i r_j = r_k t_{ij}$, where $r_i = \{p_i|\boldsymbol{a}_i\}$ are representatives in Eq. (A.3.3) and t_{ij} is given by

$$t_{ij} = \{E|p_k^{-1}(\boldsymbol{a}_i + p_i\boldsymbol{a}_j - \boldsymbol{a}_k)\} \in T. \tag{A.3.8}$$

Here, we have used the fact $\gamma_{\boldsymbol{k}} \downarrow T = \hat{1}F_{\boldsymbol{k}}$. Note that, if we consider usual space groups (i.e., SO(3) rotations as the spin space rotations), there can appear an additional phase factor in Eq. (A.3.7) describing the double-valuedness of the electron spin.

Eq. (A.3.7) implies that if we introduce a representation $\bar{\gamma}_{\boldsymbol{k}}$ of $\bar{K}_{\boldsymbol{k}}$ to satisfy $\bar{\gamma}_{\boldsymbol{k}}(\alpha) = \gamma_{\boldsymbol{k}}(r_\alpha)$ for all $\alpha \in \bar{K}_{\boldsymbol{k}}$, then $\bar{\gamma}_{\boldsymbol{k}}$ forms a projective representation of $\bar{K}_{\boldsymbol{k}}$ with the factor system $\omega_{ij} = F_{\boldsymbol{k}}(t_{ij})$, namely,

$$\bar{\gamma}_{\boldsymbol{k}}(\alpha_i)\bar{\gamma}_{\boldsymbol{k}}(\alpha_j) = \omega_{ij}\bar{\gamma}_{\boldsymbol{k}}(\alpha_k), \tag{A.3.9}$$

for $\alpha_i \in \bar{K}_{\boldsymbol{k}}$, where $\alpha_i\alpha_j = \alpha_k$ in the sense of quotient group. Inversely, by use of $\bar{\gamma}_{\boldsymbol{k}}$ defined in Eq. (A.3.9), we can redefine $\gamma_{\boldsymbol{k}}$ as $\gamma_{\boldsymbol{k}}(g_\alpha) = F_{\boldsymbol{k}}(t_\alpha)\bar{\gamma}_{\boldsymbol{k}}(\alpha)$ for all $g_\alpha = r_\alpha t_\alpha \in K_{\boldsymbol{k}}$ since the decomposition of $g \in G$ into the form $g = rt$ with $r \in R$ and $t \in T$ is unique. We can easily see that they indeed satisfy eq. (A.3.7), and also, corresponding to $g_ig_j = g_k$,

$$\gamma_{\boldsymbol{k}}(g_i)\gamma_{\boldsymbol{k}}(g_j) = \gamma_{\boldsymbol{k}}(g_k), \tag{A.3.10}$$

for all $g_i = r_it_i \in K_{\boldsymbol{k}}$. This is shown by,

$$l.h.s = F_{\boldsymbol{k}}(t_i + t_j)\bar{\gamma}_{\boldsymbol{k}}(i)\bar{\gamma}_{\boldsymbol{k}}(j) = F_{\boldsymbol{k}}(t_i + t_j + t_{ij})\bar{\gamma}_{\boldsymbol{k}}(k), \tag{A.3.11}$$

$$r.h.s = F_{\boldsymbol{k}}(t_k)\bar{\gamma}_{\boldsymbol{k}}(k) = F_{\boldsymbol{k}}(t_{ij} + g_j^{-1}t_ig_j + t_j)\bar{\gamma}_{\boldsymbol{k}}(k). \tag{A.3.12}$$

Here, we have used $t_k = \{E|p_k^{-1}(\boldsymbol{a}_i + p_i\boldsymbol{a}_j - \boldsymbol{a}_k + p_i\boldsymbol{t}_i + p_k\boldsymbol{t}_j)\} = t_{ij} + g_j^{-1}t_ig_j + t_j$. Because $F_{\boldsymbol{k}}(g_j^{-1}tg_j) = F_{\boldsymbol{k}}(t)$ for all $g = \{p|\boldsymbol{a}\} \in K_{\boldsymbol{k}}$ and $t \in T$, Eqs. (A.3.11) and (A.3.12) show that $\gamma_{\boldsymbol{k}}$ satisfies Eq.(A.3.10).

If $\bar{\gamma}_{\boldsymbol{k}}$ is irreducible, then $\gamma_{\boldsymbol{k}}$ is also irreducible since $\gamma_{\boldsymbol{k}}$ is an constant multiple of $\bar{\gamma}_{\boldsymbol{k}}$. Therefore, we can obtain the small representations $\gamma_{\boldsymbol{k}}$ from the irreducible projective representations $\bar{\gamma}_{\boldsymbol{k}}$ of the little co-group $\bar{K}_{\boldsymbol{k}}$ with the factor system ω_{ij}. This is the practical prescription to obtain the Bloch states in a given $\boldsymbol{k}$.

Note that, if we decompose G in terms of its left cosets with respect to $K_{\boldsymbol{k}}$,

$$G = \sum_{i \in \{\boldsymbol{k}\}} r_iF_{\boldsymbol{k}}, \tag{A.3.13}$$

then the set $\{\boldsymbol{k}\}$ forms what is called the star (or orbit) of $F_{\boldsymbol{k}}$. Now, the irreducible representation of G can be obtained as the induced representation $\gamma_{\boldsymbol{k}} \uparrow G$. However, this is not necessary for our purpose.

A.3.4 Small corepresentations

Similarly, we can obtain the small corepresentation $\lambda_{\boldsymbol{k}}$ for the magnetic little group $Q_{\boldsymbol{k}}$. By the definition of corepresentations, $\lambda_{\boldsymbol{k}}$ meets the following relations,

$$r_ir_j = r_kt_{ij} \quad \Leftrightarrow \quad \lambda_{\boldsymbol{k}}(r_i)\lambda_{\boldsymbol{k}}(r_j) = F_{\boldsymbol{k}}(t_{ij})\lambda_{\boldsymbol{k}}(r_k), \tag{A.3.14}$$

$$r_ir_J = r_Kt_{iJ} \quad \Leftrightarrow \quad \lambda_{\boldsymbol{k}}(r_i)\lambda_{\boldsymbol{k}}(r_J) = F^*_{\boldsymbol{k}}(t_{iJ})\lambda_{\boldsymbol{k}}(r_K), \tag{A.3.15}$$

$$r_Ir_j = r_Kt_{Ij} \quad \Leftrightarrow \quad \lambda_{\boldsymbol{k}}(r_I)\lambda^*_{\boldsymbol{k}}(r_j) = F^*_{\boldsymbol{k}}(t_{Ij})\lambda_{\boldsymbol{k}}(r_K), \tag{A.3.16}$$

$$r_Ir_J = r_kt_{IJ} \quad \Leftrightarrow \quad \lambda_{\boldsymbol{k}}(r_I)\lambda^*_{\boldsymbol{k}}(r_J) = F_{\boldsymbol{k}}(t_{IJ})\lambda_{\boldsymbol{k}}(r_k), \tag{A.3.17}$$

where r_i, r_j, and r_k (r_I, r_J, and r_K) are representatives of quotient group $\bar{Q}^u_{\boldsymbol{k}}$ ($\bar{Q}^a_{\boldsymbol{k}}$) in Eq. (A.3.6). Note that the double-valuedness of the time reversal operation, i.e., $\theta^2 = -1$, can be absorbed

into the space group as the same manner of that of electron spin. Then, we introduce a projective corepresentation $\bar{\lambda}_{\boldsymbol{k}}$ of $\bar{Q}_{\boldsymbol{k}} = \bar{Q}^u_{\boldsymbol{k}} + \bar{Q}^a_{\boldsymbol{k}}$ to meet $\bar{\lambda}_{\boldsymbol{k}}(\alpha_i) = \lambda_{\boldsymbol{k}}(r_{\alpha_i})$ and $\bar{\lambda}_{\boldsymbol{k}}(\alpha_I) = \lambda_{\boldsymbol{k}}(r_{\alpha_I})$ for all $\alpha_i \in \bar{Q}^u_{\boldsymbol{k}}$ and $\alpha_I \in \bar{Q}^a_{\boldsymbol{k}}$. Thus,

$$\alpha_i\alpha_j = \alpha_k \quad \Leftrightarrow \quad \bar{\lambda}_{\boldsymbol{k}}(\alpha_i)\bar{\lambda}_{\boldsymbol{k}}(\alpha_j) = \omega_{ij}\bar{\lambda}_{\boldsymbol{k}}(\alpha_k), \tag{A.3.18}$$

$$\alpha_i\alpha_J = \alpha_K \quad \Leftrightarrow \quad \bar{\lambda}_{\boldsymbol{k}}(\alpha_i)\bar{\lambda}_{\boldsymbol{k}}(\alpha_J) = \omega^*_{iJ}\bar{\lambda}_{\boldsymbol{k}}(\alpha_K), \tag{A.3.19}$$

$$\alpha_I\alpha_j = \alpha_K \quad \Leftrightarrow \quad \bar{\lambda}_{\boldsymbol{k}}(\alpha_I)\bar{\lambda}^*_{\boldsymbol{k}}(\alpha_j) = \omega^*_{Ij}\bar{\lambda}_{\boldsymbol{k}}(\alpha_K), \tag{A.3.20}$$

$$\alpha_I\alpha_J = \alpha_k \quad \Leftrightarrow \quad \bar{\lambda}_{\boldsymbol{k}}(\alpha_I)\bar{\lambda}^*_{\boldsymbol{k}}(\alpha_J) = \omega_{IJ}\bar{\lambda}_{\boldsymbol{k}}(\alpha_k), \tag{A.3.21}$$

where $\alpha_i \in \bar{Q}^u_{\boldsymbol{k}}$ and $\alpha_I \in \bar{Q}^a_{\boldsymbol{k}}$. Here, the set $\omega_{ij}, \omega_{iJ}, \omega_{Ij}$, and ω_{IJ} are defined for all $l, m \in \bar{Q}_{\boldsymbol{k}}$ to meet $\omega_{lm} = F_{\boldsymbol{k}}(t_{lm})$ as the same as the unitary little co-group. In this definition, the set ω_{lm} forms the factor system of a projective corepresentation in $\bar{Q}_{\boldsymbol{k}}$, which satisfies

$$\omega_{(lm)i}\omega_{lm} = \omega_{l(mi)}\omega_{mi} \tag{A.3.22}$$

$$\omega_{(lm)I}\omega^*_{lm} = \omega_{l(mI)}\omega_{mI} \tag{A.3.23}$$

where $l, m \in \bar{Q}_{\boldsymbol{k}}$, $i \in \bar{Q}^u_{\boldsymbol{k}}$, and $I \in \bar{Q}^a_{\boldsymbol{k}}$.

Inversely, by use of $\bar{\lambda}_{\boldsymbol{k}}$ defined in Eqs. (A.3.18)-(A.3.21), we can obtain $\lambda_{\boldsymbol{k}}$ as $\lambda_{\boldsymbol{k}}(g_i) = F_{\boldsymbol{k}}(t_i)\bar{\lambda}_{\boldsymbol{k}}(i)$ and $\lambda_{\boldsymbol{k}}(g_I) = F^*_{\boldsymbol{k}}(t_I)\bar{\lambda}_{\boldsymbol{k}}(I)$ where $g_i = r_i t_i$ ($g_I = r_I t_I$) is any unitary (anti-unitary) operation in $Q_{\boldsymbol{k}}$. This satisfies, for example,

$$g_i g_j = g_k \quad \Leftrightarrow \quad \lambda_{\boldsymbol{k}}(g_i)\lambda_{\boldsymbol{k}}(g_j) = \omega'_{ij}\lambda_{\boldsymbol{k}}(g_k), \tag{A.3.24}$$

$$g_i g_J = g_K \quad \Leftrightarrow \quad \lambda_{\boldsymbol{k}}(g_i)\lambda_{\boldsymbol{k}}(g_J) = \omega'^*_{iJ}\lambda_{\boldsymbol{k}}(g_K), \tag{A.3.25}$$

$$g_I g_j = g_K \quad \Leftrightarrow \quad \lambda_{\boldsymbol{k}}(g_I)\lambda^*_{\boldsymbol{k}}(g_j) = \omega'^*_{Ij}\lambda_{\boldsymbol{k}}(g_K), \tag{A.3.26}$$

$$g_I g_J = g_k \quad \Leftrightarrow \quad \lambda_{\boldsymbol{k}}(g_I)\lambda^*_{\boldsymbol{k}}(g_J) = \omega'_{IJ}\lambda_{\boldsymbol{k}}(g_k), \tag{A.3.27}$$

which are shown by, for example,

$$l.h.s \text{ in Eq. (A.3.25)} = F_{\boldsymbol{k}}(t_i - t_J)\bar{\gamma}_{\boldsymbol{k}}(i)\bar{\gamma}_{\boldsymbol{k}}(J) \tag{A.3.28}$$

$$= F_{\boldsymbol{k}}(t_i - t_J - t_{iJ})\bar{\gamma}_{\boldsymbol{k}}(k), \tag{A.3.29}$$

$$r.h.s \text{ in Eq. (A.3.25)} = F^*_{\boldsymbol{k}}(t_k)\bar{\gamma_{\boldsymbol{k}}}(k) \tag{A.3.30}$$

$$= F_{\boldsymbol{k}}(-t_{iJ} - g_J^{-1}t_i g_J - t_J)\bar{\gamma_{\boldsymbol{k}}}(k), \tag{A.3.31}$$

and the relation $F_{\boldsymbol{k}}(g_J^{-1}t_i g_J) = F^*_{\boldsymbol{k}}(t_i) = F_{\boldsymbol{k}}(-t_i)$ to be satisfied for all $t_i \in T$ and the anti-unitary operations $g_J \in Q_{\boldsymbol{k}}$. The others are also shown in the similar way. Since $\lambda_{\boldsymbol{k}}$ is irreducible when $\bar{\lambda}_{\boldsymbol{k}}$ is irreducible, we can obtain the small corepresentations $\lambda_{\boldsymbol{k}}$ from the irreducible projective corepresentations $\bar{\lambda}_{\boldsymbol{k}}$ of the magnetic little co-group $\bar{Q}_{\boldsymbol{k}}$ with the factor system ω_{lm}.

A.3.5 Representations of Cooper pairs

The Bloch states are regarded as the bases of the small representations $\gamma_{\boldsymbol{k}}$ (or a small corepresentations $\lambda_{\boldsymbol{k}}$). As shown in the previous sections, $\gamma_{\boldsymbol{k}}$ ($\lambda_{\boldsymbol{k}}$) can be obtained from the irreducible projective (co)representations $\bar{\gamma}_{\boldsymbol{k}}$ ($\bar{\lambda}_{\boldsymbol{k}}$) in the (magnetic) little co-groups $\bar{K}_{\boldsymbol{k}}$ ($\bar{Q}_{\boldsymbol{k}}$), which have the appropriate factor systems ω. Here, we show how to calculate the representations describing the Cooper pair wave functions, which we call representations of Cooper pairs, when the correct small (co)representations $\gamma_{\boldsymbol{k}}(\lambda_{\boldsymbol{k}})$ are given. In the following discussion, because it is irrelevant whether the space group is unitary or non-unitary, we do not distinguish them and simply use $\gamma_{\boldsymbol{k}}$ and $K_{\boldsymbol{k}}$.

Let Ψ_i^{Γ} be a BCS mean field term in a BdG Hamiltonian. Here, Γ and i, which are the irreducible representation of P and its basis respectively, specify the realized superconducting symmetry. As shown in Sec. 3.1, this takes the form like

$$\Psi_i^{\Gamma} = \sum_{\boldsymbol{k}} \sum_{12} [\varphi_i^{\Gamma}(\boldsymbol{k})]_{12} c_1^{\dagger}(\boldsymbol{k}) c_2^{\dagger}(-\boldsymbol{k}), \tag{A.3.32}$$

in the band basis. Here, $c_1^{\dagger}(\boldsymbol{k})$ is a creation operator of Bloch state with the crystal momentum $\boldsymbol{k}$. The suffix $1, 2$ generally denotes the band index n and the others such as Kramers index $\pm$. $\varphi_i^{\Gamma}(\boldsymbol{k})$ is a band based gap function belonging to Γ. According to the Fermion anti-symmetry, the relation

$$[\varphi_i^{\Gamma}(\boldsymbol{k})]_{12} = -[\varphi_i^{\Gamma}(-\boldsymbol{k})]_{21}, \tag{A.3.33}$$

holds for any superconductivity.

Here, we focus on the fact that the (zero-momentum) Cooper pairs have to be formed between the degenerate states present at $\boldsymbol{k}$ and $-\boldsymbol{k}$ within the weak coupling BCS theory. Thus, in the following, we neglect the inter-band pairing and only focus on a single state labeled by $\gamma_{\boldsymbol{k}}$ for simplicity. Due to the degeneracy of paired states, these should be connected by some symmetry operations except for an accidentally degenerate case. Here, we assume that a space group operation $d = \{p_d|\boldsymbol{a}_d\} \in G$ connects two states of the paired electrons, namely, its rotation/inversion part p_d meets $p_d\boldsymbol{k} = -\boldsymbol{k}$ modulo a reciprocal lattice vector. In this case, the creation operator $c_i^{\dagger}(\gamma_{\boldsymbol{k}}; \boldsymbol{k})$, which corresponds to a basis i of a small representation $\gamma_{\boldsymbol{k}}$, can form a pair with $d\, c_j^{\dagger}(\gamma_{\boldsymbol{k}}; \boldsymbol{k})\, d^{-1}$ and the corresponding mean field term takes the form as,

$$\Psi_k^{\Gamma}(\gamma_{\boldsymbol{k}}; \boldsymbol{k}) = \sum_{ij} [\varphi_k^{\Gamma}(\gamma_{\boldsymbol{k}}; \boldsymbol{k})]_{ij} c_i^{\dagger}(\gamma_{\boldsymbol{k}}; \boldsymbol{k})\, d\, c_j^{\dagger}(\gamma_{\boldsymbol{k}}; \boldsymbol{k})\, d^{-1}. \tag{A.3.34}$$

Note that, as shown later, the representation of Cooper pair does not depend on the chose of d, and thus, we can neglect its label in $\Psi_k^{\Gamma}(\gamma_{\boldsymbol{k}})$. Since the transformations of $[\varphi_k^{\Gamma}(\gamma_{\boldsymbol{k}}; \boldsymbol{k})]_{ij}$ and of $c_i^{\dagger}(\gamma_{\boldsymbol{k}}; \boldsymbol{k})\, d\, c_j^{\dagger}(\gamma_{\boldsymbol{k}}; \boldsymbol{k})\, d^{-1}$ are convertible, we will consider the symmetry property of

later term. For the discussion based on the small representations, we introduce the ordered pairs of two basis function $\phi_i^{\gamma_{\boldsymbol{k}}}$ and $d\phi_j^{\gamma_{\boldsymbol{k}}}$, which we denote by $(\phi_i^{\gamma_{\boldsymbol{k}}}, d\phi_j^{\gamma_{\boldsymbol{k}}})$. Here, $\phi_i^{\gamma_{\boldsymbol{k}}}$ is a basis of $\gamma_{\boldsymbol{k}}$ and $d\phi_j^{\gamma_{\boldsymbol{k}}}$ is a possible paired states at $-\boldsymbol{k}$. Taking into account the anti-symmetry of creation operators, we find the following correspondence,

$$\begin{aligned} & c_i^\dagger(\gamma_{\boldsymbol{k}};\boldsymbol{k})\, d\, c_j^\dagger(\gamma_{\boldsymbol{k}};\boldsymbol{k})\, d^{-1}, \\ & \qquad \Leftrightarrow \quad \Phi_{ij}(\gamma_{\boldsymbol{k}}) := (\phi_i^{\gamma_{\boldsymbol{k}}}, d\phi_j^{\gamma_{\boldsymbol{k}}}) - (d\phi_j^{\gamma_{\boldsymbol{k}}}, \phi_i^{\gamma_{\boldsymbol{k}}}). \end{aligned} \tag{A.3.35}$$

Namely, the representation of the Cooper pairs is the same as that of $\Phi_{ij}(\gamma_{\boldsymbol{k}})$.

Note that $\Phi_{ij}(\gamma_{\boldsymbol{k}})$ can be regarded as an anti-symmetrized Kronecker square with zero total momentum of the induced representation $\gamma_{\boldsymbol{k}} \uparrow K_{\boldsymbol{k}} + dK_{\boldsymbol{k}}$ [59]. The character of its representation, denoted by $P_{\gamma_{\boldsymbol{k}}}$, is given by,

$$\chi^{P_{\gamma_{\boldsymbol{k}}}}(g) = \chi^{\gamma_{\boldsymbol{k}}}(g)\chi^{\gamma_{\boldsymbol{k}}}(d^{-1}gd), \tag{A.3.36}$$

$$\chi^{P_{\gamma_{\boldsymbol{k}}}}(dg) = -\chi^{\gamma_{\boldsymbol{k}}}(dgdg). \tag{A.3.37}$$

This is a key relation to investigate the nodal structure in non-symmorphic superconductors in Chapter 4. Note that Eqs. (A.3.36) and (A.3.37) are special cases of Mackey-Bradley theorem deduced with the double coset decomposition [59]. Before showing the derivation of Eqs. (A.3.36) and (A.3.37), we make some remarks.

1. First, we note that the little group $K_{-\boldsymbol{k}}$ at $-\boldsymbol{k}$ point is the same as $K_{\boldsymbol{k}}$ at $\boldsymbol{k}$ point. This is simply because the condition $p\boldsymbol{k} = \boldsymbol{k} + \boldsymbol{g}$ for all $\{p|\boldsymbol{a}\} \in K_{\boldsymbol{k}}$ is identical with $p(-\boldsymbol{k}) = -\boldsymbol{k} + \boldsymbol{g}'$ for all $\{p|\boldsymbol{a}\} \in K_{-\boldsymbol{k}}$, where $\boldsymbol{g}' = -\boldsymbol{g}$. This implies $K_{\boldsymbol{k}} = dK_{\boldsymbol{k}}d^{-1}$, in other words, $K_{\boldsymbol{k}}$ is an invariant subgroup of $M_{\boldsymbol{k}} = K_{\boldsymbol{k}} + dK_{\boldsymbol{k}}$. Therefore, we can define the induced representation $\gamma_{\boldsymbol{k}} \uparrow M_{\boldsymbol{k}}$ for any d. Moreover, *r.h.s* of Eq. (A.3.36) makes sense because $d^{-1}gd \in K_{\boldsymbol{k}}$. Note that, by the definition,

$$g\phi_i^{\gamma_{\boldsymbol{k}}} = \sum_{i'} \phi_{i'}^{\gamma_{\boldsymbol{k}}}[\gamma_{\boldsymbol{k}}(g)]_{i'i}, \tag{A.3.38}$$

$$gd\phi_j^{\gamma_{\boldsymbol{k}}} = \sum_{j'} d\phi_{j'}^{\gamma_{\boldsymbol{k}}}[\gamma_{\boldsymbol{k}}(d^{-1}gd)]_{j'j}, \tag{A.3.39}$$

   hold for any $g \in K_{\boldsymbol{k}}$.

2. For any $d = \{p_d|\boldsymbol{a}_d\}$, $d^2 \in K_{\boldsymbol{k}}$ because d^2 is an element of G and satisfies $(p_d^2)\boldsymbol{k} = \boldsymbol{k}$. $K_{\boldsymbol{k}} = dK_{\boldsymbol{k}}d^{-1}$ and $d^2 \in K_{\boldsymbol{k}}$ immediately lead $dgdg = d^2 \cdot d^{-1}gd \cdot g \in K_{\boldsymbol{k}}$, and thus, *r.h.s* of Eq. (A.3.37) makes sense. Note that

$$dg\phi_i^{\gamma_{\boldsymbol{k}}} = \sum_{i'} d\phi_{i'}^{\gamma_{\boldsymbol{k}}}[\gamma_{\boldsymbol{k}}(g)]_{i'i}, \tag{A.3.40}$$

$$dgd\phi_j^{\gamma_{\boldsymbol{k}}} = \sum_{j'} \phi_{j'}^{\gamma_{\boldsymbol{k}}}[\gamma_{\boldsymbol{k}}(dgd)]_{j'j}, \tag{A.3.41}$$

   hold for any $dg \in dK_{\boldsymbol{k}}$, and thus, $\Phi_{ij}(\gamma_{\boldsymbol{k}})$ indeed forms a representation of $K_{\boldsymbol{k}} + dK_{\boldsymbol{k}}$. This originates from the fact $d \in dK_{\boldsymbol{k}} \cap K_{\boldsymbol{k}}d^{-1}$.

3. For any d and d', the induced basis $d\phi_i^{\gamma_{\boldsymbol{k}}}$ and $d'\phi_i^{\gamma_{\boldsymbol{k}}}$ are convertible by a unitary transformation. Therefore, the character of $P(\gamma_{\boldsymbol{k}})$ is independent of the choice of d. This is guaranteed by the fact that $K_{\boldsymbol{k}}$ is an invariant subgroup of $M_{\boldsymbol{k}}$.

Now, we are ready to prove Eqs. (A.3.36) and (A.3.37). After the straightforward calculations using Eqs. (A.3.38)-(A.3.41), we get,

$$g\Phi_{ij}(\gamma_{\boldsymbol{k}}) = \sum_{i'j'} \Phi_{i'j'}(\gamma_{\boldsymbol{k}})[\gamma_{\boldsymbol{k}}(g)]_{i'i}[\gamma_{\boldsymbol{k}}(d^{-1}gd)]_{j'j}, \tag{A.3.42}$$

$$dg\Phi_{ij}(\gamma_{\boldsymbol{k}}) = -\sum_{i'j'} \Phi_{j'i'}(\gamma_{\boldsymbol{k}})[\gamma_{\boldsymbol{k}}(g)]_{i'i}[\gamma_{\boldsymbol{k}}(dgd)]_{j'j}, \tag{A.3.43}$$

$$= -\sum_{i'j'} \Phi_{i'j'}(\gamma_{\boldsymbol{k}})[\gamma_{\boldsymbol{k}}(g)]_{j'i}[\gamma_{\boldsymbol{k}}(dgd)]_{i'j}. \tag{A.3.44}$$

Thus, their characters are given by,

$$P^{\gamma_{\boldsymbol{k}}}_{i'j',ij}(g) = [\gamma_{\boldsymbol{k}}(g)]_{i'i}[\gamma_{\boldsymbol{k}}(d^{-1}gd)]_{j'j} \quad \Rightarrow \quad \chi^{P_{\gamma_{\boldsymbol{k}}}}(g) = \chi^{\gamma_{\boldsymbol{k}}}(g)\chi^{\gamma_{\boldsymbol{k}}}(d^{-1}gd), \tag{A.3.45}$$

$$P^{\gamma_{\boldsymbol{k}}}_{i'j',ij}(dg) = -[\gamma_{\boldsymbol{k}}(g)]_{j'i}[\gamma_{\boldsymbol{k}}(dgd)]_{i'j} \quad \Rightarrow \quad \chi^{P_{\gamma_{\boldsymbol{k}}}}(dg) = -\chi^{\gamma_{\boldsymbol{k}}}(dgdg). \tag{A.3.46}$$

Note that as shown above, the original Mackey-Bradley theorem, which is a theorem for the double coset decomposition [59] and is used in the previous works [138, 139, 3], is not necessary in the symmetry consideration on the zero-momentum Cooper pairs. It may be applied, for example, to the classification of order parameters in the superconductivity or the other long range orders with finite ordering momentum.

Bibliography

[1] M. Sigrist and K. Ueda, Reviews of Modern Physics **63**, 239 (1991).

[2] T. Nomoto and H. Ikeda, Physical Review Letters **117**, 217002 (2016).

[3] T. Micklitz and M. R. Norman, Physical Review B **80**, 100506(R) (2009).

[4] T. Nomoto, K. Hattori, and H. Ikeda, Physical Review B **94**, 174513 (2016).

[5] T. Nomoto and H. Ikeda, Journal of the Physical Society of Japan **86**, 023703 (2017).

[6] J. Bardeen, L. N. Cooper, and J. R. Schrieffer, Physical Review **108**, 1175 (1957).

[7] G. R. Stewart, Reviews of Modern Physics **56**, 755 (1984).

[8] W. E. Pickett, Reviews of Modern Physics **61**, 433 (1989).

[9] K. Miyake, S. Schmitt-Rink, and C. M. Varma, Physical Review B **34**, 6554 (1986).

[10] D. J. Scalapino, E. Loh, and J. E. Hirsch, Physical Review B **34**, 8190(R) (1986).

[11] A. J. Leggett, Reviews of Modern Physics **47**, 331 (1975).

[12] D. Van Harlingen, Reviews of Modern Physics **67**, 515 (1995).

[13] K. Izawa, H. Yamaguchi, Y. Matsuda, H. Shishido, R. Settai, and Y. Onuki, Physical Review Letters **87**, 057002 (2001).

[14] K. An, T. Sakakibara, R. Settai, Y. Onuki, M. Hiragi, M. Ichioka, and K. Machida, Physical Review Letters **104**, 037002 (2010).

[15] G. Volovik and L. Gor'kov, JETP Letter **39**, 647 (1984).

[16] G. Volovik and L. Gor'kov, Sov. Phys. JETP **61**, 843 (1985).

[17] K. Ueda and T. M. Rice, Physical Review B **31**, 7114 (1985).

[18] J. A. Sauls, Adv. Phys. **43**, 113 (1994).

[19] R. Joynt and L. Taillefer, Reviews of Modern Physics **74**, 235 (2002).

[20] C. Pfleiderer, Reviews of Modern Physics **81**, 1551 (2009).

[21] J. F. Annett, Adv. Phys. **39**, 83 (1990).

[22] T. Rice and M. Sigrist, J. Phys. Condens. Matter **7**, L643 (1995).

[23] K. Machida, M.-a. Ozaki, and T. Ohmi, Journal of the Physical Society of Japan **65**, 3720 (1996).

[24] A. P. Mackenzie and Y. Maeno, Reviews of Modern Physics **75**, 657 (2003).

[25] M.-a. Ozaki, K. Machida, and T. Ohmi, Progress of Theoretical Physics **74**, 221 (1985).

[26] M.-a. Ozaki, K. Machida, and T. Ohmi, Progress of Theoretical Physics **75**, 442 (1986).

[27] T. Shibauchi, H. Ikeda, and Y. Matsuda, Philosophical Magazine **94**, 3747 (2014).

[28] E. Bauer, G. Hilscher, H. Michor, C. Paul, E. W. Scheidt, A. Gribanov, Y. Seropegin, H. Noël, M. Sigrist, and P. Rogl, Physical Review Letters **92**, 027003 (2004).

[29] T. Akazawa, H. Hidaka, H. Kotegawa, T. C. Kobayashi, T. Fujiwara, E. Yamamoto, Y. Haga, R. Settai, and Y. Onuki, Journal of the Physical Society of Japan **73**, 3129 (2004).

[30] G. Goll, M. Marz, A. Hamann, T. Tomanic, K. Grube, T. Yoshino, and T. Takabatake, Physica B: Condensed Matter **403**, 1065 (2008).

[31] L. P. Gor'kov and E. I. Rashba, Physical Review Letters **87**, 037004 (2001).

[32] N. Hayashi, K. Wakabayashi, P. A. Frigeri, and M. Sigrist, Physical Review B **73**, 092508 (2006).

[33] Y. Yanase and M. Sigrist, Journal of the Physical Society of Japan **77**, 124711 (2008).

[34] M. Sato, Physical Review B **73**, 214502 (2006).

[35] P. A. Frigeri, D. F. Agterberg, A. Koga, and M. Sigrist, Physical Review Letters **92**, 097001 (2004).

[36] M. Sato and S. Fujimoto, Physical Review B **79**, 094504 (2009).

[37] V. M. Edelstein, Physical Review Letters **75**, 2004 (1995).

[38] S. K. Yip, Physical Review B **65**, 144508 (2002).

[39] S. Fujimoto, Physical Review B **72**, 024515 (2005).

[40] J. Paglione and R. L. Greene, Nature Physics **6**, 645 (2010).

[41] G. R. Stewart, Reviews of Modern Physics **83**, 1589 (2011).

[42] P. J. Hirschfeld, M. M. Korshunov, and I. I. Mazin, Reports on Progress in Physics **74**, 124508 (2011).

[43] Y. Wan and Q.-H. Wang, Europhysics Letters **85**, 57007 (2009).

[44] I. I. Mazin, D. J. Singh, M. D. Johannes, and M. H. Du, Physical Review Letters **101**, 057003 (2008).

[45] K. Kuroki, S. Onari, R. Arita, H. Usui, Y. Tanaka, H. Kontani, and H. Aoki, Physical Review Letters **101**, 087004 (2008).

[46] S. Raghu, X. L. Qi, C. X. Liu, D. J. Scalapino, and S. C. Zhang, Physical Review B **77**, 220503 (2008).

[47] Y. Zhou, W. Q. Chen, and F. C. Zhang, Physical Review B **78**, 064514 (2008).

[48] W. L. You, S. J. Gu, G. S. Tian, and H. Q. Lin, Physical Review B **79**, 014508 (2009).

[49] M. Daghofer, A. Nicholson, A. Moreo, and E. Dagotto, Physical Review B **81**, 014511 (2010).

[50] M. H. Fischer, New Journal of Physics **15**, 073006 (2013).

[51] P. A. Lee and X. G. Wen, Physical Review B **78**, 144517 (2008).

[52] J. Hu and N. Hao, Physical Review X **2**, 021009 (2012).

[53] T. T. Ong and P. Coleman, Physical Review Letters **111**, 217003 (2013).

[54] M. H. Fischer, F. Loder, and M. Sigrist, Physical Review B **84**, 184533 (2011).

[55] D. Maruyama, M. Sigrist, and Y. Yanase, Journal of the Physical Society of Japan **81**, 034702 (2012).

[56] S. J. Youn, M. H. Fischer, S. H. Rhim, M. Sigrist, and D. F. Agterberg, Physical Review B **85**, 220505(R) (2012).

[57] J. Goryo, M. H. Fischer, and M. Sigrist, Physical Review B **86**, 100507(R) (2012).

[58] T. Yoshida, M. Sigrist, and Y. Yanase, Journal of the Physical Society of Japan **82**, 074714 (2013).

[59] C. J. Bradley and B. L. Davies, Reviews of Modern Physics **40**, 359 (1968).

[60] E. I. Blount, Physical Review B **32**, 2935 (1985).

[61] S. Kobayashi, K. Shiozaki, Y. Tanaka, and M. Sato, Physical Review B **90**, 024516 (2014).

[62] F. Steglich, J. Aarts, C. D. Bredl, W. Lieke, D. Meschede, W. Franz, and H. Schäfer, Physical Review Letters **43**, 1892 (1979).

[63] C. D. Bredl, H. Spille, U. Rauchschwalbe, W. Lieke, F. Steglich, G. Cordier, W. Assmus, M. Herrmann, and J. Aarts, Journal of Magnetism and Magnetic Materials **31-34**, 373 (1983).

[64] Y. Kitaoka, K.-i. Ueda, K. Fujiwara, H. Arimoto, H. Iida, and K. Asayama, Journal of the Physical Society of Japan **55**, 723 (1986).

[65] K. Ishida, Y. Kawasaki, K. Tabuchi, K. Kashima, Y. Kitaoka, K. Asayama, C. Geibel, and F. Steglich, Physical Review Letters **82**, 5353 (1999).

[66] S. Kittaka, Y. Aoki, Y. Shimura, T. Sakakibara, S. Seiro, C. Geibel, F. Steglich, H. Ikeda, and K. Machida, Physical Review Letters **112**, 067002 (2014).

[67] H. Ikeda, M.-T. Suzuki, and R. Arita, Physical Review Letters **114**, 147003 (2015).

[68] S. Kittaka, Y. Shimizu, T. Sakakibara, Y. Haga, and E. Yamamoto, Journal of the Physical Society of Japan **85**, 033704 (2016).

[69] G. M. Pang, M. Smidman, J. L. Zhang, L. Jiao, Z. F. Weng, E. M. Nica, Y. Chen, W. B. Jiang, Y. J. Zhang, H. S. Jeevan, P. Gegenwart, F. Steglich, Q. Si, and H. Q. Yuan, arXiv:1605.04786 .

[70] H. R. Ott, H. Rudigier, Z. Fisk, and J. L. Smith, Physical Review Letters **50**, 1595 (1983).

[71] G. R. Stewart, Z. Fisk, J. O. Willis, and J. L. Smith, Physical Review Letters **52**, 679 (1984).

[72] T. T. M. Palstra, A. A. Menovsky, J. van den Berg, A. J. Dirkmaat, P. H. Kes, G. J. Nieuwenhuys, and J. A. Mydosh, Physical Review Letters **55**, 2727 (1985).

[73] W. Schlabitz, J. Baumann, B. Pollit, U. Rauchschwalbe, H. M. Mayer, U. Ahlheim, and C. D. Bredl, Zeitschrift für Physik B **62**, 171 (1986).

[74] C. Geibel, C. Schank, S. Thies, H. Kitazawa, C. D. Bredl, A. Böhm, M. Rau, A. Grauel, R. Caspary, R. Helfrich, U. Ahlheim, G. Weber, and F. Steglich, Zeitschrift für Physik B **84**, 1 (1991).

[75] C. Geibel, S. Thies, D. Kaczorowski, A. Mehner, A. Grauel, B. Seidel, U. Ahlheim, R. Helfrich, K. Petersen, C. D. Bredl, and F. Steglich, Zeitschrift für Physik B **83**, 305 (1991).

[76] S. Saxena, P. Agarwal, K. Ahilan, F. Grosche, R. Haselwimmer, M. Steiner, E. Pugh, I. Walker, S. Julian, P. Monthoux, G. Lonzarich, A. Huxley, I. Sheikin, D. Braithwaite, and J. Flouquet, Nature **406**, 587 (2000).

[77] D. Aoki, A. Huxley, E. Ressouche, D. Braithwaite, J. Flouquet, J. P. Brison, E. Lhotel, and C. Paulsen, Nature **413**, 613 (2001).

[78] N. T. Huy, A. Gasparini, D. E. De Nijs, Y. Huang, J. C. P. Klaasse, T. Gortenmulder, A. De Visser, A. Hamann, T. Görlach, and H. V. Löhneysen, Physical Review Letters **99**, 067006 (2007).

[79] V. P. Mineev, Physical Review B **66**, 134504 (2002).

[80] K. V. Samokhin and M. B. Walker, Physical Review B **66**, 174501 (2002).

[81] T. Nomoto and H. Ikeda, Physical Review B **90**, 125147 (2014).

[82] T. Das, J.-X. Zhu, and M. J. Graf, Scientific reports **5**, 8632 (2015).

[83] Y. Tsutsumi, K. Machida, T. Ohmi, and M.-a. Ozaki, Journal of the Physical Society of Japan **81**, 074717 (2012).

[84] K. Izawa, Y. Machida, A. Itoh, Y. So, K. Ota, Y. Haga, E. Yamamoto, N. Kimura, Y. Onuki, Y. Tsutsumi, and K. Machida, Journal of the Physical Society of Japan **83**, 061013 (2014).

[85] S. Adenwalla, S. W. Lin, Q. Z. Ran, Z. Zhao, J. B. Ketterson, J. A. Sauls, L. Taillefer, D. G. Hinks, M. Levy, and B. K. Sarma, Physical Review Letters **65**, 2298 (1990).

[86] R. A. Fisher, S. Kim, B. F. Woodfield, N. E. Phillips, L. Taillefer, K. Hasselbach, J. Flouquet, A. L. Giorgi, and J. L. Smith, Physical Review Letters **62**, 1411 (1989).

[87] G. Bruls, D. Weber, B. Wolf, P. Thalmeier, B. Lüthi, A. D. Visser, and A. Menovsky, Physical Review Letters **65**, 2294 (1990).

[88] B. S. Shivaram, T. F. Rosenbaum, and D. G. Hinks, Physical Review Letters **57**, 1259 (1986).

[89] E. I. Blount, C. M. Varma, and G. Aeppli, Physical Review Letters **64**, 3074 (1990).

[90] D. F. Agterberg and M. B. Walker, Physical Review B **51**, 8481 (1995).

[91] M. E. Zhitomirsky and K. Ueda, Physical Review B **53**, 6591 (1996).

[92] P. L. Krotkov and V. P. Mineev, Physical Review B **65**, 224506 (2002).

[93] K. Machida, T. Ohmi, and M.-a. Ozaki, Journal of the Physical Society of Japan **62**, 3216 (1993).

[94] C. H. Choi and J. A. Sauls, Physical Review Letters **66**, 484 (1991).

[95] C. H. Choi and J. A. Sauls, Physical Review B **48**, 13684 (1993).

[96] J. A. Sauls, Journal of Low Temperature Physics **95**, 153 (1994).

[97] M. J. Graf, S. K. Yip, and J. A. Sauls, Physical Review B **62**, 14393 (2000).

[98] P. Frings, B. Renker, and C. Vettier, Physica B: Condensed Matter **151**, 499 (1988).

[99] G. Aeppli, E. Bucher, C. Broholm, J. K. Kjems, J. Baumann, and J. Hufnagl, Physical Review Letters **60**, 615 (1988).

[100] S. M. Hayden, L. Taillefer, C. Vettier, and J. Flouquet, Physical Review B **46**, 8675 (1992).

[101] G. Luke, A. Keren, L. Le, W. Wu, Y. Uemura, D. Bonn, L. Taillefer, and J. Garrett, Physical Review Letters **71**, 1466 (1993).

[102] J. D. Strand, D. J. Bahr, D. J. Van Harlingen, J. P. Davis, W. J. Gannon, and W. P. Halperin, Science **328**, 1368 (2010).

[103] E. R. Schemm, W. J. Gannon, C. M. Wishne, W. P. Halperin, and A. Kapitulnik, Science **345**, 190 (2014).

[104] B. S. Shivaram, Y. H. Jeong, T. F. Rosenbaum, and D. G. Hinks, Physical Review Letters **56**, 1078 (1986).

[105] J. Brison, N. Keller, P. Lejay, J. Tholenee, A. Huxley, N. Bernhoeft, A. Buzdin, B. Fak, J. Flouquet, L. Schmidt, A. Stepanov, C. Vettier, R. A. Fisher, and N. Phillips, Journal of Low Temperature Physics **95**, 145 (1994).

[106] B. Lussier, B. Ellman, and L. Taillefer, Physical Review B **53**, 5145 (1996).

[107] H. Suderow, J. Brison, A. Huxley, and J. Flouquet, Physical Review Letters **80**, 165 (1998).

[108] H. Tou, Y. Kitaoka, K. Ishida, K. Asayama, N. Kimura, Y. Onuki, E. Yamamoto, Y. Haga, and K. Maezawa, Physical Review Letters **80**, 3129 (1998).

[109] Y. Machida, A. Itoh, Y. So, K. Izawa, Y. Haga, E. Yamamoto, N. Kimura, Y. Onuki, Y. Tsutsumi, and K. Machida, Physical Review Letters **108**, 157002 (2012).

[110] K. Machida and M.-a. Ozaki, Physical Review Letters **66**, 3293 (1991).

[111] J. Gouchi, A. Sumiyama, G. Motoyama, A. Yamaguchi, N. Kimura, E. Yamamoto, Y. Haga, and Y. Onuki, Journal of the Physical Society of Japan **81**, 113701 (2012).

[112] S. Kittaka, K. An, T. Sakakibara, Y. Haga, E. Yamamoto, N. Kimura, Y. Onuki, and K. Machida, Journal of the Physical Society of Japan **82**, 024707 (2013).

[113] M. R. Norman, Physical Review Letters **59**, 232 (1987).

[114] W. Putikka and R. Joynt, Physical Review B **37**, 2372 (1988).

[115] M. R. Norman, Physical Review Letters **72**, 2077 (1994).

[116] H. Ikeda, M.-T. Suzuki, R. Arita, T. Takimoto, T. Shibauchi, and Y. Matsuda, Nature Physics **8**, 528 (2012).

[117] L. Taillefer and G. G. Lonzarich, Physical Review Letters **60**, 1570 (1988).

[118] N. Kimura, T. Komatsubara, D. Aoki, Y. Onuki, Y. Haga, E. Yamamoto, H. Aoki, and H. Harima, Journal of the Physical Society of Japan **67**, 2185 (1998).

[119] P. Blaha, "WIEN2K package," .

[120] P. A. Midgley, S. M. Hayden, L. Taillefer, B. Bogenberger, and H. v. Löhneysen, Physical Review Letters **70**, 678 (1993).

[121] D. A. Walko, J.-I. Hong, T. V. Chandrasekhar Rao, Z. Wawrzak, D. N. Seidman, W. P. Halperin, and M. J. Bedzyk, Physical Review B **63**, 054522 (2001).

[122] J. P. Perdew, K. Burke, and M. Ernzerhof, Physical Review Letters **77**, 3865 (1996).

[123] J. Kuneš, R. Arita, P. Wissgott, A. Toschi, H. Ikeda, and K. Held, Computer Physics Communications **181**, 1888 (2010).

[124] N. Marzari and D. Vanderbilt, Physical Review B **56**, 12847 (1997).

[125] I. Souza, N. Marzari, and D. Vanderbilt, Physical Review B **65**, 035109 (2001).

[126] A. A. Mostofi, J. R. Yates, Y. S. Lee, I. Souza, D. Vanderbilt, and N. Marzari, Computer Physics Communications **178**, 685 (2008).

[127] J. Kuneš, Physical Review B **83**, 1 (2011).

[128] M. Norman, R. Albers, A. Boring, and N. Christensen, Solid State Communications **68**, 245 (1988).

[129] G. J. McMullan, P. M. C. Rourke, M. R. Norman, A. D. Huxley, N. Doiron-Leyraud, J. Flouquet, G. G. Lonzarich, A. McCollam, and S. R. Julian, New Journal of Physics **10**, 053029 (2008).

[130] G. Aeppli, A. Goldman, G. Shirane, E. Bucher, and M.-C. Lux-Steiner, Physical Review Letters **58**, 808 (1987).

[131] A. I. Goldman, G. Shirane, G. Aeppli, E. Bucher, and J. Hufnagl, Physical Review B **36**, 8523 (1987).

[132] Y. Yanase, Physical Review B **94**, 174502 (2016).

[133] H. Kontani, Physical Review B **70**, 054507 (2004).

[134] R. Shiina, H. Shiba, and P. Thalmeier, Journal of the Physical Society of Japan **66**, 1741 (1997).

[135] S. Yip and A. Garg, Physical Review B **48**, 3304 (1993).

[136] H. Kim, K. Wang, Y. Nakajima, R. Hu, S. Ziemak, P. Syers, L. Wang, H. Hodovanets, J. D. Denlinger, P. M. R. Brydon, D. F. Agterberg, M. A. Tanatar, R. Prozorov, and J. Paglione, arXiv:1603.03375 .

[137] P. M. R. Brydon, L. Wang, M. Weinert, and D. F. Agterberg, Physical Review Letters **116**, 177001 (2016).

[138] V. G. Yarzhemsky and E. N. Murav'ev, Journal of Physics: Condensed Matter **4**, 3525 (1992).

[139] V. Yarzhemsky, physica status solidi B **209**, 101 (1998).

[140] C. B. Bishop, G. Liu, E. Dagotto, and A. Moreo, Physical Review B **93**, 224519 (2016).

[141] K. Matsubayashi, T. Tanaka, A. Sakai, S. Nakatsuji, Y. Kubo, and Y. Uwatoko, Physical Review Letters **109**, 187004 (2012).

[142] M. Tsujimoto, Y. Matsumoto, T. Tomita, A. Sakai, and S. Nakatsuji, Physical Review Letters **113**, 267001 (2014).

[143] J. Effantin, J. Rossat-Mignod, P. Burlet, H. Bartholin, S. Kunii, and T. Kasuya, Journal of Magnetism and Magnetic Materials **47**, 145 (1985).

[144] T. Tayama, T. Sakakibara, K. Kitami, M. Yokoyama, K. Tenya, H. Amitsuka, D. Aoki, Y. Onuki, and Z. Kletowski, Journal of the Physical Society of Japan **70**, 248 (2001).

[145] T. Onimaru, T. Sakakibara, N. Aso, H. Yoshizawa, H. S. Suzuki, and T. Takeuchi, Physical Review Letters **94**, 197201 (2005).

[146] T. Onimaru, K. T. Matsumoto, Y. F. Inoue, K. Umeo, T. Sakakibara, Y. Karaki, M. Kubota, and T. Takabatake, Physical Review Letters **106**, 177001 (2011).

[147] Y. Mizuguchi, Journal of Physics and Chemistry of Solids **84**, 34 (2015).

[148] H. Usui, K. Suzuki, and K. Kuroki, Physical Review B **86**, 220501 (2012).

[149] J. Lee, M. B. Stone, A. Huq, T. Yildirim, G. Ehlers, Y. Mizuguchi, O. Miura, Y. Takano, K. Deguchi, S. Demura, and S.-H. Lee, Physical Review B **87**, 205134 (2013).

[150] A. Athauda, J. Yang, S. Lee, Y. Mizuguchi, K. Deguchi, Y. Takano, O. Miura, and D. Louca, Physical Review B **91**, 144112 (2015).

[151] S. Kittaka, T. Sakakibara, M. Hedo, Y. Onuki, and K. Machida, Journal of the Physical Society of Japan **82**, 123706 (2013).

[152] K. Izawa, Y. Nakajima, J. Goryo, Y. Matsuda, S. Osaki, H. Sugawara, H. Sato, P. Thalmeier, and K. Maki, Physical Review Letters **90**, 117001 (2003).

[153] Y. Matsuda, K. Izawa, and I. Vekhter, Journal of Physics: Condensed Matter **18**, R705 (2006).

[154] T. Shibauchi, A. Carrington, and Y. Matsuda, Annual Review of Condensed Matter Physics **5**, 113 (2014).

[155] N. D. Mathur, F. M. Grosche, S. R. Julian, I. R. Walker, D. M. Freye, R. K. W. Haselwimmer, and G. G. Lonzarich, Nature **394**, 39 (1998).

[156] S. Kawasaki, T. Mito, Y. Kawasaki, H. Kotegawa, G.-Q. Zheng, Y. Kitaoka, H. Shishido, S. Araki, R. Settai, and Y. Onuki, Journal of the Physical Society of Japan **73**, 1647 (2004).

[157] T. Park, F. Ronning, H. Q. Yuan, M. B. Salamon, R. Movshovich, J. L. Sarrao, and J. D. Thompson, Nature **440**, 65 (2006).

[158] G. Knebel, D. Aoki, D. Braithwaite, B. Salce, and J. Flouquet, Physical Review B **74**, 020501(R) (2006).

[159] N. Kimura, K. Ito, K. Saitoh, Y. Umeda, H. Aoki, and T. Terashima, Physical Review Letters **95**, 247004 (2005).

[160] I. Sugitani, Y. Okuda, H. Shishido, T. Yamada, A. Thamizhavel, E. Yamamoto, T. D. Matsuda, Y. Haga, T. Takeuchi, R. Settai, and Y. Onuki, Journal of the Physical Society of Japan **75**, 043703 (2006).

[161] K. Ishida, D. Ozaki, T. Kamatsuka, H. Tou, M. Kyogaku, Y. Kitaoka, N. Tateiwa, N. K. Sato, N. Aso, C. Geibel, and F. Steglich, Physical Review Letters **89**, 037002 (2002).

[162] N. Sato, N. Koga, and T. Komatsubara, Journal of the Physical Society of Japan **65**, 1555 (1996).

[163] M. Jourdan, A. Zakharov, M. Foerster, and H. Adrian, Physical Review Letters **93**, 097001 (2004).

[164] H. Tou, Y. Kitaoka, T. Kamatsuka, K. Asayama, C. Geibel, F. Steglich, S. Süllow, and J. Mydosh, Physica B: Condensed Matter **230**, 360 (1997).

[165] A. Krimmel, P. Fischer, B. Roessli, H. Maletta, C. Geibel, C. Schank, A. Grauel, A. Loidl, and F. Steglich, Zeitschrift für Physik B **86**, 161 (1992).

[166] Y. Inada, H. Aono, A. Ishiguro, J. Kimura, N. Sato, A. Sawada, and T. Komatsubara, Physica B: Condensed Matter **199-200**, 119 (1994).

[167] Y. Inada, A. Ishiguro, J. Kimura, N. Sato, A. Sawada, T. Komatsubara, and H. Yamagami, Physica B: Condensed Matter **206-207**, 33 (1995).

[168] Y. Inada, H. Yamagami, Y. Haga, K. Sakurai, Y. Tokiwa, T. Honma, E. Yamamoto, Y. Onuki, and T. Yanagisawa, Journal of the Physical Society of Japan (1999).

[169] G. Zwicknagl, A. Yaresko, and P. Fulde, Physical Review B **68**, 052508 (2003).

[170] N. K. Sato, N. Aso, K. Miyake, R. Shiina, P. Thalmeier, G. Varelogiannis, C. Geibel, F. Steglich, P. Fulde, and T. Komatsubara, Nature **410**, 340 (2001).

[171] K. Miyake and N. K. Sato, Physical Review B **63**, 052508 (2001).

[172] M. Jourdan, M. Huth, and H. Adrian, Nature **398**, 47 (1999).

[173] M. Kyogaku, Y. Kitaoka, K. Asayama, C. Geibel, C. Schank, and F. Steglich, Journal of the Physical Society of Japan **62**, 4016 (1993).

[174] M. Kyogaku, Y. Kitaoka, K. Asayama, N. Sato, T. Sakon, T. Komatsubara, C. Geibel, C. Schank, and F. Steglich, Physica B: Condensed Matter **186-188**, 285 (1993).

[175] T. Watanabe, K. Izawa, Y. Kasahara, Y. Haga, Y. Onuki, P. Thalmeier, K. Maki, and Y. Matsuda, Physical Review B **70**, 184502 (2004).

[176] Y. Shimizu, S. Kittaka, T. Sakakibara, Y. Tsutsumi, T. Nomoto, H. Ikeda, K. Machida, Y. Homma, and D. Aoki, Physical Review Letters **117**, 037001 (2016).

[177] S. Fujimoto, Journal of the Physical Society of Japan **75**, 083704 (2006).

[178] L. N. Bulaevskii and A. I. Buzdin, Adv. Phys. **34**, 175 (1985).

[179] F. Levy, I. Sheikin, B. Grenier, and A. D. Huxley, Science **309**, 1343 (2005).

[180] T. Hattori, Y. Ihara, Y. Nakai, K. Ishida, Y. Tada, S. Fujimoto, N. Kawakami, E. Osaki, K. Deguchi, N. K. Sato, and I. Satoh, Physical Review Letters **108**, 1 (2012).

[181] Y. Tada, S. Fujimoto, N. Kawakami, T. Hattori, Y. Ihara, K. Ishida, K. Deguchi, N. K. Sato, and I. Satoh, Journal of Physics: Conference Series **449**, 012029 (2013).

[182] V. P. Mineev and T. Champel, Physical Review B **69**, 144521 (2004).

[183] V. P. Mineev, Physical Review B **81**, 180504(R) (2010).

[184] V. P. Mineev, Physical Review B **83**, 064515 (2011).

[185] Y. Tada, N. Kawakami, and S. Fujimoto, Journal of the Physical Society of Japan **80**, SA006 (2011).

[186] K. Hattori and H. Tsunetsugu, Physical Review B **87**, 064501 (2013).

[187] Y. Tada, S. Takayoshi, and S. Fujimoto, Physical Review B **93**, 174512 (2016).

[188] T. Ohta, Y. Nakai, Y. Ihara, K. Ishida, K. Deguchi, N. K. Sato, and I. Satoh, Journal of the Physical Society of Japan **77**, 023707 (2008).

[189] T. Ohta, T. Hattori, K. Ishida, Y. Nakai, E. Osaki, K. Deguchi, N. K. Sato, and I. Satoh, Journal of the Physical Society of Japan **79**, 023707 (2010).

[190] M. Sato and S. Fujimoto, Journal of the Physical Society of Japan **85**, 072001 (2016).

[191] M. Taupin, L. Howald, D. Aoki, and J. P. Brison, Physical Review B **90**, 180501(R) (2014).

[192] C. J. Bradley and A. P. Cracknell, *The Mathematical Theory of Symmetry in Solids* (Oxford University Press, Oxford, 1972).

[193] M. V. Murthy, Journal of Mathematical Physics **7**, 853 (1966).

[194] G. W. Mackey, American Journal of Mathematics **75**, 387 (1953).

[195] C. J. Bradley and B. L. Davies, Journal of Mathematical Physics **11**, 1536 (1970).

[196] S. Kobayashi, Y. Yanase, and M. Sato, Physical Review B **94**, 134512 (2016).

[197] N. Bernhoeft, The European Physical Journal B **13**, 685 (2000).

[198] R. Feyerherm, A. Amato, F. N. Gygax, A. Schenck, C. Geibel, F. Steglich, N. Sato, and T. Komatsubara, Physical Review Letters **73**, 1849 (1994).

[199] K. Matsuda, Y. Kohori, and T. Kohara, Physical Review B **55**, 15223 (1997).

[200] L. M. Sandratskii, J. Kübler, P. Zahn, and I. Mertig, Physical Review B **50**, 15834 (1994).

[201] P. M. Oppeneer and G. Varelogiannis, Physical Review B **68**, 214512 (2003).

[202] M. Samsel-Czekała, S. Elgazzar, P. M. Oppeneer, E. Talik, W. Walerczyk, and R. Troć, Journal of Physics: Condensed Matter **22**, 015503 (2010).

[203] D. Aoki, I. Sheikin, T. D. Matsuda, V. Taufour, G. Knebel, and J. Flouquet, Journal of the Physical Society of Japan **80**, 013705 (2011).

[204] S.-i. Fujimori, T. Ohkochi, I. Kawasaki, A. Yasui, Y. Takeda, T. Okane, Y. Saitoh, A. Fujimori, H. Yamagami, Y. Haga, E. Yamamoto, and Y. Onuki, Physical Review B **91**, 174503 (2015).

[205] E. Hassinger, D. Aoki, G. Knebel, and J. Flouquet, Journal of the Physical Society of Japan **77**, 073703 (2008).

[206] E. Hassinger, D. Aoki, G. Knebel, and J. Flouquet, Journal of Physics: Conference Series **200**, 012055 (2010).

[207] G. C. Psaltakis and E. W. Fenton, Journal of Physics C: Solid State Physics **16**, 3913 (1983).

[208] A. Aperis, G. Varelogiannis, P. B. Littlewood, and B. D. Simons, Journal of Physics: Condensed Matter **20**, 434235 (2008).

[209] P.-D. Fan, J.-Q. Chen, L. McAven, and P. Butler, International Journal of Quantum Chemistry **75**, 1 (1999).

Acknowledgment

I would like to thank my mentor, Hiroaki Ikeda, for his help and support during my five years graduate course. I am grateful for his guidance and patience in discussing physical topics. His valuable comments have been important for me to complete this work. I would also like to thank Kazumasa Hattori for many fruitful and stimulating discussions.

I would like to thank the faculty in the condensed matter theory group at Kyoto, Norio Kawakami, Ryusuke Ikeda, Youichi Yanase, Masaki Tezuka, and Robert Peters for their help in various academic matters. I also benefited from discussions and interactions with many inspiring colleagues in the condensed matter theory group. I am especially grateful to Fuyuki Matsuda, Masaya Nakagawa, Hiroaki Sumiyoshi, and Yasuharu Nakamura for everyday discussions about physics and others. I appreciate financial support I have received over the past two years from the Japan Society for the Promotion of Science.